University of Alberta

LOW COMPLEXITY DETECTION TECHNIQUES FOR MIMO AND
COOPERATIVE NETWORKS

by

Shuangshuang Han

A thesis submitted to the Faculty of Graduate Studies and Research
in partial fulfillment of the requirements for the degree of

Doctor of Philosophy

in

Communications

Department of Electrical and Computer Engineering

©Shuangshuang Han
Fall 2013
Edmonton, Alberta

Abstract

This thesis investigates detection technologies for multiple-input multiple-output (MIMO) systems and cooperative communications. The exploitation of detection methods and relay strategies to achieve near-optimal performance (measured by symbol error rate or minimum mean squared error) and reductions of the running time of detection methods are the main focus of this thesis. A signal-to-noise ratio (SNR)-dependent radius control sphere detector (SD) algorithm, a general framework of statistical pruning SD, and an improved K-best SD are proposed. These SD algorithms reduce the detection running time in terms of the average number of visited nodes, with negligible performance loss compared with that of optimal maximum likelihood (ML) detection. In order to optimize the MIMO relay performance, an estimate-and-forward (EF) relay strategy is also developed. The emerging trend towards large MIMO and cooperative communication systems makes the development of low running time strategies with near-optimal performance more important. Thus, an EF list generated by SD is also proposed to reduce the number of computational operations for the EF scheme in large MIMO relay networks; this method is called list EF.

Overall, the research findings should help to reduce the running time and improve the reliability of detection algorithms, to achieve a desirable trade-off between running time and performance, and to provide efficiently-implementable MIMO and cooperative detection algorithms.

$\sim$

Acknowledgement

I express my sincere gratitude and respect to my supervisor, Dr. Chintha Tellambura, for his brilliant advice and constant encouragement. He guided me on how to think critically and how to identify and solve research problems. His insight, kindness and genuine concerns for his students made working with him a memorable experience. I am grateful to him for supporting me throughout my graduate studies.

My thanks also go to members of PhD examining committee, Dr. Xianbin Wang, Dr. Mike MacGregor, Dr. Bruce Cockburn and Dr. Hai Jiang, for their time reviewing my thesis and for their valuable suggestions for improvement. I am also grateful to the faculty and the staff of the ECE for their support and for creating an environment conducive to research excellence.

I would also like to thank Dr. Tao Cui for his invaluable feedback and collaboration while coauthoring publications. Much respect to my labmates, including Dr. Damith Senaratne, Dr. Gongpu Wang, Saman Atapattu and Gayan Amarasuriya, for providing me with invaluable help and advice for my study and research and the pleasant times we spent together.

My heartfelt and deepest gratitude goes to my beloved parents, my sister and my boyfriend for their immeasurable dedication, faithful support and great encouragement.

Last but not least, I also wish to thank the China Scholarship Council (CSC) for the financial support I received in the form of a CSC Scholarship.

$\sim$

Table of Contents

List of Tables

List of Figures

List of Abbreviations

Abbreviation	Definition
3GPP	3rd-generation partnership project
AF	amplify-and-forward
AWGN	additive white Gaussian noise
BER	bit error rate
BPSK	binary phase shift keying
CDF	cumulative distribution function
CDMA	code division multiple access
CPD	cooperative partial detection
CSC	China Scholarship Council
CSI	channel state information
DF	decode-and-forward
ECC	error correction code
EF	estimate-and-forward
FER	frame error rate
FP	Fincke-Pohst
i.i.d.	independent and identically distributed
IKSD	improved K-best sphere detector
LLR	log-likelihood ratio
LMMSE	linear minimum mean squared error
LTE	long-term evolution
MAN	metropolitan area networks
MIMO	multiple-input multiple-output
ML	maximum likelihood
MMSE	minimum mean squared error

Abbreviation	Definition
MSE	mean squared error
PAM	pulse amplitude modulation
PDF	probability density function
PTP-SD	probabilistic tree-pruning sphere detector
QAM	quadrature amplitude modulation
SD	sphere detector
SE	Schnorr-Euchner
SER	symbol error rate
SNR	signal-to-noise ratio
SPSD	statistical pruning sphere detector
SRC-SD	SNR-dependent radius control sphere detector
VLSI	very-large-scale integration

List of Symbols

$\lvert a \rvert$	absolute value of scalar a
$\mathbb{R}$	real number set
$\Re\{x\}$	real component of (complex) scalar x
$\Im\{x\}$	imaginary component of (complex) scalar x
$z \sim \mathcal{CN}(\mu, \sigma^2)$	A circularly complex Gaussian variable with mean μ and variance σ^2
$\lVert (\cdot) \rVert^2$	square of the L^2-norm
$\mathbf{A}^c$	complement event of $\mathbf{A}$
$(\mathbf{A})^{-1}$	inverse of $\mathbf{A}$
$\mathbf{A}^\dagger$	Moore-Penrose pseudo inverse of $\mathbf{A}$
$(\mathbf{A})^T$	transpose of $(\mathbf{A})$
$(\mathbf{A})^H$	Hermitian of $(\mathbf{A})$
$\mathbf{A}^*$	conjugate of $\mathbf{A}$
$\mathbf{I_n}$	identity matrix of rank n
$\arg\min_i(a_i)$	index i corresponding to the smallest a_i
$\arg\max_i(a_i)$	index i corresponding to the largest a_i
$\max_i(a_i)$	the maximum a_i
$\min_i(a_i)$	the minimum a_i
$\mathcal{E}(x)$	expectation of x
$\log(\cdot)$	natural logarithm
$\log_2(\cdot)$	logarithm to base 2
$\sum_{i=1}^{m}(x_i)$	sum of x_i for $i = 1, 2, \ldots, m$
∞	infinity
$\lceil x \rceil$	the smallest integer greater than or equal to x
$\lfloor x \rfloor$	the largest integer less than or equal to x
$\lceil x \rfloor$	the nearest integer around x
$\lim_{x \to \infty} f(x)$	the limit of function $f(x)$ as x tends to ∞
$\exp(x)$	exponential function of x
$\gamma(k, x)$	incomplete Gamma function
$\Gamma(k)$	Gamma function

Chapter 1

Introduction

1.1   The Growth of Wireless Communications

Wireless communications is one of the most vibrant areas in the communication field today. A topic of study since the 1960s, it has seen a surge of research activity in the past decade. Two fundamental challenges are to improve the reliability and spectral efficiency of wireless networks. The reliability of the delivery of messages to the intended recipients may be measured by the bit error rates, while spectral efficiency refers to the delivered bit rate for a given bandwidth. The improvement in these metrics has helped the growth of wireless traffic.
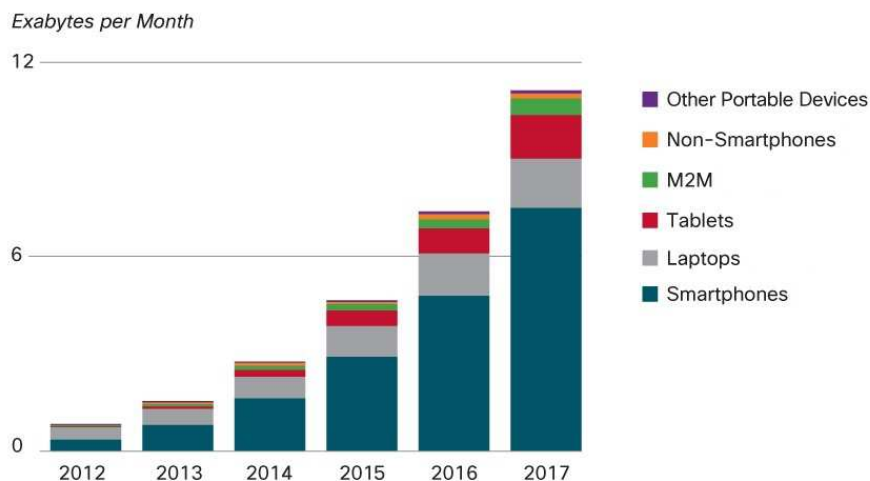
Figure 1.1: Mobile data traffic of wireless communications devices [1]

One of the primary contributors to traffic growth is the increasing number of wireless devices accessing mobile networks worldwide, as shown in the mobile
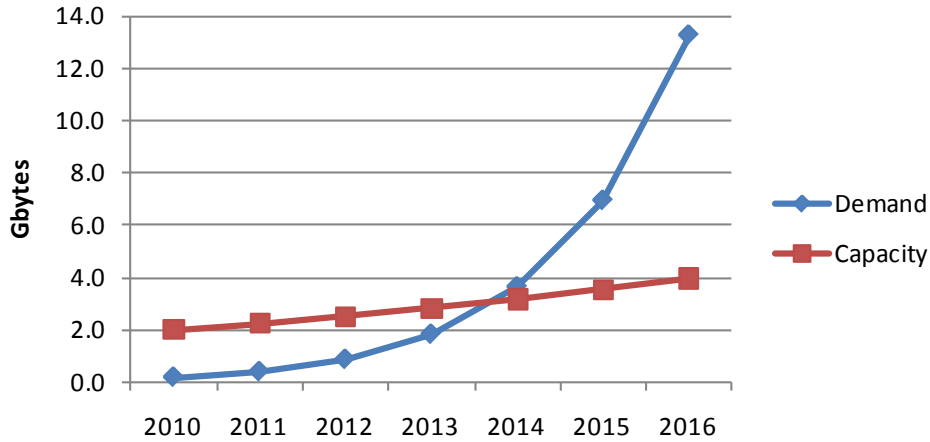
Figure 1.2: Average demand per user and average capacity per user [2]

wireless traffic forecast by Cisco systems (Fig. 1.1). The data rate demand and the system capacity (Fig. 1.2) drive the need for more sophisticated communications technologies.

Two such technologies under consideration for the wireless networks are

- Multiple-input multiple-output (MIMO) technology [3], which uses multiple antennas at both the transmitter and receiver to improve communication performance. MIMO offers significant increases in data throughput and link range without additional bandwidth or increased transmit power.

- Cooperative communication [4], which most commonly involves multiple-hop techniques. The basic idea is to have one or more intermediate nodes (relays) that will repeat or retransmit the signal from one node (sender) to another (destination).

These two technologies are introduced next.

1.1.1 MIMO Technology

As mentioned above, MIMO technology has attracted attention due to its significant improvements in the spectral efficiency and/or reliability. Fig. 1.3 shows a MIMO system that uses multiple antennas to create multiple links between the transmitter and receiver. These multiple links create the space dimension, which can be

exploited for reliability and/or efficiency gains. MIMO technology is exploited in the latest WiFi (IEEE 802.11n [5]) data communication standard, 3rd-generation partnership project (3GPP) long-term evolution (LTE) cellular communication standard [6], and in the IEEE 802.16e (WiMAX) metropolitan area networks (MAN) standard [7].
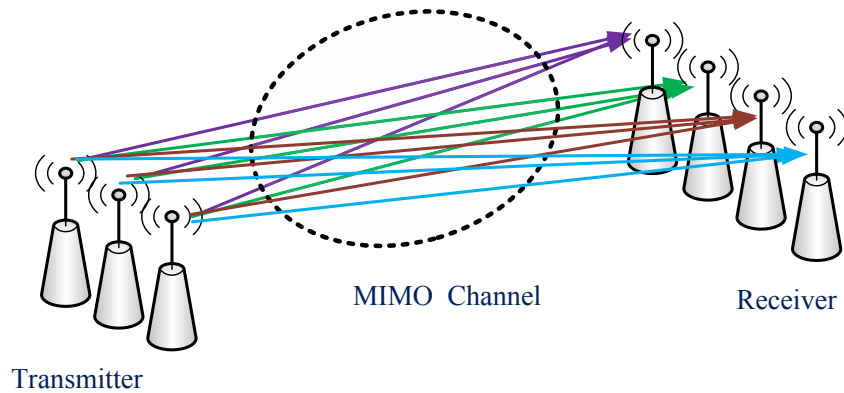
Figure 1.3: MIMO Channel

MIMO can be used to mitigate wireless channel impairments and resource constraints. This mitigation is possible by exploiting the time, frequency, and spatial dimensions. The resulting MIMO performance gains are array gain, spatial diversity gain, spatial multiplexing gain and interference reduction [3]:

- Array gain means a power gain of the transmitted signals that is achieved by using multiple-antennas at the transmitter and/or receiver, with respect to the single-input single-output case. It can be simply called the power gain resulting from a coherent combining effect of the wireless signals at the receiver. It improves resistance to noise, thus improving the coverage of a wireless network.

- Spatial diversity gain refers to the ability to mitigate multipath fading by using multiple antennas to improve the quality and reliability of a wireless link. This gain arises because the multiple links created by MIMO offer a receiver several observations of the same transmitted signal.

- Spatial multiplexing, a special case of MIMO, transmits multiple independent data signals, so-called streams, from each of the multiple transmit antennas. Thus, the space dimension is reused, or multiplexed, more than once. Spatial multiplexing gain refers to the increased data rate due to the use of MIMO.

- Interference reduction refers to the ability of MIMO to exploit the spatial dimension to increase the separation between users who share time and frequency resources.

In general, simultaneously exploiting all the benefits above might be impossible. However, using some combination of the benefits across a wireless network will result in improved capacity, coverage and reliability.

1.1.2 Coded MIMO

MIMO systems use digital modulations and codes to be able to recover from errors made during the transmission. Channel codes, also known as error correction codes (ECCs) [8, 9], play an indispensable role in all modern wireless communication systems.

The ECC encoder computes additional bits (also called check bits) from the original information bits. In a block ECC, information bits and the additional redundant bits form a block of bits called a codeword. This codeword is transmitted to the receiver, whose decoder exploits the redundancy in the received data to determine the original data bits.

Therefore, over unreliable or noisy communication channels, channel codes (ECCs) provide redundancy for guarding against bursty fading, interference, and additive receiver noise. Receiver design for channel-coded systems dates from the 1960s, while that for multiple-antenna channels began largely in the 1980s [3].

By using channel codes, the reliability of a MIMO channel can be improved, leading to the development of coded MIMO systems with suitable detection and decoding techniques. For instance, the iterative MIMO receiver [10] enables high-throughput transmission at low signal-to-noise ratios (SNRs). Such transmission approaches the theoretical capacity limit.

1.1.3 Cooperative Relays

The additional constraints posed by limited power and scarce frequency bandwidth make the task of designing high-data-rate, high-reliability wireless communication systems challenging. Because even with MIMO technology, the difficulties of meeting the demands and expectations on wireless communication systems (e.g., over a 10-fold increase in data rates) are challenging, additional means to enhance wireless performance are necessary. Consequently, cooperation among wireless nodes that enables intermediate nodes (relays) to forward messages from source to destination is potentially very useful. Such cooperative relays and MIMO are being considered for next-generation wireless systems such as LTE-Advanced [11, 12] and IEEE 802.11ad [13].

In cooperative communications, several independent paths between the source and the destination are created using relay channels, as illustrated in Fig. 1.4. The relay channels can be thought of as providing independent auxiliary channels to the direct channel between the source and destination.
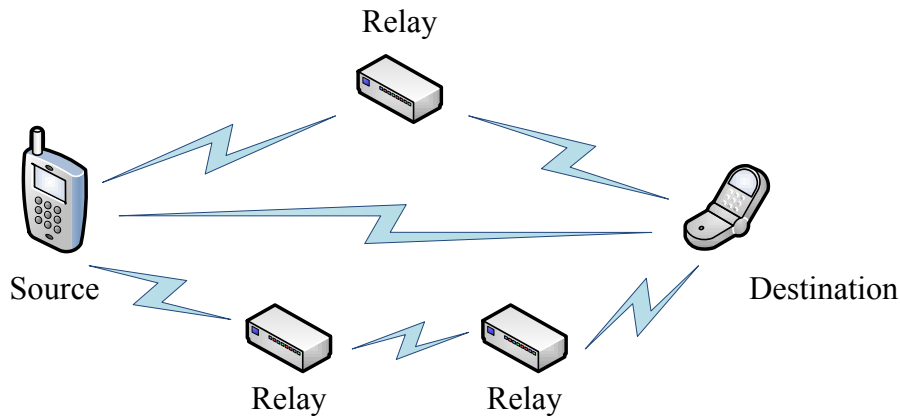
Figure 1.4: Relay channels

These relay channels improve wireless performance due to cooperation diversity. That is, the destination receives independent copies of the transmit signal, which can be combined to achieve performance gains such as diversity and multiplexing gains. These gains may translate into decreased transmission powers, higher capacity or better cell coverage [4].

A key aspect of the cooperative relays is the processing of the signal received from the source node. While different relaying schemes result in different system performance, they can be categorized generally into amplify-and-forward (AF) and decode-and-forward (DF) relaying schemes [4].

- An AF relay simply scales the received signal and transmits an amplified version to the destination. Although this relay process amplifies noise, the destination receives multiple versions of the transmitted signal.

- A DF relay decodes the received signal, re-encodes, and then retransmits to the receiver. In this case, if the relay makes decoding errors, the digital errors will propagate to the destination.

Section 2.4 provides more discussion of relays.

1.2   Motivation

As mentioned in Section 1.1, extraordinary wireless growth (1300% between 2012 and 2017 as shown in Fig. 1.1) has driven the need for MIMO and cooperative relays. Reliability and spectral efficiency are the main performance gains. However, these gains depend critically on the detection algorithms employed by the receiver. In particular, guaranteeing statistically optimal performance requires maximum likelihood (ML) detection. However, ML detection for MIMO and relays is significantly more complicated than that for single-antenna systems. Naive detection algorithms require computational complexity[1] that increases exponentially with the number of transmit antennas and the order of the signal constellation. Consequently, the optimal detection algorithms at the receiver end require very high computing power, which typically exceeds the capabilities of the typical integrated circuits currently being used in wireless communication [14].

Therefore, this thesis focuses on the development of low-complexity MIMO and/or relay detection algorithms. Low-complexity and near-optimal detection algorithms have the potential for adoption in emerging wireless standards. Their

---

[1]Computational complexity is a functional form that is inferred by observing the run-times of a series of solutions to successively larger problem instances.

reduced computational complexity can simplify hardware implementation, without compromising the higher data rates and quality of service envisioned for future wireless networks. Moreover, the algorithms and the insights gained while designing them may be used elsewhere in wireless communication.

1.3 Thesis Outline & Contributions

Chapter 2 presents the background techniques related to this thesis, including MIMO detection techniques and conventional relaying methods for relay networks. Chapters 3–6 deal with either uncoded/coded MIMO detection or relay forwarding strategies, establishing a background and framework for future research. Chapter 7 presents the conclusions and future research.

- Chapter 3 introduces a novel sphere detector (SD) algorithm, which is called SNR-dependent radius control sphere detector (SRC-SD), for uncoded/coded spatial multiplexing MIMO systems. The SRC-SD overcomes the drawbacks of traditional SDs, which are variable running time and high running time in low SNRs. The main idea of the SRC-SD is to scale the search radius by a heuristic SNR-dependent factor. Due to this scaling, this new SRC-SD offers a near-ML performance over the entire range of SNRs, while keeping its running time roughly constant. This new algorithm also incorporates channel ordering to save running time and is also extended for MIMO-relay networks.

- In Chapter 4, node-pruning strategies based on probability distributions are developed for ML detection for MIMO systems. Uniform pruning, geometric pruning, threshold pruning, hybrid pruning and depth-dependent pruning are thus developed in detail. The desirable diversity order of uniform pruning and the threshold level for threshold pruning are derived. Threshold pruning is shown to save running time compared to popular SD algorithms such as K-best, fixed complexity and probabilistic tree-pruning sphere detector (PTP-SD), especially for high SNRs and large antenna MIMO systems. Furthermore, the application to other systems, including coded MIMO systems and relay networks, is discussed.

7

- Chapter 5 investigates a breadth-first SD algorithm, which we called the improved K-best sphere detector (IKSD). At each iteration, this algorithm retains the best K nodes and all the nodes whose costs are within a certain margin of the cost of the K-th best node. Three IKSD variants – fixed threshold, normalized threshold and adaptive threshold IKSD – are developed. The proposed IKSD requires a smaller K (indicating lower running time) while achieving near-ML performance compared to the conventional K-best SD. These gains are confirmed by simulation results. The IKSD is also extended as a hybrid SD algorithm, which uses full enumeration in the top layers of the search tree and applies the IKSD for the remaining layers. The IKSD is also extended as a list SD for joint iterative detection and decoding of coded MIMO.

- MIMO relay networks are the main focus in Chapter 6. An estimate-and-forward (EF) scheme is proposed and analyzed. This relay scheme forwards the unconstrained minimum mean squared error (MMSE) estimate of the source data to the destination. The relay thus performs like AF and DF for the low and high SNR regions, respectively, and achieves the conventional AF and DF performance across all SNRs without the need to switch algorithms for different SNRs. Its number of computational operations is, however, high for relays with a relatively large number of antennas (large MIMO) and/or high-order constellations. Two approximate EF schemes for large MIMO relay networks are thus proposed. The first one, called list EF, computes a list SD-based MMSE estimate and retains the advantages of the exact EF relay at a negligible performance loss, while the second one computes a Gaussian estimate. For parallel relay networks, the EF scheme achieves increased performance gains.

$\sim$

Chapter 2

Background

This thesis develops new signal detection and transmission techniques for MIMO systems and relay networks. The basic background techniques are reviewed in this chapter: MIMO detection, sphere detection, coded MIMO systems and cooperative relay networks.

2.1 Basic Concepts

2.1.1 Detection vs. Decoding

Signal detection [15] is broadly concerned with the analysis of received signals to determine the presence or absence of signals of interest, to classify the signals present, and to extract useful information included in these signals. Specifically, for this thesis, the process of retrieving transmitted data from a noise-corrupted and faded signal is called detection.

To enable detection, the data bits are modulated into transmitted symbols using a modulation scheme $\mathcal{Q}$. For example, in a quadrature amplitude modulation (QAM), the signal constellation is given by

$$\mathcal{Q} = \{\kappa(a + bi) \,|\, a, b \in \{\ldots - 3, -1, 1, 3, \ldots\}\},\qquad(2.1)$$

where $i = \sqrt{-1}$, and κ is an energy-normalizing constant. Thus, if $x \in \mathcal{Q}$ is transmitted and signal vector y is received, detection refers to the recovering of x from y.

In a coded system, the recovery of data bits from the transmitted version of the

9

coded bit sequence is called decoding. Note that, decoding refers to the recovery of coded data while detection refers to the recovery of uncoded data.

However, for uncoded MIMO systems, many authors have used sphere detection and decoding interchangeably. In this thesis, sphere detection or detector is used.

2.1.2 Complexity

Currently, over 90% of the energy consumption of wireless communications is consumed in the outdoor cellular network, of which 75% is consumed by base stations [16]. The complexity of applied techniques significantly impacts the power consumption of communication systems. The time complexity characterizes the amount of time an algorithm will take to solve successively larger instances of a problem. This can be used to evaluate its time efficiency and power consumption. Therefore, the measure of running time [17] is a very important issue described as follows.

The running time of hardware implementation is evaluated by the number of floating-point operations per second (FLOPS). Typical operations are addition, subtraction, multiplication, division, square root, exponential and so on. The amount of energy being consumed per operation is determined by the power consumption of a design [18]. This factor impacts critical design decisions, such as those involving the power-supply capacity and the battery lifetime. Therefore, power dissipation is an important property of a design that affects feasibility and reliability, and energy costs will be much greater for high running time algorithms.

Therefore, to save energy, low-complexity algorithms are needed. In computer science, the analysis of algorithms is the determination of the amount of resources (such as time and storage) necessary to execute them. It is common to estimate their running time in the asymptotic sense. Big O notation is used to specify an asymptotic upper bound [19] of running time, and it is a convenient way to express the worst-case scenario for a given algorithm. For a given function $g(n)$ (n is the input size), $\mathcal{O}(g(n))$ denotes the set of functions that satisfy

$$\mathcal{O}(g(n)) = \{f(n) : \text{there exist positive constants } c \text{ and } n_0 \\ \text{such that } 0 \leq f(n) \leq cg(n) \text{ for all } n \geq n_0\}. \tag{2.2}$$

For example, $\mathcal{O}(n^2)$ means that the running time is asymptotically no worse than cn^2.

However, for sphere detection algorithms in communications, its running time is evaluated by the expected number of nodes visited in the search tree [20]. The reasons for this measure are (1) the detection problem is a tree-search problem, (2) the number of floating-point operations is constant for all the nodes at the same layer [21], and (3) running time is in proportion to the number of nodes visited by the algorithm. Since the detector algorithms eliminate as many nodes as possible, this number is a random variable. Hence, the average number of nodes visited by the sphere decoder is referred to as the measure of the expected running time of the detection algorithm.

2.2 MIMO Detection

MIMO appears in three main categories [3]:

- Spatial multiplexing MIMO partitions a high-rate signal into multiple lower-rate streams, and then each stream is transmitted from a different transmit antenna.

- Beamforming MIMO attempts to maximize the diversity gain and thus reduce the error rate.

- MIMO space-time coding involves coding across space and time to gain diversity and/or capacity benefits.

Among these three MIMO categories, spatial multiplexing MIMO achieves the highest data rates [3].

As spatial multiplexing MIMO systems are capable of providing enormous capacity improvements without increasing the bandwidth or the total transmit power, these systems are the focus of this thesis. An uncoded spatial multiplexing system is considered with $N_T \geq 1$ transmit antennas and $N_R \geq 1$ receive antennas (Fig. 2.1). A rich scattering memoryless (flat fading) channel $\tilde{\mathbf{H}}$ is assumed [3]. $\tilde{\mathbf{H}}$ is
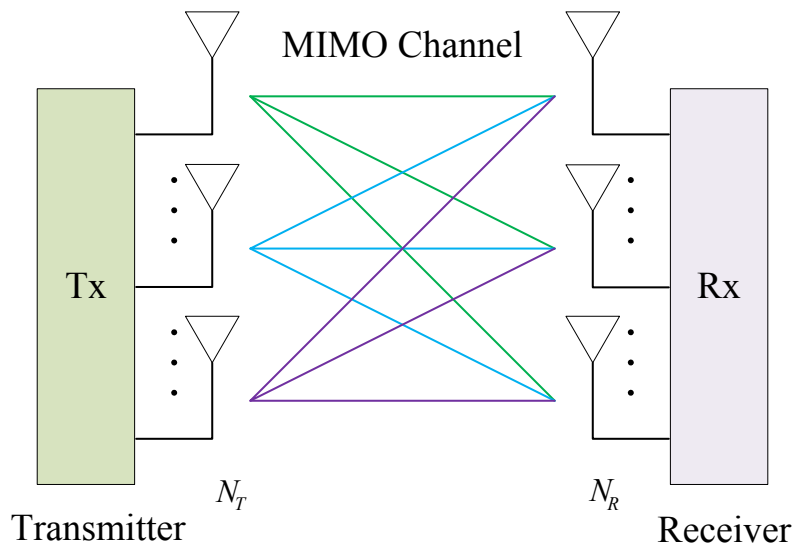
Figure 2.1: $N_T \times N_R$ MIMO system

assumed to be full rank. At the receiver, the received signal vector can be written as [3]

$$\tilde{\mathbf{y}} = \tilde{\mathbf{H}}\tilde{\mathbf{s}} + \tilde{\mathbf{n}}, \tag{2.3}$$

where $\tilde{\mathbf{s}} = (\tilde{s}_1, \tilde{s}_2, \ldots, \tilde{s}_{N_T})^T$ is the transmitted symbol vector, $\tilde{s}_i \in \mathcal{Q}$ (a complex constellation such as M^2-QAM), $\tilde{\mathbf{y}} = (\tilde{y}_1, \tilde{y}_2, \ldots, \tilde{y}_{N_R})^T$, and $\tilde{y}_i$ is the signal received at the i-th antenna ($i = 1, 2, \ldots, N_R$). $\tilde{\mathbf{H}}$ denotes an $N_R \times N_T$ Rayleigh fading channel matrix with independent and identically distributed (i.i.d.) elements $\tilde{h}_{ij} \sim \mathcal{CN}(0, 1)$, where $\mathcal{CN}(0, 1)$ denotes a complex Gaussian distribution with zero mean and unit variance. $\tilde{\mathbf{n}} = (\tilde{n}_1, \tilde{n}_2, \ldots, \tilde{n}_{N_R})^T$ is the vector of i.i.d. additive white Gaussian noise (AWGN) where $\tilde{n}_i \sim \mathcal{CN}(0, \sigma^2)$. It is assumed that the channel matrix $\tilde{\mathbf{H}}$ is perfectly known by the receiver. Following a common assumption in the literature, we will assume $N_T = N_R = N$. For $N_T \neq N_R$ cases, ML detection is also feasible, however, generalized sphere detection will be needed [22]

2.2.1 ML Detection

The detection process determines the original bits sequence based on the signal received over the channel. For statistically optimal detection performance (minimum error rate), a MIMO system requires an optimal detector [3], which minimizes the average error probability. In other words, given a received vector $\tilde{\mathbf{y}}$, the optimal receiver selects $\hat{\tilde{\mathbf{s}}} = \tilde{\mathbf{s}}_i$ corresponding to the constellation symbol vector $\tilde{\mathbf{s}}_i$ that satisfies $p(\tilde{\mathbf{s}}_i|\tilde{\mathbf{y}}) > p(\tilde{\mathbf{s}}_j|\tilde{\mathbf{y}})$, $\forall j \neq i$. By the Bayes rule [23],

$$p(\tilde{\mathbf{s}}_i|\tilde{\mathbf{y}}) = \frac{p(\tilde{\mathbf{y}}|\tilde{\mathbf{s}}_i)p(\tilde{\mathbf{s}}_i)}{p(\tilde{\mathbf{y}})}. \tag{2.4}$$

Assuming equally likely messages $p(\tilde{\mathbf{s}}_i) = \frac{1}{|\mathcal{Q}|^N}$, for all i, the detected symbol vector must satisfy

$$\hat{\tilde{s}} = \arg\max_{\tilde{\mathbf{s}} \in \mathcal{Q}^N} p(\tilde{\mathbf{y}}|\tilde{\mathbf{s}}_i). \tag{2.5}$$

Because of $\tilde{\mathbf{n}} \sim \mathcal{CN}(0, \sigma^2)$, the conditional probability density function (PDF) may be written as

$$p(\tilde{\mathbf{y}}|\tilde{\mathbf{s}}_i) = \frac{1}{(\pi\sigma^2)^N} \exp\left(-\frac{\|\tilde{\mathbf{y}} - \tilde{\mathbf{H}}\tilde{\mathbf{s}}\|^2}{\sigma^2}\right). \tag{2.6}$$

Therefore, by taking the log likelihood of (2.6), the optimal ML detection rule is given as [24]

$$\hat{\tilde{s}} = \arg\min_{\tilde{\mathbf{s}} \in \mathcal{Q}^N} \|\tilde{\mathbf{y}} - \tilde{\mathbf{H}}\tilde{\mathbf{s}}\|^2, \tag{2.7}$$

where $\|x\|$ denotes the Frobenius norm of x, and $\mathcal{Q}^N$ is the set of all possible N-dimensional transmitted symbol vectors for constellation $\mathcal{Q}$.

This detection rule (2.7) is formulated by using complex signals and matrices. However, real versions of these quantities are somewhat easier to handle. Fortunately, the complex channel matrix can be transformed into a real matrix representation $\mathbf{y} = \mathbf{H}\mathbf{s} + \mathbf{n}$, where $\mathbf{y}, \mathbf{n} \in \mathcal{R}^n$, $\mathbf{H} \in \mathcal{R}^{n \times m}$, and $\mathbf{s} \in \mathcal{R}^m$ with $m = n = 2N$; that is,

$$\begin{bmatrix} \Re(\tilde{\mathbf{y}}) \\ \Im(\tilde{\mathbf{y}}) \end{bmatrix} = \begin{bmatrix} \Re(\tilde{\mathbf{H}}) & -\Im(\tilde{\mathbf{H}}) \\ \Im(\tilde{\mathbf{H}}) & \Re(\tilde{\mathbf{H}}) \end{bmatrix} \begin{bmatrix} \Re(\tilde{\mathbf{s}}) \\ \Im(\tilde{\mathbf{s}}) \end{bmatrix} + \begin{bmatrix} \Re(\tilde{\mathbf{n}}) \\ \Im(\tilde{\mathbf{n}}) \end{bmatrix}, \tag{2.8}$$

where $\Re(\cdot)$ and $\Im(\cdot)$ are the real and the imaginary parts of $(\cdot)$, respectively.

Therefore, for the equivalent real constellation, the optimal ML detection rule is given by

$$\hat{\mathbf{s}} = \arg\min_{\mathbf{s} \in \Omega^m} \|\mathbf{y} - \mathbf{H}\mathbf{s}\|^2, \tag{2.9}$$

13

where Ω^m is all possible m-dimensional transmit symbol vectors for the real constellation Ω, and $\hat{\mathbf{s}}$ is the element in Ω^m which minimizes $\|\mathbf{y} - \mathbf{H}\mathbf{s}\|^2$. We take the real and imaginary parts of $\mathcal{Q}$ to form Ω. For example, 16-QAM in (2.3) can be transformed into two 4-pulse amplitude modulation (PAM) $\Omega = \{-3, -1, 1, 3\}$. The naive ML detector exhaustively searches (2.9) and its complexity is

$$C = \mathcal{O}(|\mathcal{Q}|^N) = \mathcal{O}(2^{n_c N}), \tag{2.10}$$

where $n_c = \log_2 |\mathcal{Q}|$ is the order of constellation. Thus, the detection running time grows exponentially with the number of transmit antennas and with the order of the signal constellation.

2.2.2 Sphere Detection

Because of the exponential running time of naive ML detection (2.10), the SD algorithm [25] and its variants are designed to reduce the running time of the search.

The main idea of the SD is to restrict the search space for detection from all the constellation points to a hypersphere with a certain radius d around a preliminary signal vector estimated from the received signal. This idea is efficiently realized by the Fincke-Pohst (FP) SD and Schnorr-Euchner (SE) SD [26, 27]. Here, before discussing these two SDs, we briefly introduce the basic principle of the SD algorithm. Based on the QR factorization of $\mathbf{H}$ ($\mathbf{H} = \mathbf{Q}\mathbf{R}$), where $\mathbf{R}$ is an upper-triangular matrix and $\mathbf{Q}$ is an unitary matrix, and letting $\mathbf{z} = \mathbf{Q}^H \mathbf{y}$ ($\mathbf{Q}^H$ denotes the Hermitian of matrix $\mathbf{Q}$), (2.9) is equivalent to

$$\hat{\mathbf{s}} = \arg\min_{\mathbf{s} \in \Phi} \|\mathbf{z} - \mathbf{R}\mathbf{s}\|^2, \tag{2.11}$$

where Φ should be the set of all points which satisfy $\|\mathbf{z} - \mathbf{R}\mathbf{s}\|^2 \leq d^2$. Here, $\|\mathbf{z} - \mathbf{R}\mathbf{s}\|^2$ is the total cost metric of signal vector $\mathbf{s}$.

The SD detector restricts the search space to this hypersphere Φ. We use the real-system formulation (2.8) to briefly explain the conventional FP and SE SDs (depth-first). To generate the candidate point set Φ, all points $\mathbf{s} = (s_1, s_2 \ldots, s_m)^T$ such that $\|\mathbf{z} - \mathbf{R}\mathbf{s}\|^2 \leq d^2$ can be expanded as

$$\sum_{i=1}^{m} \left(z_i - \sum_{j=i}^{m} r_{i,j} s_j \right)^2 \leq d^2. \tag{2.12}$$

Since the cost metric in (2.12) involves a sum of m terms, a tree with m layers can be used to represent the search problem. Then, Φ will be a set of leaf nodes (layer 1) in the tree.
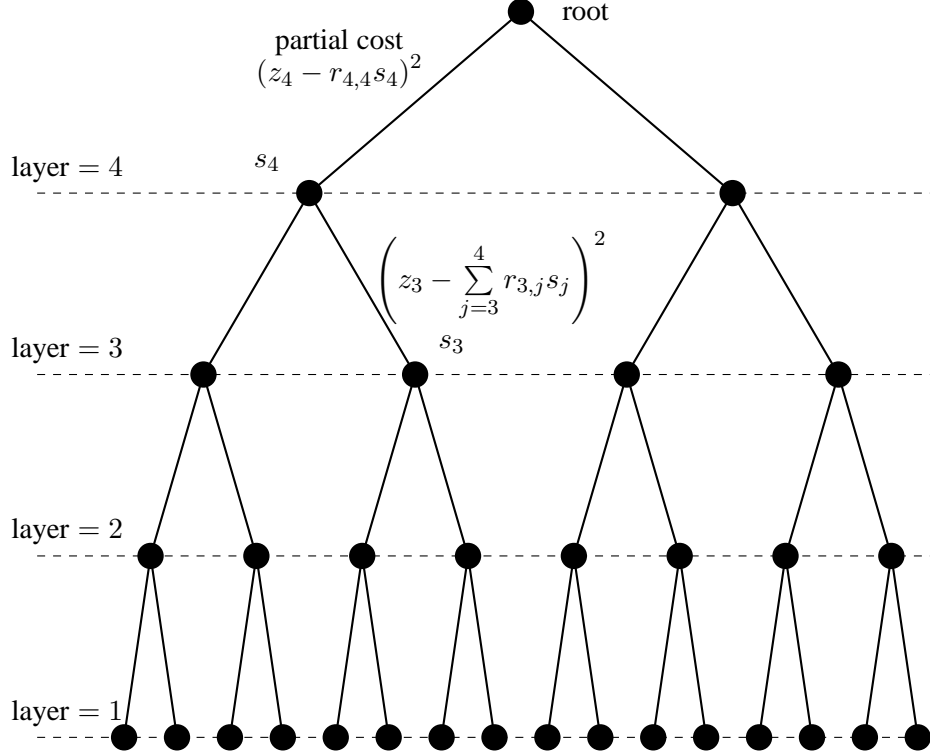
Figure 2.2: An example of tree search

For example, a search tree for a 2×2 4-QAM system is given in Fig. 2.2. The search process starts from layer 4 to layer 1 because matrix $\mathbf{R}$ is an upper-triangular matrix, and by convention the SD algorithm first detects the m-th element s_m in the transmitted signal vector $\mathbf{s} = [s_1, s_2, \ldots, s_m]^T$. The accumulated cost c_i of the nodes at the i-th layer is given by

$$c_i = \sum_{k=i+1}^{m} \left(z_k - \sum_{j=k}^{m} r_{k,j} s_j \right)^2, \tag{2.13}$$

where $s_j \in \{-1, 1\}$ for 2-PAM. In this example, there are $m = 4$ layers, called the depth of the search tree, and each node has 2 child nodes. Following (2.12), when the SD algorithm visits a node i and its partial cost c_i exceeds d^2, then the partial tree emanating from the node is removed totally from further searches. That is, the partial tree is discarded without further searching, and we refer to this activity as

15

the pruning of node i. Clearly, this pruning process does not discard the optimal solution and it certainly saves running time.

The two main categories of SD algorithms are depth-first and breadth-first SD. The basic ideas of these SDs are given in the following.

Depth-first SD

The depth-first algorithm traverses the tree from layer m (top) to layer 1 (bottom) and backtracks as necessary. For example, in the conventional FP SD (Pohst enumeration [28]), given the symbols $s_{i+1}, \ldots, s_m$, the element s_i can be chosen from the range of

$$\left\lceil \frac{1}{r_{i,i}} \left(z_i - \sum_{j=i+1}^{m} r_{i,j} s_j - d_i \right) \right\rceil \leq s_i \leq \left\lfloor \frac{1}{r_{i,i}} \left(z_i - \sum_{j=i+1}^{m} r_{i,j} s_j + d_i \right) \right\rfloor, \quad (2.14)$$

where $d_i^2 = d^2 - \sum_{k=i+1}^{m} \left(z_k - \sum_{j=k}^{m} r_{k,j} s_j \right)^2$, $r_{i,j}$ is the element in the i-th row and the j-th column of matrix $\mathbf{R}$, $\lceil x \rceil$ is the smallest integer greater than or equal to x, and $\lfloor x \rfloor$ is the largest integer less than or equal to x.

In the SE SD (SE enumeration [29]), the admissible points are searched in a zig-zag order from the midpoint $s_{k,mid} = \left\lceil \frac{1}{r_{k,k}} \left(z_k - \sum_{j=k+1}^{n} r_{k,j} s_j \right) \right\rfloor$, where $\lceil s \rfloor$ is the nearest integer around s. The spanning order is $s_{k,mid}, s_{k,mid} + 1, s_{k,mid} - 1, s_{k,mid}+2, \ldots$, when $z_k - d_k - r_{k,k} s_{k,mid} \geq 0$ ($d_k^2 = d^2 - \sum_{j=k+1}^{n} |p_j(\mathbf{s})|^2 = d_{k+1}^2 - |p_{k+1}(s_{k+1}, \ldots, s_n)|^2$), and $s_{k,mid}, s_{k,mid} - 1, s_{k,mid} + 1, s_{k,mid} - 2, \ldots$, otherwise. Further, the SE SD updates the radius d^2 to be the new cost of the currently found solution (leaf node). This method is more efficient than the FP SD [27].

Breadth-first SD

Instead of a depth-first traversing, a SD can process the nodes on a breadth-first basis. The K-best SD [14] is an example, which searches the tree layer by layer and keeps only the best K candidates at each layer. This SD sorts all the child nodes based on their partial costs and selects the K best paths. Finally, when the bottom layer is reached, the leaf node with the minimum cost is selected as the solution.

Thus, the search running time of the K-best algorithm is fixed and depends only on K and the number of layers in the tree.

The K-best SD search procedure is briefly described as follows: (1) Initialize the partial cost to be 0 at the root of the search tree; (2) Expand all the nodes at the current layer and compute the partial costs for all these potential successors; (3) Sort these nodes in the ascending order of their costs, and retain the best K nodes with the smallest costs; (4) Prune all other nodes and update the partial cost for each candidate; (5) Check if the bottom layer is reached; if yes, then the leaf node with the smallest cost is the estimate; or if no, reduce the layer number, and go to (2).

Fixed SD

The fixed SD algorithm, proposed in [30], is a derivative of the K-best SD algorithm. It introduces a parameter set $(k_1, \ldots, k_l, \ldots, k_m)$, where k_l refers to the number of visited nodes per surviving parent node at the l-th layer and $1 \leq l \leq m$. For example, in the first layer, $k_m = |\Omega|$, more candidates need to be considered for the top layer; while the number of candidates will be reduced in the last layers. In this case, an exhaustive search is performed in the top layer; thus full enumeration is required in the top layer, and all nodes are concurrently visited. Therefore, the running time of this Fixed SD is less than that of the conventional K -best SD, given the same number of visited nodes.

The K-best and Fixed SD are hardware-friendly because they have predetermined visited node and constant throughput. However, neither of them can guarantee the ML solution when the number of visited nodes is severely constrained.

2.3 Coded MIMO Systems

Consider the coded MIMO system in Fig. 2.3). The information vector $\mathbf{b}$ is a frame of M_b bits encoded by the ECC module, whose output $\mathbf{c}$ goes through an interleaver Π. The interleaver rearranges the input data in a noncontiguous manner such that consecutive data are spaced apart. The interleaver here ensures statistical independence. The ECC can be a convolutional code or a turbo code with code rate R; thus, the length of the coded sequence $\mathbf{c}$ is $M_c = M_b/R$. The interleaved bits $\underline{\mathbf{x}}$ are mod-
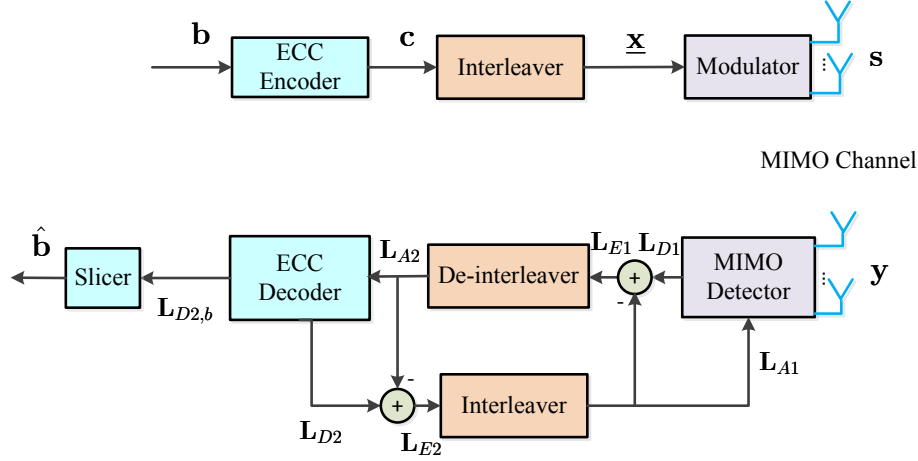
Figure 2.3: The system model of iterative detection and decoding

ulated to channel symbols $\underline{s}$ and transmitted. M_x and M_s are the frame length of $\underline{x}$ and $\underline{s}$, respectively, where $M_x = M_s \log_2(|\mathcal{Q}|)$. Therefore, a frame of M_s symbols requires the transmission of $M_{ch} = M_s/N$ blocks of data where N is the number of transmit antennas, corresponding to M_{ch} different channel realizations.

At the receiver, several iterations of soft information exchange [10] occur between the ECC decoder and MIMO detector. The MIMO detector in this case generates soft *a posteriori* information $\mathbf{L}_{D1}$ by processing the received signal $\underline{y}$ and the *a priori* information $\mathbf{L}_{A1}$ from the ECC decoder. This reliability information is expressed by *a posteriori* probability (APP) in the form of log-likelihood ratios (LLR). For example, The LLR of bit $\underline{x}_i (i = 1, 2, \ldots, M_x)$ is defined as

$$L(\underline{x}_i) = \log \frac{\Pr[\underline{x}_i = +1]}{\Pr[\underline{x}_i = -1]}. \tag{2.15}$$

Note that the amplitude levels -1 and $+1$ represent binary 0 and 1, respectively.

For the first iteration, the $\mathbf{L}_{A1}$ is initialized to 0, and the extrinsic information $\mathbf{L}_{E1} = \mathbf{L}_{D1} - \mathbf{L}_{A1}$ generated by the MIMO detector is deinterleaved by Π^{-1} to serve as the *a priori* information for the ECC decoder. The ECC decoder then generates the extrinsic information for the next iteration. This process continues until a stopping criterion is met, such as a predefined iteration number or a performance bound. In the final iteration, the ECC decoder obtains the *a posteriori* information $\mathbf{L}_{D2,b}$ on the uncoded bits $\mathbf{b}$ [31], which is sent to the slicer that outputs the final bit

estimates $\hat{\mathbf{b}}$.

As discussed above, soft information needs to be exchanged between the detector and decoder. The naive SD algorithm can be modified to produce the required soft information. The running time of this process has been widely investigated [10, 32, 33]. One jointly iterative detection and decoding method has been proposed [10], which generates soft information by a list version of the SD (LSD). In this scheme, the ECC can be any code that could be decoded by using soft inputs and outputs, such as a convolutional code or a turbo code [34]. Many SDs, for example, the K-best SD [14] and a list fixed-complexity SD [35], are capable of providing the necessary soft outputs in LSD.

2.4 Cooperative Relays
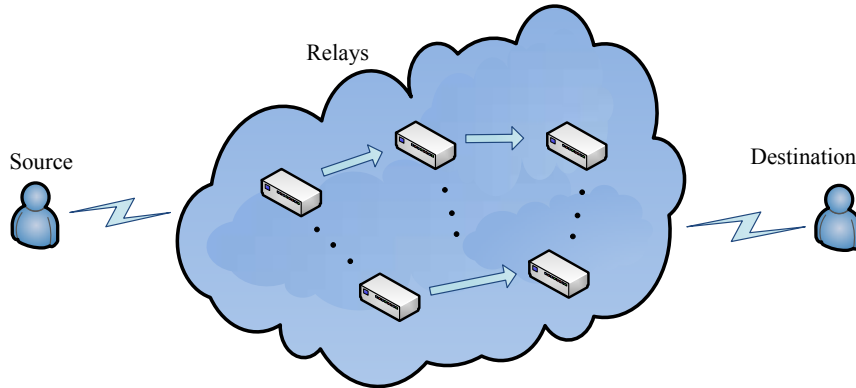
Figure 2.4: MIMO relay network

The MIMO relay network is illustrated in Fig. 2.4, where the source has M_s transmit antennas, all the relays have N_r receive antennas and M_r transmit antennas, and the destination has N_d receive antennas. In this network, the data signals from the source to the destination travel via the relays. Assuming there are N_{sr} relays receiving the transmitted signal from the source, the received signal $\mathbf{r}_k$ at the k-th ($k = 1, 2, \ldots, N_{sr}$) relay can be given as

$$\mathbf{r}_k = \mathbf{H}_k \mathbf{x} + \mathbf{n}_{1k}, \tag{2.16}$$

19

where $\mathbf{H}_k = [h_{ij}] \in \mathcal{C}^{N_r \times M_s}$ denotes the MIMO channel between the source and the k-th relay, and the elements of $\mathbf{H}_k$ are i.i.d. complex Gaussian ($h_{ij} \sim \mathcal{CN}(0, 1)$); $\mathbf{n}_{1k} = [n_{11}, n_{12}, \ldots n_{1N_r}]^T$ and $n_{1i} \sim \mathcal{CN}(0, \sigma_1^2)$ $(i = 1, 2, \ldots, N_r)$ is an AWGN with mean zero and variance σ_1^2. The transmitted signal is denoted by $\mathbf{x} = [x_1, x_2, \ldots, x_{M_s}]^T$, assuming i.i.d. elements in $\mathbf{x}$. It is also assumed that each transmitted symbol is chosen from the same constellation; i.e., $x_i \in \mathcal{Q}$, and the average transmitted power is $\mathcal{E}[\|\mathbf{x}\|^2] = P_s$, where P_s is the source power and $\mathcal{E}(x)$ is the expectation of x.

A memoryless relay receives the source signal from the source, generates and transmits the processed signal to the destination, and its relay function $\mathcal{G}(\mathbf{r})$ uses the current received signal $\mathbf{r}$ only. The assumption is that the average relay power P_r of the transmitted signal $\mathcal{G}(\mathbf{r})$ should satisfy the power constraint $\mathcal{E}[\|\mathcal{G}(\mathbf{r})\|^2] = P_r$. Therefore, if N_{rd} relays retransmit their processed signals, the received signal at the destination may be written as

$$\mathbf{y} = \sum_{k=1}^{N_{rd}} \mathbf{G}_k \, \mathcal{G}(\mathbf{r}_k) + \mathbf{n_2}, \tag{2.17}$$

where $\mathbf{G}_k = [g_{ij}] \in \mathcal{C}^{N_d \times M_r}$ $(k = 1, 2, \ldots, N_{rd})$ denotes the MIMO channel between the k-th relay and the destination, and the elements of $\mathbf{G}_k$ are also i.i.d. complex Gaussian ($g_{ij} \sim \mathcal{CN}(0, 1)$), and $\mathbf{n_2} = [n_{21}, n_{22}, \ldots n_{2N_d}]^T$ ($n_{2i} \sim \mathcal{CN}(0, \sigma_2^2)$ and $i = 1, 2, \ldots, N_d$).

The performance of MIMO memoryless relay networks depends critically on the relay function. Relay strategies have thus been studied in [4, 36–44]. Several relay functions of memoryless forwarding strategies for MIMO relay systems are discussed next.

2.4.1 Amplify-and-Forward

Pure AF: Among the classical relay strategies, AF relaying is the most basic relay strategy [45]. For each transmit symbol, the relay retransmits a scaled version of the received signal to the destination. Thus, a linear relay function is used. Furthermore, to satisfy the average power constraint, the AF relay function can be given

as

$$\mathcal{G}_{AF}(\mathbf{r}) = \alpha \mathbf{r} = \sqrt{\frac{P_r}{\mathcal{E}[\|\mathbf{H}\|^2]P_s + N_r\sigma_1^2}}\mathbf{r}, \tag{2.18}$$

where α is the scaling factor, and $\mathbf{r}$ is derived by (2.16); P_s and P_r are the source and the relay average power levels, respectively. Then, the scaled version of the received signal is sent per (2.18).

Because it it easy to implement, the AF relaying is one of the most attractive cooperative diversity schemes. While the absence of a detection process at the relay facilitates the use of simple relay units, this simple processing enables full spatial diversity at high SNRs [4, 36]. However, the main disadvantage is the performance loss due to the noise amplification at the relay.

LMMSE AF: Pure AF (2.18) can be viewed as a linear estimation scheme with the scaling factor α being normalized to satisfy the relay power constraint. In contrast, LMMSE AF begins with a scaling factor derived from MMSE principles and performs the required power normalization. Thus, an LMMSE estimator may be given as [3, 46]

$$\hat{\mathbf{x}}_{LMMSE} = \left(\mathbf{H}^H\mathbf{H} + N_r\sigma_1^2\mathbf{I}\right)^{-1}\mathbf{H}^H\mathbf{r}. \tag{2.19}$$

However the estimated signal must be scaled by a factor α_{LMMSE} under the relay power constraint. Thus, the relay function for the LMMSE AF relay may be given as

$$\mathcal{G}_{LMMSE}(\mathbf{r}) = \alpha_{LMMSE}\,\hat{\mathbf{x}}_{LMMSE}, \tag{2.20}$$

where $\alpha_{LMMSE} = \sqrt{\frac{P_r}{\mathcal{E}(\|\hat{\mathbf{x}}_{LMMSE}\|^2)}}$.

2.4.2   Decode-and-Forward

This relay method has attracted much attention recently because it outperforms AF in the high-SNR region. It detects data from the incoming signal, remodulates the detected data and forwards them to the destination. This method may use an ML detection of data from the incoming signal. The detected signal vector may be given as

$$\hat{\mathbf{x}} = \arg\min_{\mathbf{x} \in \mathcal{Q}^{M_s}} \|\mathbf{r} - \mathbf{H}\mathbf{x}\|^2. \tag{2.21}$$

where $\arg\min_x f(x)$ denotes the value of x that minimizes $f(x)$.

The SD [22, 47, 48] may be employed to perform (2.21) to reduce the detection running time. Although $\hat{\mathbf{x}}$ can be directly transmitted, the relay power constraints must be satisfied. Thus, the DF relay function may be given as

$$\mathcal{G}_{DF}(\mathbf{r}) = \sqrt{\frac{P_r}{\mathcal{E}(\|\hat{\mathbf{x}}\|^2)}}\hat{\mathbf{x}} = \sqrt{\frac{P_r}{P_s}}\hat{\mathbf{x}}. \tag{2.22}$$

However, when the source-relay link suffers from deep fading, the decoding errors at the relay propagate to the destination.

Besides AF and DF, EF [49] strategies have been proposed for single-antenna cooperative networks. The EF relay generates an unconstrained MMSE estimate of the received signal and then transmits a scaled version of it to the destination. EF MIMO relays will be developed in Chapter 6, the details will be provided there.

2.5 Conclusions

The optimal MIMO detection method is ML detection. Full or near-ML detection is possible with the SD algorithm and its variants. Two main categories (depth-first and breadth-first search) of the SD algorithm were discussed in this chapter. Coded MIMO, iterative detection and decoding schemes, were also discussed. Finally, the relay network model was given, followed by a review of conventional relay strategies.

$\sim$

Chapter 3

SNR-Dependent Radius Control Sphere Detector

This chapter introduces a new MIMO SD algorithm for uncoded systems. The main new idea is to scale the search radius by using a heuristic SNR-dependent factor. The use of this scaling offers near-ML performance over the entire range of SNRs, while keeping the running time roughly constant. This algorithm also incorporates channel ordering to save running time. As a measure of the variability of the running time, its normalized variance is evaluated. This algorithm is also extended for joint iterative detection and decoding in coded MIMO systems and for MIMO-relay networks. Simulation results and theoretical analysis demonstrate the benefits of the proposed algorithm. [1]

3.1   Introduction

As mentioned in Section 2.2.2, while the SD algorithm significantly reduces the running time compared to that of naive ML detection, its running time is quite high in the low-SNR region and decreases significantly as the SNR increases. These drawbacks make the very-large-scale integration (VLSI) implementation of the conventional SD algorithm infeasible. To address these challenges, many variants of SD have been developed [14, 22, 30, 32, 48, 50–58]. For example, [52] uses conditional probabilities to select more reliable candidates, but the running time is still

---
[1]*A version of this chapter has been published in Trans. Emerging Tel. Tech. (2013), doi:10.1002/ett.2620.*

high for near-ML performance and for high-order constellations. Statistical pruning approaches [48, 53, 54] sacrifice performance to obtain running time reduction. K-best [14], also known as the M-algorithm [59] or as beam search in the Artificial Intelligence literature [17], and the fixed-complexity (Fixed) [30, 60] SD have also been proposed. K-best traverses the search space in a breadth-first manner and retains only the several best nodes in each layer. Despite its fixed running time, K-best requires higher running time than that of the naive SD for exact ML performance [14]. Although Fixed SD ensures a fixed running time, regardless of the noise level and channel conditions, it has higher running time than that of SE in the high SNR regime [30]. Many adaptive methods have also been developed including search radius adjustments [61–64], channel-adaptive MIMO detection [65] and an early-pruned K-best algorithm [66].

SD is also required to provide soft information for coded MIMO systems. Soft information is needed for jointly iterative detection and decoding of coded systems [10]. This information is provided by using a list version of SD (LSD). In this scheme, the ECC can be any code that can be decoded by using soft inputs and outputs, such as convolutional codes or turbo codes. Many algorithms are capable of supporting soft outputs in LSD. For example, K-best has been extended for use in an iterative MIMO receiver [14], and a list Fixed SD has been proposed [35] as a list extension of the Fixed SD algorithm [30] for coded MIMO systems.

SD is also required for MIMO-relay networks. As mentioned in Section 1.1.3, the benefits of relays [4] are (1) increased diversity, (2) increased code rates, (3) reduction of transmit power and (4) extension of coverage area. The relay detection problem has thus been considered [67] for DF relaying and AF relaying. Low-complexity detection by applying zero-forcing at the relay terminals [68] fails to achieve ML performance. To achieve near-ML performance, detection at DF relays is computationally intensive; thus, cooperative partial detection (CPD) has been proposed [43]. The relay in this case detects a subset of the transmit symbols, and only these are relayed to the destination. Although the running time is low, this method performs poorly when the number of detected symbols is small [43].

In this chapter, a new SNR-dependent radius control SD is proposed [69], which

is also applied for soft MIMO detection and MIMO-relay detection. The main contributions are as follows:

1. A new SRC-SD is proposed with a low and roughly fixed level of running time over the whole SNR region and near-ML performance. This SD scales the search radius by using a heuristic SNR-dependent factor, which approaches one in the high-SNR region, guaranteeing that SRC-SD's performance converges to that of the conventional SD; however, in the low-SNR region, this factor is less than unity, resulting in more aggressive pruning of nodes and thereby significantly reducing the running time.

2. The SRC-SD is modified to generate soft information for coded MIMO systems. This modified version is called the list SRC-SD (LSRC-SD), which generates a list of candidates and further reduces the running time of iterative detection at a negligible performance loss.

3. To leverage the benefits of the new SRC-SD, its use in MIMO AF and DF relays is developed by deriving the ML detection rules.

4. By considering the average number of visited nodes as a measure of running time, an upper bound to the running time of the proposed SRC-SD is derived. This theoretical result along with the simulation results confirms the running time savings of SRC-SD.

5. A measure η of the variability of the running time for the range of SNR is defined. If η is zero, then the running time is fixed, creating the ideal situation. The η values of the proposed SRC-SD and the conventional SDs are then examined, and the very low variability of the proposed algorithm is established.

This chapter is organized as follows: Section 3.2 briefly outlines the conventional SD and derives the new SRC-SD. Section 3.3 derives coded MIMO detection and the ML rules for MIMO-relay networks. Section 3.4 provides a brief running time analysis. Simulation results for both performance and average number of visited nodes are presented in Section 3.5, followed by the conclusions in Section 3.6. The proof of (3.17) is presented in Appendix A.

3.2 SNR-Dependent Detection

This section proposes the new SRC-SD, discusses its running time and quantifies the variability in running time.

For the original FP SD, the initial radius can be selected based on the noise level [21]. The initial radius for SE is typically set as $d = \infty$ [50]. More results for SDs are presented in [14, 22, 30, 32, 48, 51–58].

3.2.1 SNR-Dependent Scaling Function

As discussed in Section 3.1, although the traditional FP and SE SDs save running time compared to the naive ML detector, their running time is variable and high in the low-SNR region. These two problems are mitigated by the proposed SRC-SD at a negligible performance loss.

The traditional SDs achieve running time savings by pruning nodes, but the pruning is limited to the nodes that can be identified early in the search to be not on the ML path. Because such nodes are few, their pruning results in only modest running time reduction, especially in the low-SNR region. Thus, more nodes need to be pruned in order to achieve more substantial running time savings. To this end, the main idea is to scale the search radius of the hypersphere based on the SNR, which is defined as a scaling function $\phi(\rho)$ based on the SNR ρ. The requirements for the scaling factor are the following:

1. $\phi(\rho)$ has to be a positive value for all the SNRs, $\phi(\rho) \geq 0$.

2. $\phi(\rho)$ should be smaller than 1 in order to obtain more running time savings than the conventional SD provides; that is, $\phi(\rho) \leq 1$.

3. In order to prune more nodes in the low-SNR region and to keep the optimal performance in the high-SNR region, $\phi(\rho)$ should be an increasing function of ρ.

4. When the SNR is high enough, the scaling factor should approach 1; that is, $\lim_{\rho \to \infty} \phi(\rho) = 1$, which guarantees an optimal performance in the high-SNR region.

The many different possible scaling functions include $1/(\exp(-\rho) + 1)$ and $\rho/(\rho + C_0)$. Based on numerical experiments, the specific scaling function (3.1) is proposed, which is a conveniently simple function of the SNR and efficiently achieves an acceptable performance and running time trade-off.

3.2.2 SNR-Dependent Radius Control (SRC) Sphere Detector

This detector uses the scaling function to get the new radius via

$$d^2_{SRC-SD} = \phi(\rho) \times d^2 = \frac{\rho}{\rho + C_0} \times d^2, \tag{3.1}$$

where d_{SRC-SD} is the radius in the new SRC-SD, ρ is the SNR of the MIMO system, d is the radius used in the original FP or the SE, and C_0 is a predefined constant. This scaling function satisfies the conditions mentioned above. Due to the limit

$$\lim_{\rho \to \infty} \frac{\rho}{\rho + C_0} = 1, \tag{3.2}$$

the performance of the proposed algorithm reverts to that of the original SD when the SNR is sufficiently high. Here, SNR is assumed to be known at the receiver and it can be derived by parameter estimation algorithm [70].

When this idea is applied to the original FP, denoted by SRC-FP, its initial radius

$$
\begin{aligned}
d^2_{SRC-FP} &= \frac{\rho}{\rho + C_0} \times d^2 \\
&= \frac{\rho}{\rho + C_0} \times \alpha n \sigma_r^2 \\
&= \frac{\alpha n m}{4(\rho + C_0)},
\end{aligned} \tag{3.3}
$$

where $m = n = 2N$, the noise variance in the real MIMO system $\sigma_r^2 = \frac{\sigma^2}{2}$, and σ^2 is the additive noise variance. The last step for (3.3) is based on the fact that the SNR in a complex MIMO system is given by $\rho = \frac{NE(|s|^2)}{\sigma^2}$, where the average energy of each symbol $E(|s|^2) = 1$ is assumed.

Because SE has lower running time compared to FP, the former is chosen as the building block of SRC-SD (Algorithm 1). Thus, SRC-SD is derived by augmenting the SE SD with the SNR-dependent radius. Once one leaf node found, the searching radius is updated by (3.1).

Algorithm 1: The SRC-SD Algorithm

Input : ρ, C_0, $\mathbf{z}$, $\mathbf{H}$
Output: $\hat{\mathbf{s}}$

---

1 Iteratively order the m columns of the channel matrix $\mathbf{H}$. The steps of the ordering are: **for** $i \leftarrow m$ **to** 1 **do**

2   Calculate $\mathbf{H}_i^\dagger = (\mathbf{H}_i^H \mathbf{H}_i)^{-1} \mathbf{H}_i^H$, where $\mathbf{H}_i$ is the channel matrix with the columns selected in previous iterations zeroed;

3   The signal to be detected ($\hat{s}_p$) is obtained by

$$p = \underset{\mathbf{j} \in \{1,...,m\} - \{\mathbf{p}_{i+1}\}}{\arg\min} \|(\mathbf{H}_i^\dagger)_j\|^2, \qquad (3.4)$$

    where $(\mathbf{H}_i^\dagger)_j$ denotes the j-th row of $\mathbf{H}_i^\dagger$, and $\mathbf{p}_{i+1}$ is the columns selected in previous iterations;

4 **end**

5 Order the channel $\mathbf{H}$ by the index vector $\mathbf{p}$, and get the matrix $\mathbf{R}$ by QR factorization;

6 Initialize the radius $d_{SRC-SD} = \infty$ and take the root s_0 (layer $k = m$) as the start node;

7 **for** *depth* $k \leftarrow m$ **to** 1 **do**

8   Expand the Current Node, generating all its successors $\mathcal{T}$ in the k-th layer satisfying

$$\left(z_k - \sum_{j=k}^{m} r_{k,j} s_j\right)^2 \leq d_{SRC-SD}^2 - \sum_{i=k+1}^{m} \left(z_i - \sum_{j=i}^{m} r_{i,j} s_j\right)^2 ; \text{Prune}$$

    other successors;

9   Sort the components in $\mathcal{T}$ by the increasing order of all the branch weights c_i in this layer, where $c_i = \left(z_i - r_{i,i} s_i - \sum_{j=i+1}^{m} r_{i,j} s_j\right)^2$ and $s_i \in \mathcal{T}$;

10   **for** *every element* s_i **do**

11   **if** s_i *is not a leaf node,* **then** set s_i as the Current Node, $k = k - 1$ and go back to line 3;

12   **else** if s_i is a leaf node ($k = 1$), and if its cost is lower than d_{SRC-SD}^2, keep it as the best solution and update d_{SRC-SD}^2 by (3.1).

13   **end**

14 **end**

In order to further improve the proposed SRC-SD, the ordering of the channel matrix is included in the proposed algorithm. In lines 1-4, the algorithm iteratively reorders the m columns of the channel matrix. The main idea of reordering is that the signals suffering the smallest noise amplification should be selected in every iteration, as discussed in [30, 71].

As Algorithm 1 reveals, the proposed SRC-SD is a variant of the conventional SE [50] and achieves a critical improvement in running time while maintaining near-ML performance (Section 3.5).

3.2.3   Running Time Analysis for SRC-SD

An exact running time analysis of the SRC-SD algorithm appears intractable because of the updating of the radius and the zig-zag search ordering, which is retained from SE [50]. Fortunately, the running time of SE is less than that of the FP because of the radius update during searching process. Thus, the running time of the SRC-FP SD can be evaluated and will be an upper bound on the running time of SRC-SD.

A proxy of the running time of an SD may be taken as the average number of nodes visited. This average depends on the number of antennas, the initial radius and the noise variance [21]. By considering the number of nodes visited at all the layers, the expected running time of SD is evaluated by

$$C(m, \sigma_r^2, d^2) = \sum_{k=1}^{m} \varphi_k, \tag{3.5}$$

where φ_k is the number of nodes visited at the k-th layer within the hypersphere of radius d.

Furthermore, here only the theoretical result for 16-QAM is shown, which is equivalent to two real 4-PAM constellations. Other constellations may be analyzed similarly, but are omitted for the sake of brevity. For consistency with the results of [21], the average energy of the transmitted signals is not set to 1. Therefore, by using [21, Theorem 2] and the SNR-dependent radius d_{SRC-SD}^2 (3.3), the expected

29

number of visited nodes of SRC-FP is given as

$$C_{SRC-FP}(m, \rho, C_0) = \sum_{k=1}^{m} \sum_{q} \frac{1}{2^k} \sum_{l=0}^{k} \binom{k}{l} \times g_{kl}(q)$$
$$\gamma \left(\frac{\alpha n \rho}{2(\rho + C_0)(1 + \frac{12\rho q}{m(L^2-1)})}, \frac{n - m + k}{2} \right),$$

(3.6)

where $g_{kl}(q)$ is the coefficient of x^q in the polynomial $(1 + x + x^4 + x^9)^l(1 + 2x + x^4)^{k-l}$, and $\sigma_r^2 = \frac{m}{\rho} \times \frac{L^2-1}{12}$ (for 4-PAM, $L = 4$).

Variability of C: Since C is a random variable, its variability for different SNRs is of interest. Fixed C for all SNRs is beneficial for hardware implementation. Thus, the variability index η is thus proposed as the ratio between the variance of C and square mean of C:

$$\eta = \frac{E(C - \bar{C})^2}{\bar{C}^2},$$

(3.7)

where C denotes the average number of nodes visited by SD; $\bar{C}$ and $E(C)$ denote the mean and the expectation of C for all the SNRs, respectively.

Therefore, the smaller the index, the less the C varies. For example, from the above theoretical analysis, the FP and SRC-FP ($C_0 = 5$ as an example) SDs achieve $\eta = 1.78$ and $\eta = 0.69$, respectively. The reduced value η suggests that SRC-FP achieves a more constant level of running time than the original FP.

Some remarks on the proposed SRC-SD are as follows:

1. It has lower running time than the basic SD, especially in the low-SNR region, while maintaining a near-ML performance in the high-SNR region. The channel ordering method in line 1-4 of Algorithm 1 is included to further reduce the running time.

2. It effectively reduces the variability index η, which is particularly helpful for hardware implementation.

3. This idea of a SNR-dependent radius can also be applied to other types of tree-search algorithms for MIMO detection, such as many SD variants [52] [54] or different stopping criteria [72].

4. The effects of the constant C_0 in (3.1) have not been discussed in detail. This constant should be adjusted for different systems. For adjusting C_0, the conventional SE can be used as a guide. When the SNR is large enough, say $20\,\mathrm{dB}$, it has a very low running time, and further running time reductions do not appear possible. Thus, a smaller C_0 may be chosen so that SRC-SD performs close to SE in the high SNR regime.

3.3 Detection Strategies

This section introduces the coded MIMO detection and MIMO-relay detection strategies. For both AF and DF relays, the ML rule for combining the received signals from the relays and the source is derived.

3.3.1 Soft MIMO Detection

As discussed in Section 2.3, the most important step in coded MIMO systems is to compute the output information for the MIMO detector and ECC decoder. Thus, the *a posteriori* information for each bit in the transmitted frames can be derived.

In this section, for simplicity, a block of bits $\underline{\mathbf{x}}$ with $N_B = N \log_2(|\mathcal{Q}|)$ is considered, where N_B is the number of bits in one block. The optimal detector obtains the exact APP for each bit. The *a posteriori* LLRs of the bits $\underline{x}_k$ ($k = 1, 2, \ldots, N_B$) conditioned on the received signal vector $\underline{\mathbf{y}}$ [10] is

$$
\begin{aligned}
L_{D1}(\underline{x}_k|\underline{\mathbf{y}}) &= \ln \frac{\Pr[\underline{x}_k = +1|\underline{\mathbf{y}}]}{\Pr[\underline{x}_k = -1|\underline{\mathbf{y}}]} \\
&= L_{A1}(\underline{x}_k) + L_{E1}(\underline{x}_k|\underline{\mathbf{y}}).
\end{aligned}
\tag{3.8}
$$

Here, the Bayes' theorem and the independence of the bits $\underline{x}_k$ due to the interleaver are used to obtain the *a priori* LLRs $L_{A1}(\underline{x}_k)$ and the *extrinsic* LLRs $L_{E1}(\underline{x}_k|\underline{\mathbf{y}})$. From [10], the *extrinsic* information can be denoted by

$$
\begin{aligned}
L_{E1}(\underline{x}_k|\underline{\mathbf{y}}) \approx & \frac{1}{2} \max_{\underline{\mathbf{x}} \in \mathbb{X}_{k,+1}} \left\{ \underline{\mathbf{x}}_{[k]}^T \mathbf{L}_{A1[k]} - \frac{1}{\sigma^2/2} \|\underline{\mathbf{y}} - \mathbf{H}\underline{\mathbf{s}}\|^2 \right\} - \\
& \frac{1}{2} \max_{\underline{\mathbf{x}} \in \mathbb{X}_{k,-1}} \left\{ \underline{\mathbf{x}}_{[k]}^T \mathbf{L}_{A1[k]} - \frac{1}{\sigma^2/2} \|\underline{\mathbf{y}} - \mathbf{H}\underline{\mathbf{s}}\|^2 \right\}.
\end{aligned}
\tag{3.9}
$$

(3.9) is obtained by applying the definition of the extrinsic information [10] and the Max-log approximation [73]. Here, $\mathbb{X}_{k,+1}$ and $\mathbb{X}_{k,-1}$ denote the sets of the bit vectors $\underline{\mathbf{x}} = (\underline{x}_1, \underline{x}_2, \ldots, \underline{x}_{N_B})^T$ having $\underline{x}_k = +1$ and $\underline{x}_k = -1$, respectively. $\mathbf{x}_{[k]}$ represents the subvector of $\underline{\mathbf{x}}$ that omits the k-th bits $\underline{x}_k$; $\mathbf{L}_{A1[k]}$ denotes the subvector of $\mathbf{L}_{A1} = (L_{A1}(\underline{x}_1), L_{A1}(\underline{x}_2), \ldots, L_{A1}(\underline{x}_{N_B}))^T$ by omitting the $L_{A1}(\underline{x}_k)$.

In spite of these simplifications, the computing of $L_{E1}(\underline{x}_k|\mathbf{y})$ (3.9) has an exponential complexity $O(|\mathcal{Q}|^N)$ and is prohibitively complex for systems with a large number of antennas and with high-order modulations. Therefore, a list version of SRC-SD is developed.

LSRC-SD generates a list $\mathcal{L}$ of $N_{\mathcal{L}}$ candidates by searching the tree by using a rule. This list includes the ML estimate, but the size of the list satisfies $1 \leq N_{\mathcal{L}} < 2^{N_c \cdot N}$, where $N_c = \log_2(|\mathcal{Q}|)$ is the number of bits per modulated symbol. Therefore, in order to compute the $L_{E1}(\underline{x}_k|\mathbf{y})$, the search space in (3.9) is limited in the list $\mathcal{L}$, and the extrinsic information can be rewritten as

$$
\begin{aligned}
L_{E1}(\underline{x}_k|\mathbf{y}) \approx & \frac{1}{2} \max_{\mathbf{x} \in \mathcal{L} \cap \mathbb{X}_{k,+1}} \left\{ \mathbf{x}_{[k]}^T \mathbf{L}_{A1[k]} - \frac{1}{\sigma^2/2} \|\underline{\mathbf{y}} - \mathbf{H}\underline{\mathbf{s}}\|^2 \right\} - \\
& \frac{1}{2} \max_{\mathbf{x} \in \mathcal{L} \cap \mathbb{X}_{k,-1}} \left\{ \mathbf{x}_{[k]}^T \mathbf{L}_{A1[k]} - \frac{1}{\sigma^2/2} \|\underline{\mathbf{y}} - \mathbf{H}\underline{\mathbf{s}}\|^2 \right\},
\end{aligned}
\tag{3.10}
$$

where $\mathcal{L} \cap \mathbb{X}_{k,+1}$ and $\mathcal{L} \cap \mathbb{X}_{k,-1}$ represent the subset of vectors $\mathcal{L}$ having $\underline{x}_k = +1$ and $\underline{x}_k = -1$, respectively.

LSRC-SD, a soft extension of SRC-SD, generates a set of candidates that can be exploited to calculate the soft extrinsic information (3.9) for iterative detection and decoding. The running time of generating the candidate list $\mathcal{L}$ can be reduced by adopting several properties of the classical LSD [10]. First, the radius is updated whenever a better candidate than the worst candidate in the current list is found. Second, the candidate list is not generated for every iteration. Once computed, it is stored in the memory and used by every iteration. Therefore, for every iteration, the only information that needs to be updated is the *a priori* information from the channel decoder.

Similar to the *a posteriori* information of the MIMO detector, that of the channel decoder can also be decomposed into the *a priori* information and *extrinsic* information for the iterative detection and decoding. Therefore, the details of the

channel decoder are not shown here.

3.3.2 MIMO-Relay Detection

A basic system model for a multi-branch dual-hop relay network is considered as shown in Fig. 3.1, which portrays the source ($\mathbb{S}$), N_{re} relays ($\mathbb{R}$) and the destination ($\mathbb{D}$), where N_{re} is the number of relays in the network. The number of antennas at the source, the relays and the destination terminal are denoted as N_s, N_r and N_d, respectively. All nodes are half-duplex (data can be transmitted back and forth between two nodes, but not simultaneously) and use orthogonal channels, and a direct link also exists from the source to the destination. Relay protocols operate in two time slots. In the first time slot, the source broadcasts a message to all the relays and the destination. In the second time slot, the relays transmit the received and/or processed signals to the destination.
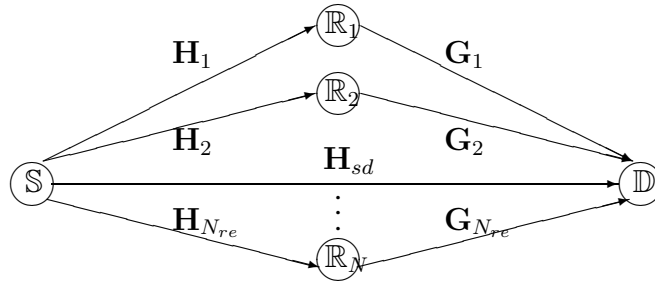
Figure 3.1: System model for multi-branch dual-hop MIMO relay network.

The channels between the source and the i-th relay, the i-th relay and the destination, the source and the destination are denoted by $\mathbf{H}_i \in \mathcal{C}^{N_r \times N_s}$, $\mathbf{G}_i \in \mathcal{C}^{N_d \times N_r}$ ($i \in \{1, 2, \ldots N_{re}\}$) and $\mathbf{H}_{sd} \in \mathcal{C}^{N_d \times N_s}$, where $\mathcal{C}$ is the set of complex numbers. For the first time slot, the received signal vector at the i-th relay ($i = 1, 2, \ldots, N_{re}$) and the destination are given by

$$\mathbf{r}_i = \mathbf{H}_i \mathbf{x} + \mathbf{n}_{1i}, \tag{3.11}$$

$$\mathbf{y}_{sd} = \mathbf{H}_{sd} \mathbf{x} + \mathbf{n}_{sd}, \tag{3.12}$$

where $\mathbf{x}$ and $\mathbf{n}_{1i}, \mathbf{n}_{sd} \sim \mathcal{CN}(0, 1)$ are the transmitted signal at the source, the AWGN at the i-th relay ($i = 1, 2, \ldots, N_{re}$) and the destination, respectively.

As before, the channel matrix entries are assumed to be independent elements. To be exact, the entries are $\mathcal{CN}(0, \frac{\text{SNR}_{sr}^{(i)}}{N_s})$, $\mathcal{CN}(0, \frac{\text{SNR}_{rd}^{(i)}}{N_r})$, $\mathcal{CN}(0, \frac{\text{SNR}_{sd}}{N_s})$ for $\mathbf{H}_i$, $\mathbf{G}_i$ and $\mathbf{H}_{sd}$, respectively. The SNRs are defined to be consistent with [43] to be $\frac{\mu P}{(d_{sr}^{(i)})^\alpha}$, $\frac{(1-\mu)P}{(d_{rd}^{(i)})^\alpha}$, $\frac{\mu P}{(d_{sd})^\alpha}$, respectively, where $\mu \in (0, 1]$ denotes the proportion factor of the transmit power between the source and the relays; the equivalent power and distance to the source at all the relays are assumed; $d_{sr}^{(i)}$, $d_{rd}^{(i)}$ and d_{sd} denote the distance between the source and the i-th relay, the i-th relay and the destination, the source and the destination, respectively; P is the total power for the source and the relays, and $\alpha \in [2, 6]$ is the path loss exponent.

Detect-and-Forward Relaying: Perfect channel state information (CSI) is assumed available at all the nodes, and it can be derived from transmitted pilot symbols [56]. Similar to the system model demonstrated in [43], the errors resulting from the detection at the relays have not been considered, in order to compare the proposed method with the method in [43].

The relays process and forward the received signal (3.11) from the source to the destination. Thus, at the end of the second time slot, the received signal vector at the destination from the i-th relay ($i = 1, 2, \ldots, N_{re}$) is given as

$$\mathbf{y}_i = \mathbf{G}_i \mathbf{x}_r^{(i)} + \mathbf{n}_{2i}, \tag{3.13}$$

where $\mathbf{x}_r^{(i)}$ is the signal detected at the i-th relay by using SD, and $\mathbf{n}_{2i} \sim \mathcal{CN}(0, 1)$ is an AWGN sample.

The detection problem at each relay is equivalent to the standard MIMO detection problem (2.9). For the first step at the i-th relay ($i = 1, 2, \ldots, N_{re}$), the ML detection rule is thus given by

$$\mathbf{x}_r^{(i)} = \arg\min_{\mathbf{x} \in \mathcal{Q}^{N_s}} ||\mathbf{r}_i - \mathbf{H}_i \mathbf{x}||^2, \tag{3.14}$$

where $\mathcal{Q}^{N_s}$ is the set of constellation symbols in the N_s dimensional constellation $\mathcal{Q}$. The running time is significantly reduced by using SD. Using the QR factorization of $\mathbf{H}_i$ ($\mathbf{H}_i = \mathbf{Q}_i \mathbf{R}_i$) and $\mathbf{z}_i = \mathbf{Q}_i^H \mathbf{r}_i$, (3.14) is equivalent to

$$\mathbf{x}_r^{(i)} = \arg\min_{\mathbf{x} \in \Phi} ||\mathbf{z}_i - \mathbf{R}_i \mathbf{x}||^2. \tag{3.15}$$

Φ should be the set of all points within the hypersphere with radius d, which satisfies $||\mathbf{z}_i - \mathbf{R}_i\mathbf{x}_i||^2 \leq d^2$.

In the second step, the relays transmit to the destination. Hence, the destination receives a total of $N_{re} + 1$ signals, including the direct source signal. All these signals are combined via the ML rule as

$$\hat{\mathbf{x}}_d = \underset{\mathbf{x}\in\mathcal{Q}^{N_s}}{\arg\min} \left(\sum_{i=1}^{N_{re}} ||\mathbf{y}_i - \mathbf{G}_i\mathbf{x}||^2 + ||\mathbf{y}_d - \mathbf{H}_{sd}\mathbf{x}||^2 \right). \tag{3.16}$$

By expanding each of the norms and regrouping some terms, the equivalent channel matrix $\mathbf{H}'$ and the equivalent received signal $\mathbf{y}'$ are derived as (see Appendix A)

$$\mathbf{H}' = \left(\sum_{i=1}^{N_{re}} \mathbf{G}_i^H\mathbf{G}_i + \mathbf{H}_{sd}^H\mathbf{H}_{sd} \right)^{1/2}, \tag{3.17a}$$

$$\mathbf{y}' = (\mathbf{H}')^{-1} \left(\sum_{i=1}^{N_{re}} \mathbf{G}_i^H\mathbf{y}_i + \mathbf{H}_{sd}^H\mathbf{y}_{sd} \right). \tag{3.17b}$$

The ML rule is then derived by (3.14).

The difference is that SD at the destination is performed by the newly combined matrix of the channel matrix and received signal vector from (3.17a) and (3.17b).

Amplify-and-Forward Relaying: The relays only amplify the received signals (3.11) from the source during the first time slot and retransmit to the destination during the second time slot. The i-th relay ($i = 1, 2, \ldots, N_{re}$) amplifies $\mathbf{y}_{sr}^{(i)}$ by a fixed gain parameter α_i [36], which is chosen to satisfy the power constraint. Therefore, the received signal at the destination from the i-th relay, $i = 1, 2, \ldots, N_{re}$, is

$$\begin{aligned} \mathbf{y}_i &= \mathbf{G}_i(\alpha_i\mathbf{r}_i) + \mathbf{n}_{2i} \\ &= \alpha_i\mathbf{G}_i\mathbf{H}_i\mathbf{x} + \mathbf{n}', \end{aligned} \tag{3.18}$$

where the noise term $\mathbf{n}' = \alpha_i\mathbf{G}_i\mathbf{n}_{1i} + \mathbf{n}_{2i}$.

The relays simply retransmit a scaled version of the received signal. Similar to the DF relaying case (Appendix A), the equivalent channel matrix and received

signal at the destination in AF relaying are given by

$$\mathbf{H}' = \left(\sum_{i=1}^{N_{re}} (\alpha_i \mathbf{G}_i \mathbf{H}_i)^H (\alpha_i \mathbf{G}_i \mathbf{H}_i) + \mathbf{H}_{sd}^H \mathbf{H}_{sd} \right)^{\frac{1}{2}}$$

$$\mathbf{y}' = (\mathbf{H}')^{-1} \left(\sum_{i=1}^{N_{re}} (\alpha_i \mathbf{G}_i \mathbf{H}_i)^H \mathbf{y}_i + \mathbf{H}_{sd}^H \mathbf{y}_{sd} \right).$$

To sum up, SD is appropriate for the receiver in both DF relaying and AF relaying networks to reduce the running time with near-ML performance.

Therefore, SRC-SD works for both DF and AF systems. Thus, the running time at both the relays and the destination can be reduced. Previously, the Fixed SD algorithm [30] was applied to obtain the fixed running time in the MIMO-relay networks. In the results section, both the Fixed SD and SRC-SD algorithms will be compared.

3.4 Running Time Analysis

The average running time for coded MIMO and MIMO-relay detection is analysed here.

Coded MIMO System: For the proposed LSRC-SD, the running time of generating the candidate list is evaluated to allow for a comparison of the proposed LSRC-SD and the original LSD [10].

MIMO-Relay Networks: SD can perform the signal detection needed in both DF and AF relays networks. For AF relays, because relay signal detection is not required, the running time is the same as that of a point-to-point MIMO link (3.5). However, the DF relays require signal detection at both the relays and the destination, so the average number of nodes visited by SD algorithms is given by

$$C_{all} = \sum_{i=1}^{N_{re}} C_i + C_d, \tag{3.20}$$

where C_i is the number of visited node evaluated at the i-th relay ($i = 1, 2, \ldots, N_{re}$), C_d is the number of visited nodes of detection at the destination, and C_i and C_d are given by (3.5).

36

3.5   Results and Discussions

MIMO Detection: This section evaluates the performance and running time of the proposed SRC-SD (Algorithm 1). An uncoded 4×4 MIMO 16-QAM system is considered over a flat Rayleigh fading channel. In order to verify the advantages of SRC-SD, both the performance as measured by the error rate (e.g., the symbol error rate (SER)) and the running time as measured by the average number of nodes visited by the new SRC-SD are compared with those of the FP, SRC-FP, K-best [14] and Fixed [30] SDs. The first two require the choice of an initial radius, and the method of [21] is used to set the probability of the lattice point inside the sphere at $1 - \varepsilon = 0.9999$. The K-best algorithm with $K = 4$ [14], and the Fixed SD with $p = 1$ (p is the number of layers with full enumeration and $p \geq \sqrt{N} - 1$) [30], for achieving the same diversity as that of ML detection are compared here. C_0 is chosen to be 10 for the proposed SRC-SD where necessary.
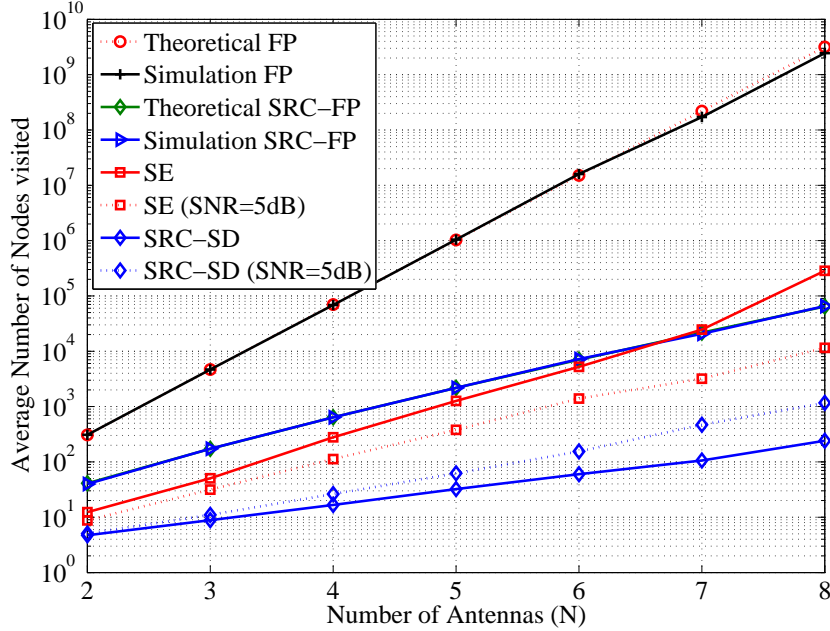
Figure 3.2: Running time (16-QAM) as a function of the number of antennas, where $\mathrm{SNR} = 0\,\mathrm{dB}$ except where stated otherwise.

Running time comparison: Because of its importance for implementation, running time is compared for the FP, SRC-FP, SE and SRC-SD algorithms for different

numbers of antennas (Fig. 3.2). The two main observations that can be made about this figure are as follows:

1. The simulation and theoretical results of both FP and SRC-FP agree, confirming the theoretical analysis of (3.6). Clearly, SRC-FP achieves lower running time than the original FP. Furthermore, the running time gap between these two algorithms increases with the number of antennas. For example, when the number of antennas increases from 3 to 5, the running time gap increases by a factor of 200. This result shows that augmenting the traditional FP SD with the SNR-dependent scaling (3.1) achieves substantial running time gains.

2. The running time of the proposed SRC-SD is also shown here. It achieves the lowest running time for all the antenna numbers. For example, for an 8×8 MIMO system at an SNR of $0\,\mathrm{dB}$, the SRC-SD, SE and FP SDs search on average about 2.4×10^2, 10^5 and 10^9, respectively. Thus, over six orders of magnitude of running time savings are achieved, confirming the high efficiency in the low-SNR region of SRC-SD and affirming its suitability for large MIMO systems. Furthermore, the running time savings depend on the operating SNR and they diminish for high SNRs.

How running time varies as a function of the SNR is an important consideration (Fig. 3.3). In Fig. 3.3, the SRC-SD with/without channel ordering are compared with the FP, SE, K-best and Fixed SDs. The SRC-SD with channel ordering obtains a running time saving compared to that obtained without channel ordering[2]. Fig. 3.3 reveals that the proposed SRC-SD has the following advantages:

1. SRC-SD significantly reduces the running time compared to the conventional SE and FP SDs. For example, for an SNR of $20\,\mathrm{dB}$, SRC-SD saves about an order of magnitude running time compared to FP, and this saving increases to 4 orders of magnitude at $0\,\mathrm{dB}$. In contrast to SE, which visits 3×10^2 nodes, SRC-SD visits only 16 nodes at $0\,\mathrm{dB}$. This advantage may, however, vanish if the SNR increases, as per (3.2).

---

[2]In the following figures, SRC-SD denotes the algorithm with channel ordering.
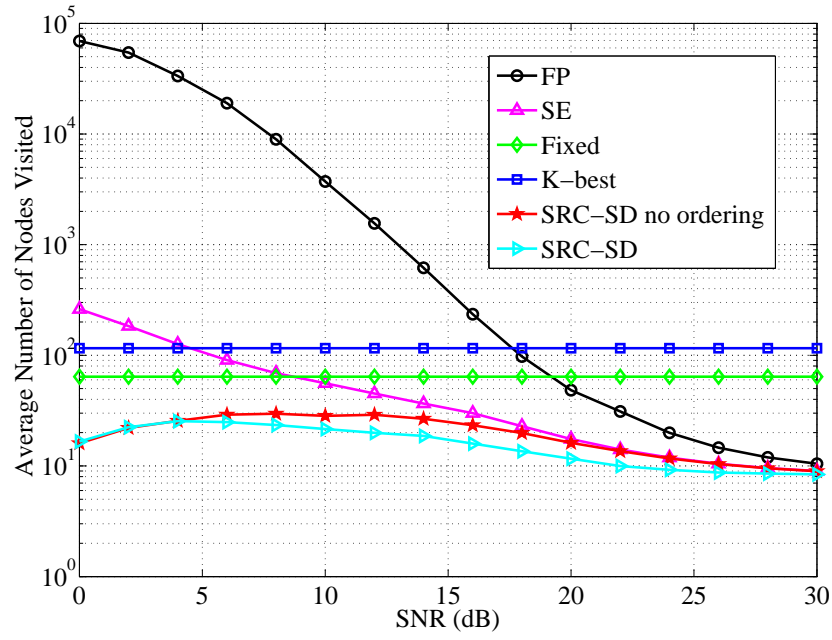
Figure 3.3: Running time of different SDs for a 4×4 16-QAM MIMO system.
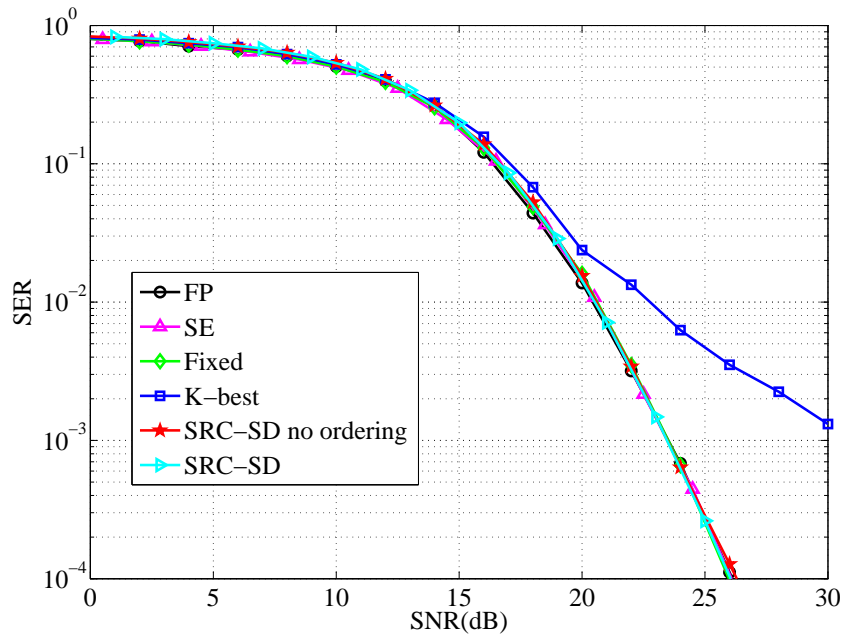
Figure 3.4: Error performance for a 4×4 16-QAM MIMO system.

2. More importantly, SRC-SD also has even lower running time than the K-best [14] and Fixed [30] SDs.

3. Notice how flat the running time curve of SRC-SD is; the variability index η of 0.14 for SRC-SD verifies the roughly fixed running time according to (3.7). SRC-SD thus achieves a roughly fixed and reduced running time.

Because of the trade-off between running time and performance, the performance of SRC-SD is examined next.

SER performance: Pruning the nodes by using SNR-dependent scaling of the hypersphere radius in the proposed SRC-SD results in a suboptimal detection performance. The impact of this suboptimality is quantified in Fig. 3.4. Note that the SER curves of SRC-SD (with/without ordering), FP and SE are almost identical. The FP, Fixed and SE SDs are full ML detectors. Clearly, SRC-SD achieves a near-ML performance, and also outperforms K-best, especially in the high-SNR region. For instance at an SER of 10^{-3}, SRC-SD gains $7\,\mathrm{dB}$ over K-best. Consequently, based on performance and running time, the new SRC-SD outperforms the Fixed and K-best SDs.

Detection for Coded MIMO system: The advantages of SRC-SD in a coded 4×4 MIMO system are assessed next. The bit error rate (BER) performance and the running time are investigated. The naive LSD is compared with LSRC-SD for several values of the parameter C_0. The systematic recursive convolutional code with rate $R = 1/2$ is exploited to encode the transmitted bits sequence $\mathbf{b}$ with a frame length $M_b = 8192$, where the feed-forward and feedback-generating polynomials are $G_1(D) = 1 + D^2$ and $G_2(D) = 1 + D + D^2$ with memory length 2 [10]. A random interleaver is exploited here. The SNR is used as the horizontal axis as defined by E_s/N_0.

In order to choose the best C_0, the performance and running time comparison of LSRC-SD for different values of C_0 is shown. An increased C_0 leads to more node pruning in the searching process, which achieves lower running time. However, the BER performance is degraded by such pruning. Thus, a proper value for C_0 may be found to attain a suitable trade-off between performance and running time. From

Table 3.1, by using 4 iterations, the performance gets closer to that of the naive LSD when C_0 decreases. To maintain the performance, a smaller value should be chosen for C_0.

Table 3.1: Bit error rate comparison for different C_0 for a 4×4 16-QAM coded MIMO system with $M_b = 8192$ transmitted bits and a maximum of 4 iterations.

SNR	LSD	LSRC-SD $(C_0 = 1)$	LSRC-SD $(C_0 = 2)$	LSRC-SD $(C_0 = 3)$	LSRC-SD $(C_0 = 5)$	LSRC-SD $(C_0 = 10)$
8 dB	0.1201	0.1180	0.1398	0.1317	0.1356	0.1659
8.5 dB	0.0639	0.0635	0.0632	0.0708	0.0799	0.1005
9 dB	0.0147	0.0146	0.0194	0.0279	0.0284	0.043
9.5 dB	0.0044	0.0045	0.006	0.0079	0.0093	0.0176
10 dB	0.0019	0.0020	0.0029	0.0037	0.0048	0.0081

Table 3.2: Comparison of the average number of visited nodes for different C_0 for a 4×4 16-QAM coded MIMO system with $M_b = 8192$ transmitted bits.

SNR	LSD	LSRC-SD $(C_0 = 1)$	LSRC-SD $(C_0 = 2)$	LSRC-SD $(C_0 = 3)$	LSRC-SD $(C_0 = 5)$	LSRC-SD $(C_0 = 10)$
8 dB	4280.2	2561.6	2111.8	1860.5	1571.9	1199.9
8.5 dB	4243.4	2624.9	2192.4	1914.4	1633.4	1257.5
9 dB	4241.3	2675.8	2240.8	1982.0	1688.6	1314.1
9.5 dB	4196.4	2736.7	2302.7	2043.9	1737.8	1381.6
10 dB	4190.7	2767.1	2374.7	2121.6	1804.6	1435.7

The running time for LSRC-SD with different C_0 is given in Table 3.2. As C_0 increases, the running time decreases more. For example, the average number of nodes visited is about 1.7×10^3 for $C_0 = 5$, around 2×10^3 with $C_0 = 3$, and approximately 2.2×10^3 with $C_0 = 2$. Therefore, to maintain the performance and reduce the running time, $C_0 = 2$ should be chosen in this case. Similarly, an appropriate C_0 for other MIMO configurations can be found after several trials.

Detection for MIMO-Relay Networks: To confirm the benefits of SRC-SD for MIMO-relay networks, its performance and running time are evaluated for both DF and AF relays. The number of relays is one or two. The proposed SRC-SD is compared with Fixed SD, the original SE, and CPD [43]. In what follows, it is assumed that $d_{sd} = d_{sr}^{(i)} + d_{rd}^{(i)}$ with $\frac{d_{sr}^{(i)}}{d_{sd}} = 0.2$, $i \in \{1, 2, \ldots N_{re}\}$, the path loss

exponent $\alpha = 3$, and $\mu = 0.5$.

Figure 3.5: Error performance for a 4×4 16-QAM MIMO-relay network.
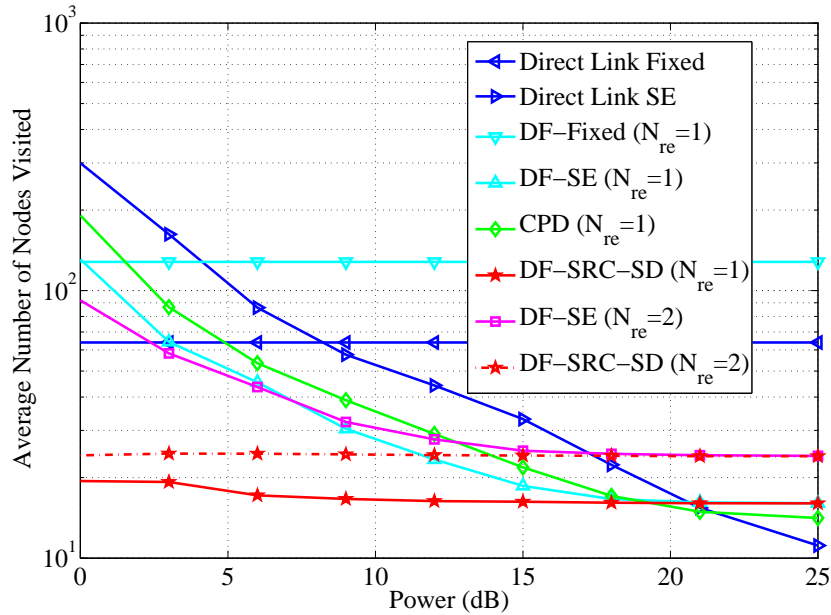
Figure 3.6: Running time for a 4×4 16-QAM MIMO-relay network.

Fig. 3.5 shows the SER performance of Fixed, SRC-SD and SE SDs. Direct source-to-destination transmissions also occur. The horizontal axis is the transmit

42

power. $p = 1$ and $C_0 = 10$ are set for Fixed SD [30] and the new SRC-SD, respectively. For CPD, the expansion factor is chosen to be 3 [43]. Note that for both the one-relay case and the two-relay case with DF, the SRC-SD, SE and Fixed SDs perform identically. This finding confirms the near-ML performance of SRC-SD. In contrast, CPD incurs performance penalties. For example, for the one-relay case, at an SER of 10^{-3}, CPD loses $5\,\mathrm{dB}$ relative to SRC-SD. Clearly, since the SER performance improves when the number of relays increases, the benefit of using relays to increase the reliability is clear.

The running time comparison for the same set-up shown in Fig. 3.5 is depicted in Fig. 3.6. For the single-relay case, SRC-SD reduces the running time compared to the CPD, Fixed and SE SDs, and approaches the running time of SE when the power increases (to higher than $15\,\mathrm{dB}$). For example, at an SNR of $0\,\mathrm{dB}$, SRC-SD visits only 190 nodes, while the CPD, Fixed SD and SE algorithms visit 190, 128 and 130 nodes, respectively. SRC-SD also achieves lower running time than that of the direct link with SE and Fixed SD for the lower power region, while SRC-SD has slightly higher running time than that of the direct transmission when the power is larger than $21\,\mathrm{dB}$. This result is caused by the path loss due to the long distance. For the two-relay network, SRC-SD reduces the running time compared to that of SE. In order to check the variability of the running time here, notice that for both one-relay and two-relay networks, SRC-SD obtains a roughly flat running time curve as a function of the SNR. For these two cases, it can be shown by using (3.7) that the variability indexes of SRC-SD are 6.5×10^{-5} and 5.7×10^{-3}, respectively. The results demonstrate the effectiveness of SRC-SD for multi-branch MIMO-relay networks, with the advantage of roughly fixed, low running time.

Both the DF and AF cases are considered in Figs. 3.7 and 3.8. Fig. 3.7 compares the performances of the SRC-SD, SE and Fixed algorithms in one-relay AF and DF systems. In AF relaying, both the SRC-SD and Fixed SDs perform close to that of SE, which provides the optimal detection. In DF relaying, SE achieves a performance gain of $1.5\,\mathrm{dB}$ higher than that in AF.

Fig. 3.8 shows a running time comparison for the same set-up. The AF SRC-SD system has lower running time than the SE and Fixed SDs, just as in DF relaying
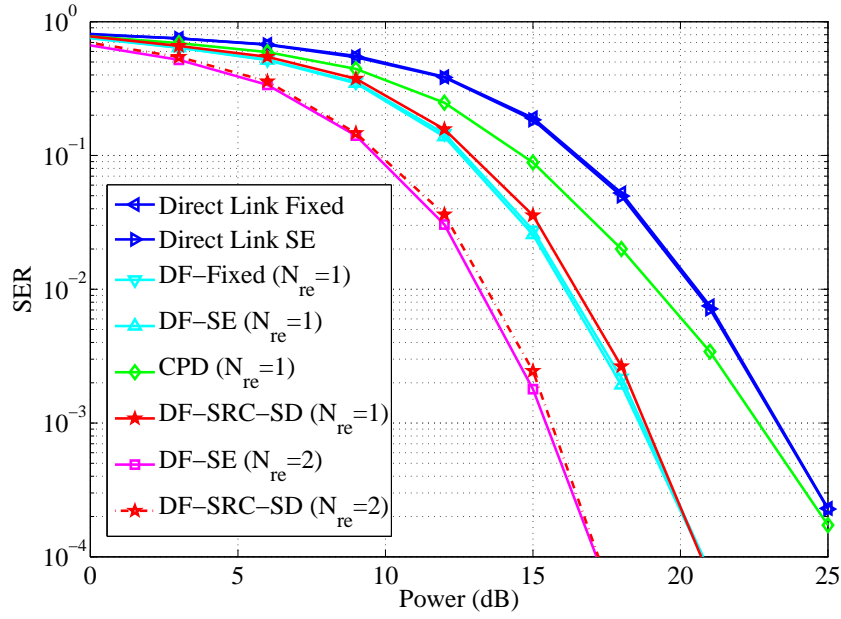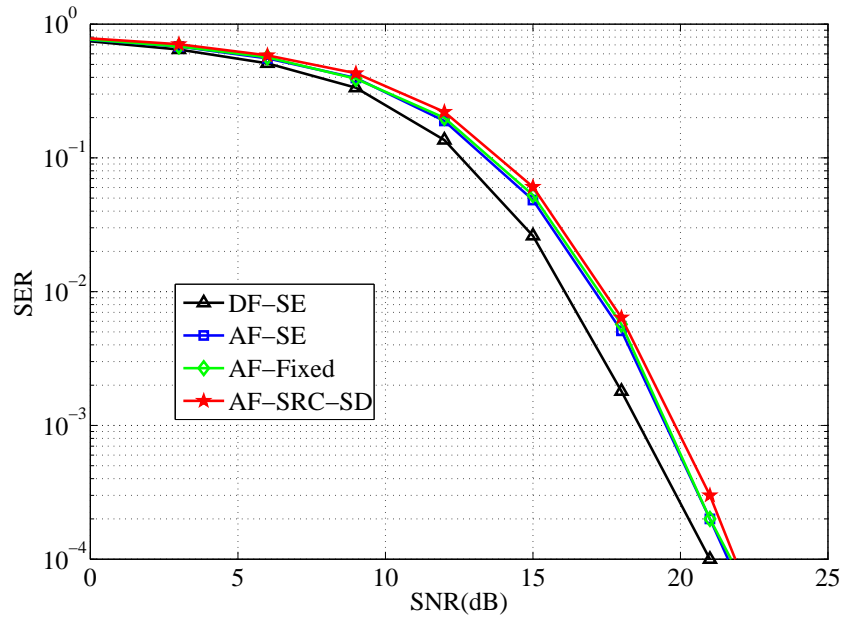
Figure 3.7: Error performance for a 4×4 16-QAM MIMO-relay network.
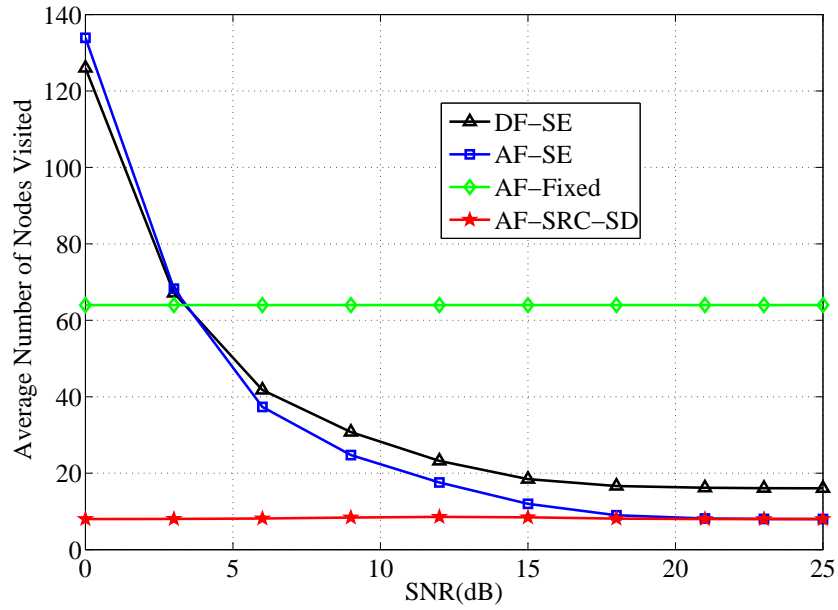
Figure 3.8: Running time for a 4×4 16-QAM MIMO-relay network.

case (Fig. 3.6). Especially in the low-power region, SRC-SD significantly reduces the running time. For example at $0\,\mathrm{dB}$, it is only 6% of that of SE. Thus, systems that operate in the low-SNR region may particularly benefit from the use of SRC-SD. As expected, however, both the SRC-SD and SE algorithms have the same level of running time in the high-SNR region ($> 20\,\mathrm{dB}$). It is interesting to compare the DF SE and AF SRC-SD systems. The running time saving varies from 93.6% to 52%. The variability index η is found to be 1.9×10^{-4} for SRC-SD, which demonstrates roughly fixed running time. These results again confirm that SRC-SD reduces the running time and its variability.

3.6 Conclusions

This chapter proposed an SNR-dependent radius control SD with reduced running time, reduced variability of running time, and near-ML performance. By tightening the search radius by a heuristic SNR-dependent factor, this SD outperforms the existing K-best and Fixed SDs in terms of SER but also saves running time. For coded MIMO systems, a soft extension called LSRC-SD was proposed. It further improves the running time of detection and decoding at a negligible performance loss. Signal detection for AF and DF MIMO-relay networks was also investigated by deriving the ML detection rules. The simulation results confirmed the benefits of the proposed SRC-SD, which provided a near-ML performance and roughly constant running time.

$\sim$

Chapter 4

Statistical Pruning-Based Detector

In this chapter, node-pruning strategies based on probability distributions are developed. Uniform pruning, geometric pruning, threshold pruning, hybrid pruning and depth-dependent pruning are developed in detail. The desirable diversity order of uniform pruning and the threshold level for threshold pruning are derived. Simulation results comparing the proposed rules with popular SD algorithms such as K-best SD, fixed complexity SD and probabilistic tree-pruning sphere detector (PTP-SD) are provided.[1]

4.1 Introduction

As discussed in Section 2.2.2, the conventional SD prunes only the nodes whose partial costs exceed the cost of the current best solution. Since this process does not discard the optimal solution, the pruned nodes are called non-essential nodes. That is, a node i is non-essential if its accumulated cost, say, c_i exceeds the cost of the current best solution denoted by c_*. Such pruning of these nodes not only eliminates large areas of the search tree, thereby reducing running time, but also preserves the optimality of the SD. On the other hand, if $c_i < c_*$, the i-th node is an essential node, whose pruning can potentially discard the ML solution. However, pruning of essential nodes creates algorithms that are not optimal but have lower running time, leading to a class of detectors with different running time and performance trade-offs.

---

[1] *A version of this chapter has been published in IEEE Trans. Veh. Technol., 62: 1586-1596 (2013).*

Thus, unless otherwise stated, the term **pruning** throughout this chapter refers to the pruning of **essential** nodes.

Several SD variants with such pruning have been developed [14, 30, 32, 53, 54, 74–82]. In [74], an increasing radii algorithm (IRA) chooses a gradually increased radius from the top layer to the bottom layer. Thus, excessive pruning may be needed to restart the IRA several times, resulting in additional running time. In addition, the IRA cannot attain different diversity orders[2] and achieve a flexible performance and running time trade-off. To extend the IRA, [53] proposes a PTP-SD, which prunes more nodes by adding a probabilistic noise constraint on top of the sphere constraint. Then, [54] extends the PTP-SD and provides further improvement of the running time with minimal extra cost and a negligible performance penalty. Additional pruning methods are proposed in [75, 76]. References [77, 79] combine the PTP-SD and a Fixed SD [30] to preserve the advantages of branch pruning by using an adaptively updated PTP-SD threshold. To prune more nodes, a new probabilistic sorting rule is developed by exploiting the properties of the path metric to yield more effective sorting [80]. The K-best SD [14], which prunes all but the K best nodes in each layer, traverses the search space in a breadth-first manner.

Many SD algorithms have been proposed [14,30,32,53,54,74–77,79–82] to implement different node-pruning strategies, with different performance and running time trade-offs. A general framework for such pruning is desirable. For this purpose, a statistical pruning sphere detector (SPSD) is proposed and developed [83]. The main contributions in this chapter are summarized as follows.

- The key idea is that each essential node, say node i, is assigned a probability $f(i)$ that indicates the likelihood of being pruned. For example, $f(i) = 0$ means i-th node is retained, and $f(i) = 1$ means i-th node is eliminated. For other cases, given the probability distribution $f(i)$, this algorithm randomly generates a pruning decision for node i based on $f(i)$. $f(i)$ could be chosen based on experimental results or common statistical distributions. For example, $f(i)$ may be set small for the nodes in the top layers of the search tree, so

---

[2]If the error probability decays proportionally to SNR^{-d}, then d is called the diversity order

that more such nodes are retained, and the ML solution is more likely to be found. Also $f(i)$ may be varied to achieve different performance and running time trade-offs. Performance and running time are measured by SER and the number of nodes visited. The SER in the high-SNR region is, however, closely related to the diversity order. Thus, a flexible trade-off between the diversity order and running time reduction is achievable. Many existing SDs (such as those in [14, 27, 74]) can be cast as special cases of the proposed approach.

- Based on several classical probability distributions, the following node pruning rules are proposed: (1) uniform pruning: all the child nodes of a node except the first one are pruned independently with equal probability; (2) geometric pruning: the child nodes are pruned dependently where the pruning probability agrees with the geometric distribution; (3) threshold pruning: the child nodes are pruned if their cost exceeds a threshold; (4) hybrid pruning: this combines the threshold rule with the uniform or geometric rule; and (5) depth-dependent pruning: the pruning probability depends on the search depth. Three cases of this rule are investigated in this chapter.

- The performance of the proposed SPSD is also analysed in this chapter. The upper bounds for the frame error rate (FER) of the uniform and threshold pruning rules are derived. These two pruning rules are shown to achieve a desired diversity order by specifically setting the pruning probability for the former and the threshold for the latter according to different SNR. Furthermore, the pruning probability of the uniform rule is analysed when a full diversity order is needed. It is also shown that the FER upper bound in the full diversity case could be affected by the predesignated SNR loss and that the achievable diversity orders or SNR gains could be controlled by the choice of pruning probability and the threshold. For example, for uniform pruning, to reduce running time, a large pruning probability should be chosen based on the achievable diversity order, and vice versa. This principle also applies to the threshold rule. With a smaller desired diversity order, the threshold could

be chosen to be a smaller value resulting in lower running time.

- The performance and running time of all the proposed rules and those of the existing SDs such as PTP-SD [53], Fixed SD [30] and K-best SD [14] as a function of the number of transmit antennas and receive antennas are compared by using simulations. The simulations show the advantages of the proposed approach for large MIMO systems at high SNRs. It is noteworthy that the proposed threshold rule obtains significant running time savings than those achieved by other SD algorithms.

This chapter is organized as follows: The SPSD is developed in Section 4.2. Five pruning rules are proposed in Section 4.3. Performance and running time analysis of the proposed SPSD is given in Section 4.4. The simulation results are presented in Section 4.5, followed by the conclusions in Section 4.6. The proof of the FER of the uniform pruning and threshold pruning rules is presented in Appendix B.

4.2   Statistical Pruning

Before describing specific pruning rules, a generic detector is described. For a search tree with n layers, this detector is given in Algorithm 2[3], where k ($k = n, n-1, \ldots 1$) denotes the current layer in the search tree, $\mathbf{g}$ is a vector which includes the pruning probabilities that are designed to use the pruning rules for the nodes in the k-th layer, and d_k^2 is the current partial upper bound obtained by the radius minus the current accumulated partial cost. The algorithm is invoked as SPSD-decode$(n, \mathbf{g}, d_n^2, \mathbf{z}, \mathbf{R})$, where d_n is the initial radius, and $\mathbf{z}$ is the received signal. The initial radius d_n can be selected based on the noise level [21] for the original FP SD, while it also can be typically set as $d_n^2 = +\infty$ for the conventional SE SD [27].

Note that Algorithm 2 is built on the top of the SE SD [29] along with additional pruning of essential nodes based on heuristic rules. The full pruning rule $\mathbf{g}$ may be dependent on the search layer. This property allows further flexibility to implement,

---

[3]A complete MATLAB-like SD algorithm description can be found in [26].

Algorithm 2: Statistical Pruning Sphere Detection
SPSD-decode (k, $\mathbf{g}$, d_k^2, $\mathbf{z}$, $\mathbf{R}$)

Input : k, $\mathbf{g}$, d_k^2, $\mathbf{z}$, $\mathbf{R}$
Output: $\mathbf{s}_{min}$

---

1 Generate all the l_0 successors $\mathcal{A}$ in the k-th layer satisfying
$(z_k - r_{k,k}a_i)^2 \leq d_k^2$ by eliminating non-essential nodes;
2 Let $[\sim, temp] = sort(\mathbf{c})$, where $\mathbf{c} = [c_1, c_2, \ldots, c_i, \ldots, c_{l_0}]$ and
$c_i = (z_k - r_{k,k}a_i)^2$; and then $A = A(temp)$;
3 **for** $i \leftarrow 1$ **to** $|\mathcal{A}|$ **do**
4 $\quad$ $p = rand(1)$;
5 $\quad$ **if** $p \leq g(i)$ **then**
6 $\quad\quad$ discard the i-th node;
7 $\quad$ **else**
8 $\quad\quad$ keep the i-th node in $\mathcal{A}$;
9 $\quad$ **end**
10 **end**
11 $l = length(\mathcal{A})$;
12 **for** $i \leftarrow 1$ **to** l *(every element in $\mathcal{A}$)* **do**
13 $\quad$ $\tilde{s}_k = a_i$;
14 $\quad$ **if** a_i *is not a leaf node* **then**
15 $\quad\quad$ Let $z_{k-1} = z_{k-1} - \sum_{j=k}^{n} r_{k-1,j}\tilde{s}_j$;
16 $\quad\quad$ **SPSD-decode** ($k - 1$, $\mathbf{g}$, $d_k^2 - c_i$, $\mathbf{z}$, $\mathbf{R}$);
17 $\quad$ **else**
18 $\quad\quad$ **if** a_i *is a leaf node ($k = 1$) and its cost is smaller than the current
best cost* **then**
19 $\quad\quad\quad$ The best solution $\mathbf{s}_{min} = \tilde{\mathbf{s}}$;
20 $\quad\quad\quad$ Update $d_n^2 = \|\mathbf{z} - \mathbf{R}\tilde{\mathbf{s}}\|^2$ and all d_i^2, $i = n - 1, \ldots, 1$;
21 $\quad\quad$ **end**
22 $\quad$ **end**
23 **end**

---

say, more aggressive/conservative pruning strategies at different search layers. Re-call that the pruning of non-essential nodes (i.e. $c_i > c_*$) preserves the optimality of the algorithm. The pruning of essential nodes by the probabilistic rules, however, is the main concern of this chapter. Specifically, consider the $|\mathcal{Q}|$ nodes that are the children of a node. Their pruning probabilities may be given as

$$g(i) = \left\{ \begin{array}{cc} 1 & if \quad c_i > c_* \\ f(i) & i = 1, \ldots t \end{array} \right. , \tag{4.1}$$

where $i \in \{1, 2, \ldots |\mathcal{Q}|\}$, c_* and c_i are the current best cost and the partial cost of the current node, respectively. t is the number of nodes whose partial cost is below c_*.

Note that pruning probability always refers to the second item $f(i)$ in (4.1), which defines the probability of pruning for the nodes with $c_i \leq c_*$ (the essential nodes). This simple but critical difference from the SD makes the SPSD terminate sooner than the latter, hopefully with the ML solution. The set $\mathcal{A}$ is sorted in line 2 of Algorithm 2 because smaller cost nodes are more likely to give high-quality solutions. Experimentally, it is known that pruning at different layers of the search tree will affect the performance and running time trade-off differently. Thus, in Algorithm 2, the heuristic rules may vary for different layers. Thus, the pruning rule can be strong in the first few layers since the bound d_k^2 itself is not tight enough to identify nonessential nodes, and can be weak in the last few layers when the bound d_k^2 is tight.

A search algorithm is **complete** if it is guaranteed to return at least one valid solution. That is, at least the Babai-point [26] or decision-feedback equalization point [3] is guaranteed. To ensure this condition, in Algorithm 2 at least one child node is always kept. Thus, the pruning probability assigned to the child node with minimum cost is always zero.

To clarify these ideas, consider a simple example where a node has four essential child nodes. Assume the child nodes are sorted by increasing cost and then assigned the pruning probabilities $[0, 0.2, 0.5, 0.8]$. That is, the first child node is never pruned, and others have more chance of being pruned because they are less likely to lead to the ML solution. Similarly, with different probability distributions,

existing SDs can be cast as special cases of the proposed framework. Some examples are as follows:

1. The SE SD [27]: this case arises when the pruning probability $f(i)$ for all the child nodes is 0. That is, SE SD does not use statistical pruning.

2. The IRA [74]: the nodes with the costs smaller than the radius are retained; that is, their pruning probabilities are 0, while the pruning probabilities are 1 for the other nodes, which are pruned. This case is an example of the uniform pruning rule.

3. The K-best SD [14]: at each layer of the search tree, the pruning probability of the best K nodes is 0, while the pruning probability of all the remaining $(K + 1, K + 2, \ldots)$ nodes is one.

In the next section, several specific pruning rules are proposed.

4.3 Pruning Rules

Five specific heuristic pruning rules are developed in this subsection: uniform, geometric, threshold, hybrid and depth-dependent pruning rules.

4.3.1 Pruning Probability Distribution Basics

To keep the statistical framework simple, the pruning probability of the k-th layer is initially defined to be $f(i, k)$, $i = 1, \ldots t$ and $k = 1, 2, \ldots n$. The value of $f(i, k)$ can be chosen to execute a strong or weak pruning regime and is not dependent on the layer number in the first several depth-independent rules, denoted by $f(i)$. However, $f(i, k)$ can also be chosen to vary with the layer. In the following, only the nodes that do not exceed the current best cost c_* are considered. The set of such nodes is $\mathcal{A}$ and its size is t (see (4.1)).

The probability that node a_i will be pruned is $f(i)$, and $f(i)$ is a non-decreasing function in i with $f(1) = 0$ and $0 \leq f(i) \leq 1$. As mentioned in Section 4.2, the boundary condition $f(1) = 0$ ensures the completeness of the SPSD. $f(i)$ is chosen as a non-decreasing function in i because, intuitively, a child with a smaller cost

is more likely to lead to the optimal solution. Based on the different probability distributions, several pruning rules are proposed next.

4.3.2 Pruning Rules

In the following, several specific pruning rules are given. Note that, the search tree is expanded from layer n (top) to layer 1 (bottom).

Uniform Pruning Rule: $f(i) = 1 - p$, for $2 \leq i \leq t$, and $f(i) = 0$, for $i = 1$.

All child nodes except the first one are pruned with equal probability and independently. This rule is rational when a priori information is not available as to which child will lead to the optimal solution and which ones should be pruned.

Geometric Pruning Rule: $f(i) = 1 - p^{i-1}$.

Because all the child nodes are ordered by increasing cost, this rule assigns geometrically pruning probabilities to the nodes $(i = 1, 2, \ldots, t)$.

Since $f(i), i \geq 2$, in the geometric pruning rule is greater than that in the uniform pruning rule, the former rule eliminates more nodes than the latter. In both pruning rules, the strength of pruning is controlled through p.

These two pruning rules are derivatives of two well-known classical probability distributions. However, the pruning probability distribution considering the cost c_i of node a_i may be designed. For example, a child node whose cost is significantly larger than its parent may not lead to an optimal solution. This idea leads to the following threshold pruning rule.

Threshold Pruning Rule: In the conventional SD, the current node is pruned if its cost exceeds the current best cost. A variation of this idea is proposed here. In order to further prune nodes, a threshold δ_k is applied at the k-th layer. As mentioned before, a_1 is never pruned ($f(1) = 0$) for the completeness of the SPSD. For $i = 2, \ldots, t$, if the cost c_i of a child node a_i is larger than δ_k, a_i is pruned; that is, $f(i) = 1$ when $c_i > \delta_k$.

Here, threshold δ_k is associated with the k-th layer. Since $\mathcal{A}$ is in a nondecreasing order of cost, if node a_i is pruned, all the children a_j for $j \geq i$ are pruned. The strength of pruning varies inversely with δ_k. For example, if $\delta_k = +\infty$, it simply reduces to the SD.

Hybrid Pruning Rule: The threshold rule can also be combined with the uniform or geometric rules to possibly take advantage of both the cost information and probabilistic pruning. Thus, the hybrid pruning rule could be constructed as $f(i) = 1 - p^{\sqrt{\frac{c_i}{c_1}}-1}$ or $f(i) = \min\{\frac{c_i-c_1}{c_1}(1-p), 1\}$, where c_1 is the minimum cost in the k-th layer. For these two examples, if the cost c_i of the child node a_i is less than or equal to c_1 (threshold rule), a_i is not pruned. Otherwise, the nodes are pruned by $f(i)$ (uniform or geometric rule).

Depth-dependent Pruning Rule: In the search process, if the pruning probability $f(i)$ at the early search layers is too high, the probability of discarding the ML solution increases. In order to keep the ML solution until the bottom search layer, $f(i)$ may be defined depending on different tree layers (depth-dependent pruning rule) denoted by $f(i, k)$, $k = 1, 2, \ldots n$. In the following, three cases are given.

Case I: $f(i, k) = 1 - \exp(-k)$, $2 \leq i \leq t$.

The children at each layer are pruned by the probability $f(i, k)$, a non-increasing function in k. For large k, the pruning probability decreases. This result helps to avoid discarding the ML solution. Once the node at the k-th layer is pruned, all the children of this node are pruned.

Case II: $f(i, k) = \frac{n-k}{2(n-1)}$, $1 \leq k \leq n$ where $2 \leq i \leq t$. The pruning probability increases linearly with the layer. For the first layer, the pruning probability is zero, and for the bottom layer, it is $1/2$.

Case III: $f(i, k) = \begin{cases} 0 & n_1 + 1 \leq k \leq n \\ p_0 & 1 \leq k \leq n_1 \end{cases}$, where $1 \leq n_1 \leq n$ and $2 \leq i \leq t$. The nodes at the early search layers ($n_1 \leq k \leq n$) are all kept and expanded, and the remaining nodes are pruned by probability p_0 ($1 \leq k \leq n_1 - 1$). That is, full enumeration at the beginning of the search process is used to improve the probability of finding the ML solution. However, in the latter search layers, nodes are pruned with probability p_0 to reduce the running time. Note that if $n_1 = 0$, this rule is the conventional SD; if $n_1 = n$, uniform pruning becomes one special case with $1 - p_k = p_0$.

In these three cases, the first node at each layer is never pruned ($f(1, k) = 0$) for the detection completeness. Because the pruning probability in Case II is larger than in Case I for each layer, the former is stronger than the latter. Only these

three cases are given in this chapter, and the many other cases for depth-dependent pruning rules are not discussed here.

Remarks:

- The idea of probability-distribution-based node pruning can be used with other tree search algorithms, e.g., best-first search, breadth-first search and iterative deepening [17].

- More importantly, the same idea can also be applied to the complex-valued SDs, such as in [30], in order to achieve a flexible performance and running time trade-off.

- The IRA in [74] is a special case of Algorithm 2. The IRA chooses a smaller radius for the lower layers of the search tree (see details in [74]). However, if the IRA cannot find a point, the radius is increased and the search resumes. The threshold pruning rule obtains at lease one point as the solution, and the threshold for each layer is different with the IRA.

- Threshold pruning rule can be readily incorporated into the SD algorithm by replacing $d_k^2 = d_{k+1}^2 - |p_{k+1}(x_{k+1}, \ldots, x_n)|^2$ in Chapter 2 with $d_k^2 = \min\{d_{k+1}^2 - |p_{k+1}(x_{k+1}, \ldots, x_n)|^2, \delta_k\}$. If d_k^2 returns a null set, $a_1 = \lceil \rho_k / r_{k,k} \rceil$ is kept in $\mathcal{A}$. In fact, δ_k can be considered as a local bound as opposed to the global bound d^2 in SD.

- The K-best SD is a special case of the depth-dependent pruning rule (Case III). When $n_1 = 0$, $p_0 = 0$ for $2 \leq i \leq K$, and $p_0 = 1$ for $K + 1 \leq i \leq t$, the K-best SD is obtained.

4.4   Performance Analysis

Here, the performance of the uniform and threshold rules is analysed. The parameters p and δ_k are determined to achieve different diversity orders and performance gains. To make the analysis tractable, detection ordering is ignored. The radius is assumed infinite, and the effect of decreasing radius as in Algorithm 2 is ignored.

The results in this section can be considered as upper bounds for those cases with column reordering.

Proposition I: The upper bound on the FER of uniform pruning is

$$P_f \leq (1-p) \sum_{i=1}^{n} \frac{|\mathcal{Q}|}{\left(1 + \frac{d_{\min}^2}{4\sigma^2}\right)^i} + \left(\frac{|\mathcal{Q}|}{1 + \frac{d_{\min}^2}{4\sigma^2}}\right)^n, \tag{4.2}$$

where $d_{\min}$ is the minimum Euclidean distance of $\mathcal{Q}$, and σ^2 is the variance of the noise. Proof: see Appendix B.1.

In the high-SNR region, the symbol error rate P_s can be approximated by P_f, $P_s \approx P_f/n$, where a frame error is caused by a single symbol error with high probability.

From (4.2), if p is fixed for all SNRs, and $p \neq 1$ (uniform pruning), the first term dominates P_f. As (4.2) is only an upper bound, this equation suggests that the diversity order of uniform pruning is at least one. The simulation results indicate that the diversity order of the uniform rule is indeed at least one. Since geometric pruning is more aggressive than uniform pruning, the diversity order in geometric pruning is also at least one for fixed p. (4.2) also indicates that, to achieve a diversity order n with uniform pruning, $1-p$ must at least decrease as fast as $\frac{1}{\left(1+d_{\min}^2/4\sigma^2\right)^{n-1}}$. Therefore, p must vary according to the SNR or σ^2. Thus,

$$p = 1 - \xi \left(\frac{1}{1 + d_{\min}^2/4\sigma^2}\right)^{K_0-1}, \tag{4.3}$$

where ξ is a constant. By substituting (4.3) into (4.2), (4.2) can be derived as

$$P_f \leq \xi \sum_{i=1}^{n} \frac{|\mathcal{Q}|}{\left(1 + \frac{d_{\min}^2}{4\sigma^2}\right)^{K_0+i-1}} + \left(\frac{|\mathcal{Q}|}{1 + \frac{d_{\min}^2}{4\sigma^2}}\right)^n \tag{4.4}$$

If $K_0 < n$, the first term dominates P_f in the high-SNR region, and the other terms can be neglected. Therefore, uniform pruning achieves at least the diversity order K_0. (4.4) reveals that ξ controls the SNR gain of statistical pruning.

In order to achieve the full diversity order n, one can choose

$$p = 1 - \beta P_{ML} \left(\frac{|\mathcal{Q}|}{1 + d_{\min}^2/4\sigma^2}\right)^{-1}, \tag{4.5}$$

where P_{ML} is the FER of the ML detector. By substituting (4.5) into (4.2), (4.2) can be derived as

$$P_f \leq \beta P_{ML} \sum_{i=1}^{n} \frac{1}{\left(1 + \frac{d_{min}^2}{4\sigma^2}\right)^{i-1}} + \left(\frac{|\mathcal{Q}|}{1 + \frac{d_{min}^2}{4\sigma^2}}\right)^n, \tag{4.6}$$

where β controls the SNR loss incurred by the statistical pruning compared with the ML detector.

From [84], when SNR becomes high, the asymptotic form of P_{ML} can be expressed as

$$P_{ML} = \alpha(n, \mathcal{Q}) \left(\frac{1}{2\gamma}\right)^n \binom{2n-1}{n-1}, \tag{4.7}$$

where γ denotes SNR. $\alpha(n, \mathcal{Q})$ is a coefficient that depends on n and the constellation. Let $\{\mathbf{d}_j\}$ denote the set of vectors with $s_k \in Q$ as their l-th element, and $\{\mathbf{d}_i\}$ denote the set of vectors that differ in their l-th element from $\mathbf{d}_j$. The α is given by [84]

$$\alpha = \frac{1}{|Q|^n} \sum_{s_k \in Q} \sum_i \sum_j \left(\frac{\|\mathbf{d}_i - \mathbf{d}_j\|^2}{2E_s}\right)^{-n}, \tag{4.8}$$

where E_s is the average symbol energy of Q. Since (4.7) scales as γ^n, from (4.6), statistical pruning by using (4.5) can still achieve a diversity order n. Note that the performance analysis in this subsection considers only a fixed pruning probability for all s_k, $k = 1, \ldots, n$. A different pruning probability for different s_k may also be assigned.

Proposition II: The FER of threshold rule is bounded as

$$P_f \leq \sum_{i=1}^{n} \int_{\frac{\delta_i}{\sigma^2}}^{+\infty} f_i(x) dx + \left(\frac{|\mathcal{Q}|}{1 + \frac{d_{min}^2}{4\sigma^2}}\right)^n, \tag{4.9}$$

where $f_i(x)$ denotes the probability density function of the chi-square distribution $\chi^2(2(n - i + 1))$ [23]. Proof: see Appendix B.2

In order to achieve a diversity order of at least K_0, δ_i may be chosen such that

$$\int_{\frac{\delta_i}{\sigma^2}}^{+\infty} f_i(x) dx = \frac{\xi}{(1 + d_{min}^2/4\sigma^2)^{K_0}}, \tag{4.10}$$

where ξ is a constant that controls the SNR gain. Since $f_i(x)$ is known, (4.10) can be solved numerically. At each SNR, (4.10) needs to be solved only once. $\delta_i = 0$

for $i \leq n - K_0 + 1$ is simply set. In this case, the upper bound on P_f is also given by (4.9).

With the same δ, it can be easily verified that

$$\int_{\frac{\delta}{\sigma^2}}^{+\infty} f_i(x)dx < \int_{\frac{\delta}{\sigma^2}}^{+\infty} f_j(x)dx \tag{4.11}$$

for $i > j$. Therefore, with the same δ, the first term in (4.9) always dominates P_f. A simplified rule to achieve a diversity order of at least K_0 can be obtained by setting δ as the solution of

$$1 - \gamma\left(1, \frac{\delta}{2\sigma^2}\right) = \frac{\xi}{(1 + d_{\min}^2/4\sigma^2)^{K_0}}. \tag{4.12}$$

Similarly, $\delta_i = \delta$ for $i > n - K_0 + 1$ and $\delta_i = 0$ for $i \leq n - K_0 + 1$ are simply set. By using (4.9), it can be readily verified that this choice of δ_i achieves a diversity order of K_0. Interestingly, the cost threshold δ depends only on SNR and K_0, but not on i.

Remarks:

- The upper bound in (4.2) may not be tight. The p given in (4.3) and (4.5) may achieve a better performance than that suggested by (4.2). This result also holds for δ_i in (4.10) and (4.12).

- The simulation results (Section 4.5) show that the performance difference between the uniform and geometric rules is small when using the same p defined in (4.3) and (4.5). For the same p, uniform pruning has only an SNR gain over geometric pruning even though the latter is stronger than the former, as remarked in Section 4.3. The value of p given by (4.3) and (4.5) along with geometric pruning achieves the same diversity order. However, the diversity order analysis for this case seems intractable.

4.5   Simulation Results

In this section, the SPSD is simulated for an uncoded MIMO system over a flat Rayleigh fading channel. The modulation formats 4-QAM and 16-QAM are used. Both the performance and running time of any SD are compared. The running time

is measured by the average number of nodes visited. The running time of the pre-processing stage is not included. The ML curve, which is the optimal performance, is obtained with the conventional SE SD. The initial radius of the SPSD is chosen to be infinity and is updated whenever the search reaches a leaf node (Algorithm 2). In hybrid pruning, $f(i) = 1 - p^{\sqrt{\frac{c_i}{c_1}} - 1}$, where c_1 is the minimum cost in the k-th layer. For the depth-dependent rule, only the result of Case I is given.

Comparison of Different Pruning Rules: Here, 4-QAM with 8 transmit and
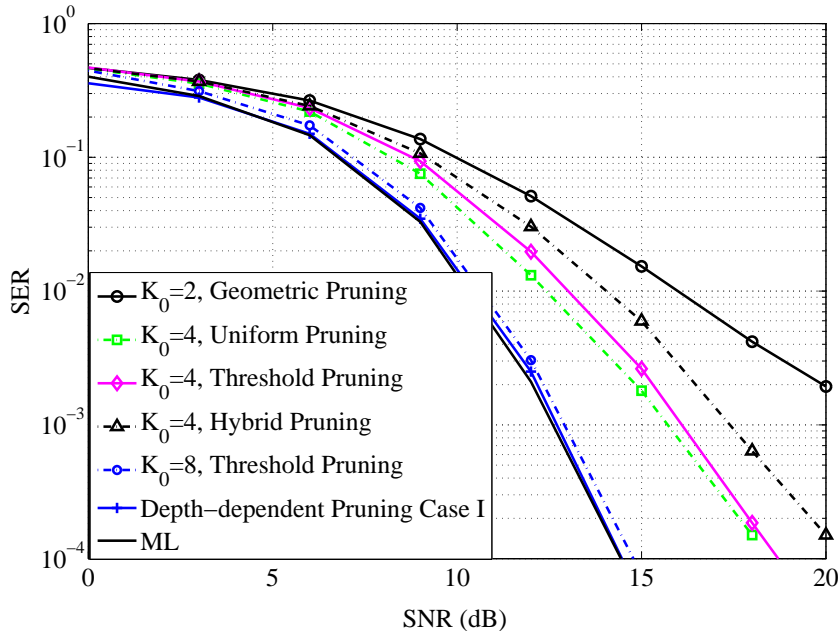
Figure 4.1: Error performance for an 8×8 4-QAM MIMO system. The ML curve is given by the simulation of SE SD.

8 receive antennas are used in Figs. 4.1 and 4.2, where ξ is set to be 0.8 (ξ is the constant in (4.3)); the achievable diversity order K_0 is set to be 2 and 4 for uniform pruning, geometric pruning and hybrid pruning; ξ is chosen to be 1; and K_0 is chosen to be 4 or 8 for threshold pruning.

Fig. 4.1 shows the SER performance of the SPSD with different statistical pruning rules. As shown, the depth-dependent pruning Case I achieves a near-ML performance, indicating that the pruning probabilities for this rule are small for all the layers. For other rules, the derivation of achievable diversity order K_0 in (4.3) and (4.12) is validated here. At the desirable diversity order K_0 of 2, geometric

pruning achieves a diversity order 2. Likewise, with the achievable diversity order 4, the uniform, threshold and hybrid pruning could achieve diversity order 4. All these rules achieve the desirable diversity order corresponding to the value of K_0, proving that the results for the uniform and threshold rules are also applicable for the geometric and hybrid rules. Another interesting observation is that by setting a greater desirable diversity order K_0, the threshold rule performs closer to optimal ML detection. For example, at an SER of 10^{-3}, the threshold rule with a diversity order K_0 of 8 attains $3\,\mathrm{dB}$ more gain than the case with diversity order 4.
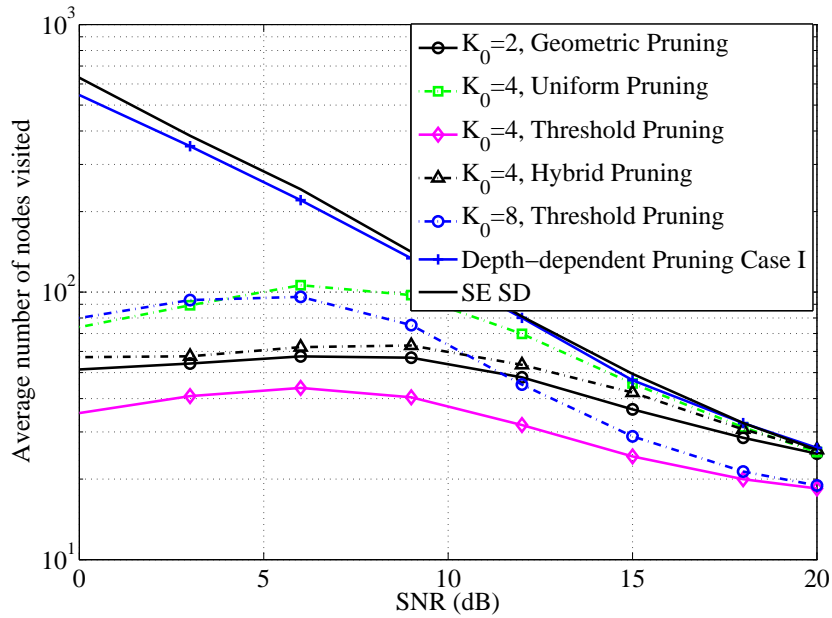
Figure 4.2: Running time for an 8×8 4-QAM MIMO system.

Fig. 4.2 compares the running time of different pruning rules with that of the optimal SE SD, which has the highest running time compared to all the proposed rules. The only exception is the depth-dependent pruning rule, which has almost the same running time as the SE SD, but does achieve the near-ML performance (Fig. 4.1). An immediate observation is that the achievable diversity order K_0 has a significant effect on running time. With a smaller desired diversity order K_0, the running time is lower. This finding shows that lower running time can be achieved by sacrificing the desirable diversity order or SER performance. All the rules, excluding the depth-dependent rule, obtain more running time savings in the

low-SNR region; however their running time savings over SE SD reduces when SNR increases. For example, at an SNR of $0\,\mathrm{dB}$, the threshold pruning (diversity order 8) obtains about 86% of the running time savings with respect to SE SD. This number reduces to 50% at $10\,\mathrm{dB}$. Furthermore, the threshold pruning obtains running time savings for very high SNRs, such as $20\,\mathrm{dB}$,S because the SE SD visits several unnecessary nodes during the early stages of the search process. However, for threshold pruning, the local bound prevents visits to these nodes, especially when the cost threshold δ_i is chosen to be 0 for $i \leq n - K_0 + 1$. Therefore, only a single node is visited at layers $1, \ldots, n - K_0 + 1$.
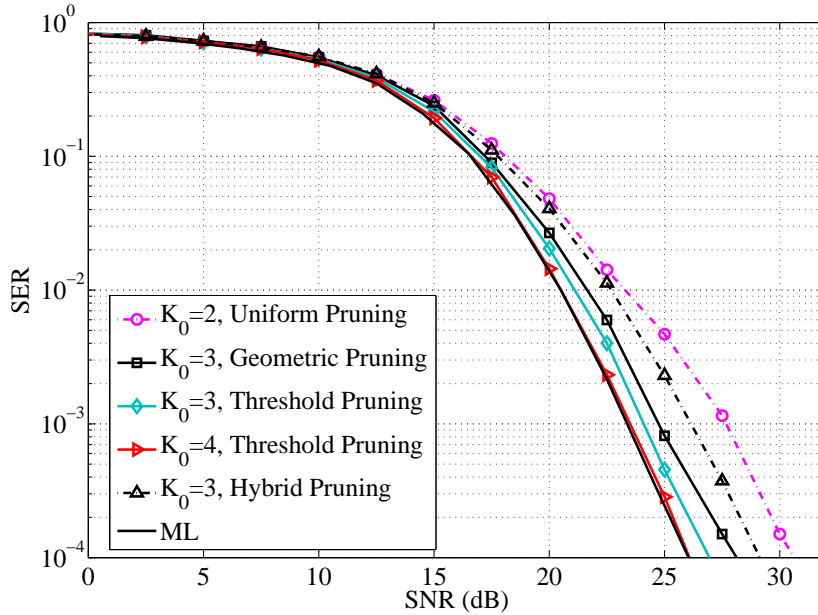
Figure 4.3: Error performance for a 4×4 16-QAM MIMO system. The ML curve is obtained by the SE SD.

The performance of the SPSD for different MIMO systems, a 16-QAM and 4×4 MIMO system, is next assessed in Figs. 4.3 and 4.4, where the parameter setting is the same as that for the 8×8 4-QAM MIMO system, except that $K_0 = 2, 3, 4$. The SER of the SPSD for different statistical pruning rules is given in Fig. 4.3. As stated in the discussion of Fig. 4.1, by varying the achievable diversity order K_0, different diversity orders are achieved. For example, the threshold rule achieves the full diversity order when the desirable diversity order is set to 4.
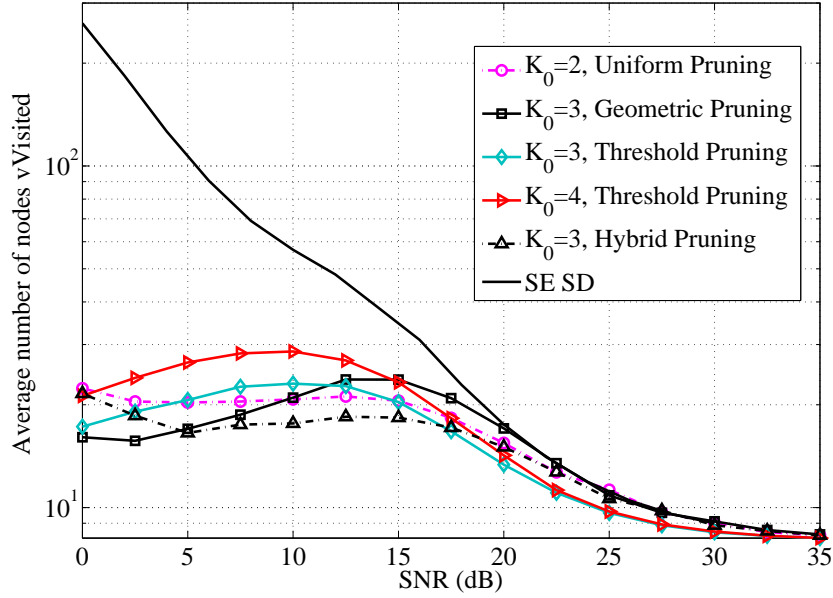
Figure 4.4: Running time for a 4×4 16-QAM MIMO system.

Fig. 4.4 shows the average number of nodes visited with different pruning rules. Trends similar to those shown in Fig. 4.2 are observed. All the rules save running time compared to the SE SD for low SNRs, but the running time saving reduces with increasing SNR. However, in the high-SNR region, threshold pruning attains lower running time than the SE SD.

Figs. 4.1-4.4 show that for achieving the full diversity order, threshold pruning obtains the lowest running time compared to the other rules. Threshold pruning is therefore the best choice for near optimal performance with significant running time savings.

Comparison with other Detectors: It is interesting to compare the proposed SPSD with other detectors that use node pruning. Thus, PTP-SD [53], Fixed SD and the K-best SD [14] are considered. For the PTP-SD, p' is set to be 0.1, where p' is the pruning probability; for the Fixed SD, the case without channel ordering is used in this chapter, and the distribution of nodes kept in each layer is $[1, 1, 1, 16]$, while K is chosen to be 4 and 16 for the K-best SD (mode 1 in [14] without channel ordering is used for fair comparison). Figs. 4.5 and 4.6 compare different detectors for a 4×4 16QAM MIMO system. Only the geometric and threshold rules are

shown because uniform pruning performs close to geometric pruning, and threshold pruning performs better than hybrid pruning.
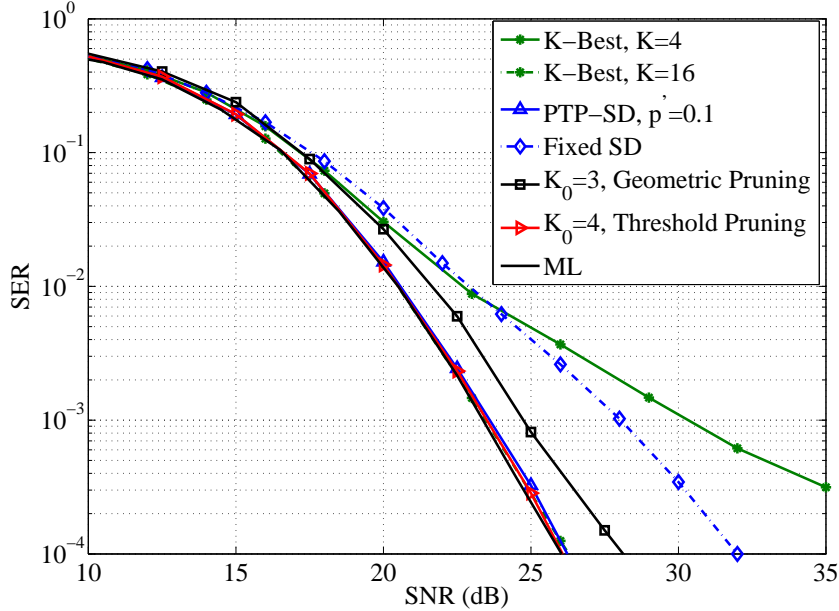
Figure 4.5: Error performance for a 4×4 16-QAM MIMO system. The ML curve is obtained by the SE SD.

Fig. 4.5 shows the SER performance comparison. The proposed threshold rule with desirable full diversity order 4, the PTP-SD, and the K-best SD ($K = 16$) achieve a near-ML performance. However, although the Fixed SD has a fixed running time because of the full enumeration in the first layers and pruning all but the first node with the minimum cost in the following layers, at an SER of 10^{-4}, the Fixed SD has 6 dB performance loss compared to the threshold rule. To be fair, this gap is due to not using channel matrix reordering. Like the Fixed SD, the K-best SD also obtains fixed running time; however, the K-best SD requires a large K to achieve a full diversity order [14]. Thus, the case ($K = 4$) achieves only a diversity order of one.

Fig. 4.6 shows the running time, i.e., the average number of nodes visited by different detectors. As mentioned before, the choice of a smaller desired diversity order K_0 leads to lower running time. For example, the geometric rule ($K_0 = 3$) has lower running time than that of the threshold rule ($K_0 = 4$). Moreover, the
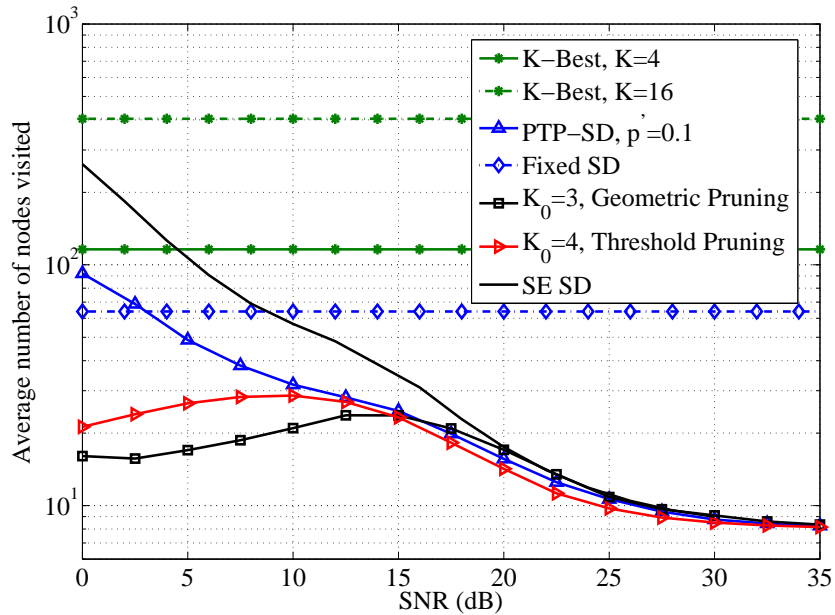
Figure 4.6: Running time for a 4×4 16-QAM MIMO system.

threshold rule has lower running time than the PTP-SD in the low-SNR region; for example, at an SNR of $0\,\text{dB}$, the former obtains 78% of the running time savings of the latter because the threshold rule prunes more nodes than the PTP-SD. Another observation is that both the geometric and threshold rules have significantly lower running time than the K-best SD, which performs a breadth-first search and always prunes all but the K best nodes at each layer. Even so, the running time of the threshold rule is only 4.5% of the K-best SD ($K = 16$) on average, while obtaining 72% more running time savings than the Fixed SD as well. To summarize, with near optimal SER performance, threshold pruning achieves the lowest running time compared to PTP-SD, Fixed SD and K-best SD.

To show the advantages of the proposed approach for a large MIMO system at high SNRs, a performance and running time comparison as a function of the number of transmit antennas and receive antennas (16-QAM) is shown in Figs. 4.7 and 4.8, where N is the number of transmit or receive antennas. The SNR is fixed at $20\,\text{dB}$.

Fig. 4.7 shows that the proposed threshold rule with full diversity order N and the PTP-SD always achieves a near-ML performance for different numbers of
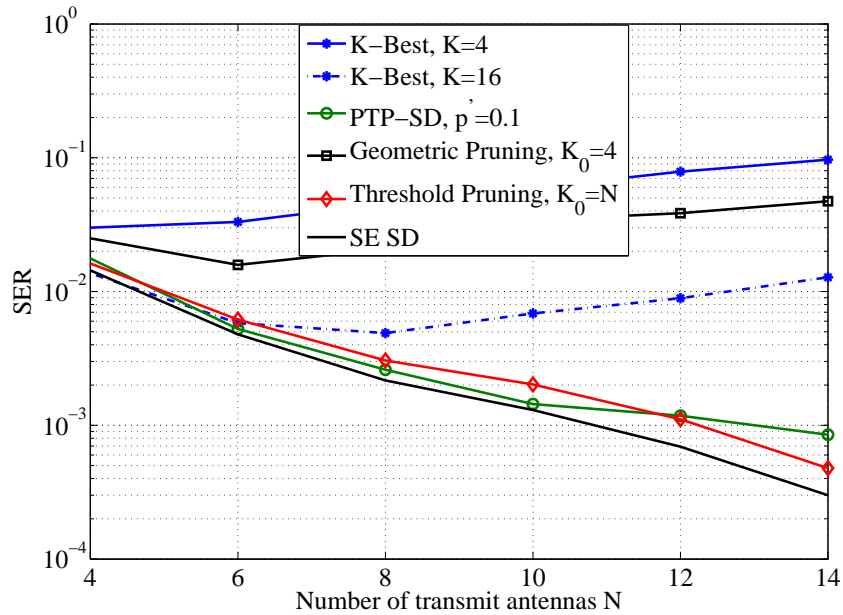
Figure 4.7: Error performance for a 16-QAM MIMO system with different numbers of transmit and receive antennas N, SNR=20 dB.

transmit antennas. However, the geometric rule with the fixed achievable diversity order 4 does not reach the optimal performance for large MIMO systems. For the same reason, the K-best SD with $K = 4$ and $K = 16$ also does not achieve a near-ML performance. This finding means that with an increasing number of antennas N, the achievable diversity order K_0 for the geometric rule and the K for the K-best SD should be larger.

The running time comparison with the same set-up as in Fig. 4.7 is given in Fig. 4.8. The running time of the PTP-SD is almost the same as that of the SE SD, which grows exponentially with N. Thus, PTP-SD does not achieve running time savings compared to SE SD for large MIMO systems and high SNRs. However, the running time of threshold pruning obtains more significant running time savings than the above two SDs. Further, the running time savings increase with the number of transmit antennas. For example, for $N = 10$ and $N = 14$, the threshold rule obtains 1 and 2 orders of magnitude of running time savings compared to SE SD and PTP-SD. Although the K-best SD has less running time when the number of antennas is large, it could not achieve the near-ML performance. Therefore, for
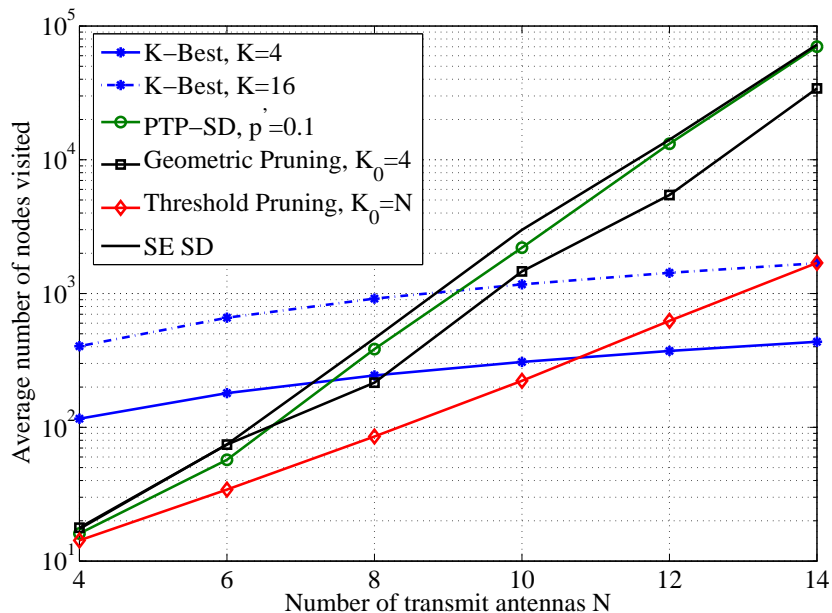
Figure 4.8: Running time for a 16-QAM MIMO system with different numbers of transmit and receive antennas N, SNR=20 dB.

high SNRs, the threshold pruning rule significantly reduces the running time while preserving near-optimal performance, especially for MIMO systems with a large number of transmit antennas.

4.6 Conclusions

Probability-distribution-based statistical pruning SD were proposed. Uniform pruning, geometric pruning, threshold pruning, hybrid pruning and depth-dependent pruning were developed. The SER performance of uniform and threshold pruning rules was analysed, and the pruning probability and the threshold for achievable diversity order K_0 were derived.

All of these rules achieved lower running time than the conventional SD in the low-SNR region. In particular, the threshold pruning rule obtained the most significant running time savings while achieving the full diversity order. For example, in low SNR, 80% and 95% running time savings were possible over the PTP-SD and K-best SD, while also achieving a slightly better SER performance. Moreover, a running time saving was also obtained for high SNRs (e.g., 20 dB), and this saving

increased with the number of transmit antennas as well.

$$\sim$$

Chapter 5

Improved K-best Sphere Detector

This chapter proposes an improved K-best sphere detector (IKSD). At each layer of the search tree, this SD keeps the best K nodes and all the nodes whose costs are within a certain margin of the cost of the K-th best node. Three IKSD variants, named fixed-threshold, normalized-threshold and adaptive-threshold, are investigated. By leveraging the IKSD, a hybrid SD algorithm is proposed by using full enumeration in the upper layers of the search tree and applying the IKSD for the remainder of the search tree. The IKSD is also extended for coded MIMO systems as a list SD for joint iterative detection and decoding.[1]

5.1   Introduction

For spatial multiplexing MIMO detection, Section 2.2.2 described the K-best SD [14], which has received significant attention recently because of its fixed throughput, fixed detection running time and parallel implementation.

Despite these advantages, the K-best SD does not guarantee a ML performance [14]. To do so, the K-best SD typically requires very large values of K, which result in a higher running time than that of the conventional SD. Nevertheless, due to the advantages of the K-best SD, several variants have been proposed to further reduce its running time or/and improve its performance, e.g., [30, 66, 85–88].

Since the performance loss of the K-best SD may be due to the likelihood of inadvertently discarding the ML solution, in this chapter, an IKSD is proposed [32]

---

[1]*A version of this chapter has been published in IEEE Wireless Commun. Lett., 1: 472 -475 (2012).*

that replaces the strict value K in the conventional K-best SD with a hypersphere radius determined by the cost of the K-th best node and a threshold Δ. The IKSD achieves a near-ML performance with a much lower running time than that of the conventional K-best SD.

The proposed algorithm, a general framework, also includes the M-algorithm [89] and T-algorithm [90] as special cases. These two algorithms are the special cases when the parameters Δ and K equal to 0 and 1, respectively.

Main Contributions:

1. An IKSD is proposed, which expands the fixed K nodes at each layer in the conventional K-best SD to a slightly bigger list, which includes all the nodes with a partial cost of f equal to or less than the K-th node cost f_K plus a small value Δ ($f \leq f_K + \Delta$). This Δ could be derived by off-line computation. The likelihood of discarding the ML solution is thus smaller than that with the conventional K-best SD.

2. Three specific IKSDs are proposed in this chapter with different choices of the threshold Δ (fixed-threshold, normalized threshold and adaptive-threshold IKSD). The parameter Δ controls the extra number of nodes visited by the IKSD. Furthermore, the closed-form expression of Δ is obtained for the normalized-threshold.

3. By leveraging the IKSD, a general hybrid SD algorithm is proposed, which expands all the nodes at the upper layers of the search tree, orders these nodes as an increasing partial cost, and then uses the proposed IKSD for the search of each subtree. This hybrid SD always updates the cost bound when one subtree search is finished and the new cost is less than the current bound, resulting in more pruned nodes.

4. The soft extension of the IKSD for coded MIMO systems is also derived in this chapter. This method increases the possibility of the candidate list including the ML point, and reduces the running time with close performance to that of conventional soft K-best SD detection [14].

This chapter is organized as follows: Section 5.2 presents the new IKSD, introduces three specific IKSD, and discusses how to derive the threshold. A hybrid IKSD is developed in Section 5.3. The soft IKSD detection in coded MIMO systems is proposed in Section 5.4. Simulation results and discussions for both the performance and the running time are given in Section 5.5. Finally, conclusions are drawn in Section 5.6.

5.2 Improved K-best Sphere Detector

The K-best SD has fixed running time only for every symbol detection, making it convenient for hardware implementation. However, a large K is necessary in order to approach a near-ML performance. This requirement results in an increased running time (even higher than that of the naive SE SD). The main reason for the performance gap is the likelihood that the K-best SD may discard the ML solution early. Mitigating this problem is the main idea in this section.

5.2.1 Improved K-best SD

The conventional K-best SD keeps K nodes for each layer, as mentioned in Section 2.2.2. However, the proposed IKSD searches the fixed K nodes and all the nodes with a partial cost equal to or less than the K-th node cost plus a small value Δ. Thus, the probability of finding the ML solution is increased compared to the probability of doing so with the conventional K-best SD. The IKSD is described in Algorithm 3.

When the initial sphere radius d is sufficiently large, the algorithm achieves its maximal running time. When it is smaller, the running time is reduced with the degradation in performance due to the lost lattice points outside the radius. In simulation results, $d^2 = \gamma n \sigma_n^2$ [14] is chosen, where $n = 2N$, σ_n^2 is the noise variance, and $\gamma \geq 1$ is chosen to guarantee the lattice point can be captured.

In this chapter, only the standard QR matrix decomposition is applied. The channel matrix ordering (e.g., [30]) is not included; however, it can improve the performance of the proposed IKSD.

Algorithm 3: The IKSD Algorithm

> **Input** : Δ, K, **z**, **H**, d
> **Output**: $\hat{\mathbf{s}}$

1   Initialize the sphere radius d and the partial cost $f_{best} = 0$, and take the root s_0 (layer $k = m$) as the start node. ;

2   **for** $p \leftarrow 1$ **to** $length(f_{best})$ **do**

3   Expand the p-th node, generate all its successors $\forall s \in \Omega$, and calculate the partial costs: $f_t = f_{best} + f_{k,t}$, where $f_{k,t} = (z_{k,p} - r_{k,k}s)^2$;

4   **end**

5   Sort all the components of f in an ascending order;

6   **if** *The number of the elements is less than K* **then**

7   Keep all the candidates with $f \leq d^2$ to obtain $\mathcal{T}$;

8   **else**

9   Only keep the elements whose cost indexes satisfy $f \leq f_K + \Delta$ in $\mathcal{T}$;

10   **end**

11   Replace the f_{best} with the adjusted f;

12   **if** $k \neq 1$ **then** Calculate $\mathbf{z}_t = \mathbf{z}_t - R_{:,k}s_t$ ($\forall s_t \in \mathcal{T}$), $k = k - 1$ and go to step 2;

13   **else** Return the first element in $\mathcal{T}$ as the estimated $\hat{\mathbf{s}}$;

For the tree search process, the conventional K-best SD sorts all the child nodes based on their partial costs, and selects the K best paths. In the proposed IKSD, instead of choosing exactly K nodes, the additional nodes are kept, whose costs are close to the cost of the K-th node, f_K. For example, at the i-th layer (where $i = 1, 2, \ldots, m$, $m = 2N$, and N is the number of transmit antennas), supposing that the nodes are also sorted, if the cost difference between the K-th node and the $(K + r)$th node ($r = 1, 2 \ldots$) is less than Δ, then all $K + r$ nodes are retained.

5.2.2   Threshold Rules

The choice of Δ is the main challenge of the IKSD, If Δ is too large, then more nodes are visited and the running time increases; while if Δ is too small, the performance improvement is limited compared to that of the conventional K-best SD. Depending on the parameterization of Δ, a flexible performance and running time trade-off could be achieved. Based on different choices of the threshold Δ, three types of IKSD are proposed next.

Fixed-Threshold IKSD: Intuitively, Δ could be a predefined constant, resulting in the fixed-threshold IKSD. This choice is motivated by the need to prune less aggressively in the early stage. A fixed Δ can perfectly serve this purpose. The value of Δ can be determined off-line through calculation, e.g., by the analysis in Section 5.2.3. For example, for the proper value for the 4×4 16-QAM MIMO system with noise variance σ_n^2, Δ could be set to be $0.25\sigma_n^2$, which is obtained by both theoretical and numerical analysis.

Normalized-Threshold IKSD: The threshold can be defined to depend on the cost of the K-th node at each layer. The theoretical analysis in Section 5.2.3 shows that this threshold will correspond to reducing the probability of pruning the true solution by a constant ratio compared to the K-best SD. Thus, the threshold can be given as

$$\Delta = \tau f_K. \tag{5.1}$$

This IKSD is called the normalized-threshold IKSD, which adaptively updates Δ in the searching process. The closed-form of Δ and τ will be derived in Section 5.2.3.

Adaptive-Threshold IKSD: If the SNR is known or can be estimated, an SNR-dependent Δ may be defined as

$$\Delta = \frac{\sigma_n^2}{\log \rho + 1}, \tag{5.2}$$

where σ_n^2 is the noise variance, and ρ is the SNR in the MIMO system. With this adaptive-threshold IKSD, Δ decreases with increasing SNR. The motivation for this threshold choice is that the cumulative costs are larger in the low-SNR region while they are smaller in the high-SNR region. Therefore, a large Δ should be chosen in the former case, and a small value for the latter case.

Other choices of the threshold may be possible. However, all the proposed threshold rules reduce the probability of dropping the ML solution early when traversing the search tree, resulting in performance gains compared to the conventional K-best SD with the same value of K. Furthermore, the proposed IKSD with K outperforms the K-best SD with $2K$, while the former also obtains lower running time than the latter. This result will be shown in Section 5.5.

5.2.3 Theoretical Analysis

Since the elements $n_1, \ldots, n_m$ in the noise vector $\mathbf{n}$ are values from independent identical distributed Gaussian noise, $\sum_{i=k}^{m} n_i^2$ becomes the chi-square random variable with $m - k + 1$ degrees of freedom. Because $f_t = \sum_{i=k}^{m} \left(z_i - \sum_{j=i}^{m} r_{i,j} s_j \right)^2 = \sum_{i=k}^{m} n_i^2$, the probability of the new cost of nodes being greater than the K-th node cost is

$$P_K = Pr(f_t > f_K) = 1 - Pr(f_t \leq f_K) = 1 - F(f_K; m - k + 1), \qquad (5.3)$$

where $F(f_K; m - k + 1) = \gamma(\frac{m-k+1}{2}, \frac{f_K}{2})\Gamma(\frac{m-k+1}{2})$ is the cumulative distribution function (CDF) of f_t, and $\gamma(k, x)$ and $\Gamma(k)$ are the incomplete Gamma function and Gamma function, respectively.

In order to reduce the probability of discarding the ML solution, the probability in (5.3) can be decreased by a predefined ratio λ ($0 < \lambda < 1$), which is given as

$$P_\Delta = Pr(f_t > f_K + \Delta) = \lambda P_K, \qquad (5.4)$$

where λ could be set to be a number close to 1 in order to constrain the incremental running time, such as $\lambda = 0.9$.

Therefore, the probability of $f_t \leq f_K + \Delta$ is $1 - \lambda P_K$. Thus, Δ can be defined as

$$\Delta = F^{-1}(1 - \lambda P_K; m - k + 1) - f_K. \qquad (5.5)$$

For the fixed-threshold IKSD, Δ can be predefined to be a deterministic value according to the above equation. By calculating the values of Δ, an interesting result is found. For example in a 4×4 MIMO system, when $\lambda = 0.9$, Δ is always between 0.2 to 0.3 for all $1, \ldots, m$ degrees of freedom, as calculated by (5.5). Thus, it is appropriate to choose $\Delta = 0.25$ for a 4×4 MIMO system. Similarly, a proper fixed threshold can also be derived by using this simple off-line calculation for other MIMO systems.

For the normalized-threshold IKSD, based on (5.1) and (5.5), τ is shown as

$$\tau = \frac{F^{-1}(1 - \lambda P_K; m - k + 1) - f_K}{f_K}. \qquad (5.6)$$

When SNR is sufficiently high, P_K can be approximated as

$$\lim_{\sigma_n^2 \to 0} P_K = \lim_{\sigma_n^2 \to 0} 1 - F(f_K; m - k + 1). \tag{5.7}$$

When $x \to 0$, the probability density function of the chi-squared distribution is

$$f(x; k) = \frac{1}{2^{\frac{k}{2}}\Gamma(\frac{k}{2})} x^{\frac{k}{2}-1} \exp(-x/2) \approx \frac{1}{2^{\frac{k}{2}}\Gamma(\frac{k}{2})} x^{\frac{k}{2}-1}. \tag{5.8}$$

Then, the CDF $F(x; k)$ is

$$F(x; k) = \int_0^x \frac{1}{2^{k/2}\Gamma(\frac{k}{2})} x^{k/2-1} dx = \frac{x^{k/2}}{(k/2)2^{k/2}\Gamma(\frac{k}{2})} \tag{5.9}$$

and $F^{-1}(P; k) = \left(\frac{k}{2} 2^{\frac{k}{2}}\Gamma(\frac{k}{2})P\right)^{\frac{2}{k}}$. Therefore, in the high-SNR region, (5.6) can be derived by the closed-form as

$$\tau = \frac{F^{-1}\left[1 - \lambda\left(1 - \frac{(f_K)^{(m-k+1)/2}}{((m-k+1)/2)2^{(m-k+1)/2}\Gamma((m-k+1)/2)}\right); m - k + 1\right] - f_K}{f_K}$$

$$= \frac{\left[\frac{(m-k+1)}{2}2^{\frac{(m-k+1)}{2}}\Gamma(\frac{(m-k+1)}{2})\left(1 - \lambda\left(1 - \frac{(f_K)^{\frac{(m-k+1)}{2}}}{(\frac{(m-k+1)}{2})2^{\frac{(m-k+1)}{2}}\Gamma(\frac{(m-k+1)}{2})}\right)\right)\right]^{\frac{2}{k}}}{f_K}$$

$$- 1. \tag{5.10}$$

Remarks:

1. The improvements of the proposed IKSD depend on the small relaxation of the number of retained nodes at each search layer. Thus, this relaxation increases the probability that the ML solution is not discarded at the early search layers. Consequently, the proposed IKSD has a roughly fixed running time and outperforms the conventional K-best SD with much smaller K.

2. According to the characteristics of the partial cost gap between K-th and $K +$ 1-th node, Δ is defined by three specific rules to obtain the new candidates at each layer for the IKSD. When $\Delta = 0$, the proposed IKSD becomes the conventional K-best SD. This Δ may have other definitions, but it always coincides with a rule – the performance is closer to the optimal performance when the Δ is increasing.

3. The running time of the proposed IKSD also depends on the margin Δ. When Δ decreases, the average number of nodes visited by the IKSD is getting closer to that of the conventional K-best SD. If Δ is sufficiently large, the search space spans the whole tree, yielding near-ML performance. Thus, the index Δ provides a flexible performance and running time for the proposed IKSD.

4. Because the proposed IKSD is intended to relax the strictly kept K nodes for the conventional K-best SD, it may be used in the variants of the original K-best SD to improve the performance with a smaller K, such as [30,85,86,91]. It also can be extended to soft MIMO detection and MIMO relay detection [78].

5.3   Hybrid Sphere Detection

In this section, the fixed-threshold IKSD is extended into a hybrid SD, as the specific IKSD of the three proposed threshold IKSDs.

In the conventional K-best SD, since only K nodes are kept at each layer of the search tree, discarding the ML solution at the early layers is thus likely. The IKSD is proposed in order to reduce this probability. Moreover, full enumeration of the early layers can also reduce this probability [65]. In this section, a general hybrid SD is proposed by combing the full enumeration and the proposed IKSD.

Hybrid SD algorithm: A general hybrid SD is proposed here, which performs two main steps in the search process.

1. In the first step, the hybrid SD expands all the branches of the early K_F layers in the search tree, i.e., performs full enumeration, where K_F is the number of layers being fully expanded. The choice of K_F depends on the number of antennas (the layers of the search tree) in MIMO systems. Intuitively, K_F may be greater when the number of antennas increases. The number of all the child nodes after the first step is $N_F = |\Omega|^{N_F}$. All these child nodes are ordered by an increasing accumulative partial cost, and become the new roots of all the generated subtrees with $m - K_F$ layers. By this process, the

probability of keeping the ML solution is increased. Moreover, the hybrid SD becomes the naive IKSD when no layer is fully expanded; i.e., $K_F = 0$.

2. In the second step, the proposed IKSD is applied for each subtree, and it updates the radius by the new cost of the estimate for the current subtree when finishing the search process of this subtree. By using this new radius as the cost bound of the next search, the proposed IKSD is more likely to prune more nodes or discard a whole subtree. Moreover, because the costs of the roots of all subtrees are already in an increasing order, once the i-th subtree is pruned, all the following $|\Omega|^{N_F} - i$ subtrees will be pruned. From the discussion in Section 5.2, it follows that the proposed IKSD needs only a smaller K than the conventional K-best SD for a similar performance. As well, the proposed IKSD provides reduced running time for the proposed hybrid SD.

The ordering of the channel matrix in the proposed hybrid SD is introduced in the following. In the first step of the hybrid SD, the signals with the largest noise amplification are detected. For the second step, the signals with the smallest noise amplification are detected.

For $i \leftarrow m$ **to** 1

1. Calculate $\mathbf{H}_i^{\dagger} = (\mathbf{H}_i^H \mathbf{H}_i)^{-1} \mathbf{H}_i^H$, where $\mathbf{H}_i$ is the channel matrix with columns selected in previous iterations zeroed;

2. The signal to be detected $(\hat{s}_p)$ is obtained by

$$p = \underset{\mathbf{j} \in \{1,\ldots,m\} - \{\mathbf{p}_{i+1}\}}{\arg\max} \|(\mathbf{H}_i^{\dagger})_j\|^2 \qquad \text{for} \qquad i = m, \ldots m - K_F, \qquad (5.11)$$

while

$$p = \underset{\mathbf{j} \in \{1,\ldots,m\} - \{\mathbf{p}_{i+1}\}}{\arg\min} \|(\mathbf{H}_i^{\dagger})_j\|^2 \qquad \text{for} \qquad i = m - K_F - 1, \ldots 1, \qquad (5.12)$$

where $(\mathbf{H}_i^{\dagger})_j$ denotes the j-th row of $\mathbf{H}_i^{\dagger}$, and $\mathbf{p}_{i+1}$ is the columns selected in previous iterations;

An SD algorithm has been proposed [85], which uses tree decomposition and pruning constraint updates to reduce the required K and terminate the search process early. This algorithm fully expands the first layer of the search tree and uses the conventional K-best SD for the search of all the subtrees. This SD algorithm is a special case of the proposed hybrid SD algorithm when $K_F = 1$ and uses the conventional K-best SD for the search of all subtrees.

Running time Measurement: The average number of nodes visited is also used to measure the running time of the proposed hybrid SD algorithm. However, the hybrid SD counts all the nodes visited by full enumeration and the search of all the subtrees.

By the full enumeration of the K_F layers, the expanded nodes N_F are directly obtained: $N_F = |\Omega|^{K_F}$. Therefore, the whole expected number of visited nodes of the hybrid SD is given by

$$C_H(m, \rho, K_F) = |\Omega|^{K_F} + \sum_{j=1}^{|\Omega|^{K_F}} \sum_{k=1}^{m-N_F} \varphi_{j,k}, \tag{5.13}$$

where $\varphi_{j,k}$ is the number of nodes visited at the k-th layer of the j-th subtree within the hypersphere of radius d. The second item of the above equation is the sum of all the nodes visited by searching $|\Omega|^{K_F}$ subtrees.

5.4 Soft Extension of the IKSD

For coded MIMO systems, the conventional K-best SD supports soft outputs [14], where the best K nodes left at the last iteration form the candidate list used by the iterative detection and decoding. However, the conventional K-best SD in coded MIMO systems results in an increasing running time in order to achieve the near-optimal performance by a sufficiently large K. Therefore, the list IKSD is proposed by extending the proposed IKSD as a list SD for coded MIMO systems.

The list IKSD generates a list $\mathcal{L}$ of $N_{\mathcal{I}}$ candidates when searching the tree. This list includes $N_{\mathcal{I}} = K + N_\Delta$ estimates, and the size of the list satisfies $1 \leq N_{\mathcal{I}} < 2^{N_c \cdot N}$, where $N_c = \log_2(|\mathcal{Q}|)$ is the number of bits per modulated symbol, and N_Δ is the number of extra nodes visited by the list IKSD compared to the list K-best

SD. The coded MIMO system model and the details of the MIMO detector and the channel decoder are presented in [10].

5.5   Simulation Results and Discussions

MIMO detection: In this section, the performance and running time of the IKSD (Algorithm 3) are assessed. Both the symbol error rate (SER) and the average number of nodes (the running time) visited by the new IKSD are compared with those of the conventional K-best SD [14]. Although the three versions of the IKSD outperform the conventional K-best SD, in this chapter only the fixed-threshold IKSD and the normalized-threshold IKSD are shown due to the space limitation. The ML curve is from the conventional SE SD. In order to compare the proposed IKSD with the K-best SD fairly, the initial radius for both the proposed IKSD and K-best SD is chosen to be the same ($\gamma = 10$). Furthermore, in order to highlight the advantage of the proposed IKSD, the channel detection ordering is not included for all the algorithms.
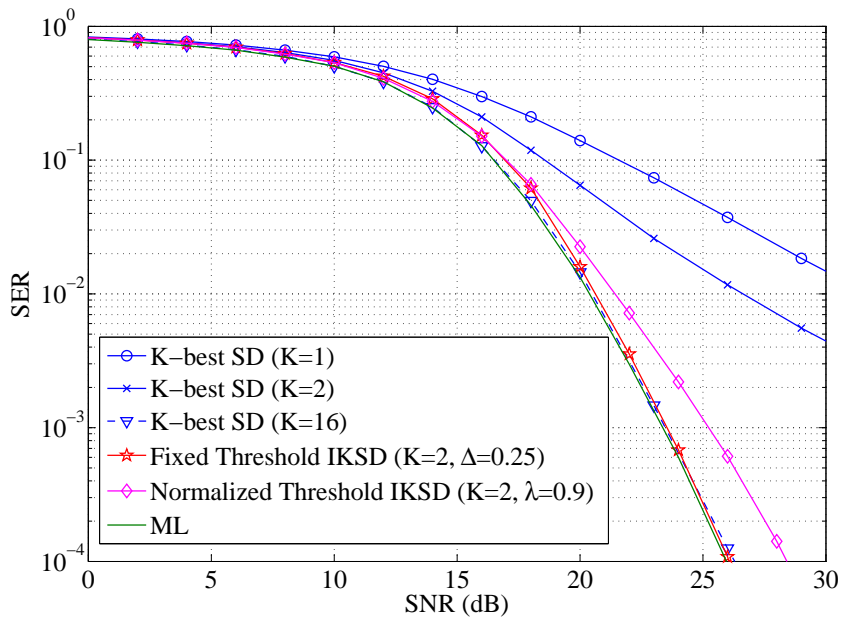
Figure 5.1: Error performance for an uncoded 4×4 MIMO 16-QAM system.

Fig. 5.1 shows the impact of the SER performance of the proposed IKSD. An

uncoded 4×4 MIMO system with 16-QAM is simulated over a flat Rayleigh fading channel ($\sigma_n^2 = 1$). Note that the performance of the IKSD by the fixed-threshold ($K = 2, \Delta = 0.25$) is very close to the ML curve, while the conventional K-best SD needs to set $K = 16$ to achieve a similar SER. Furthermore, the fixed-threshold IKSD outperforms the normalized-threshold ($K = 2, \lambda = 0.9$).
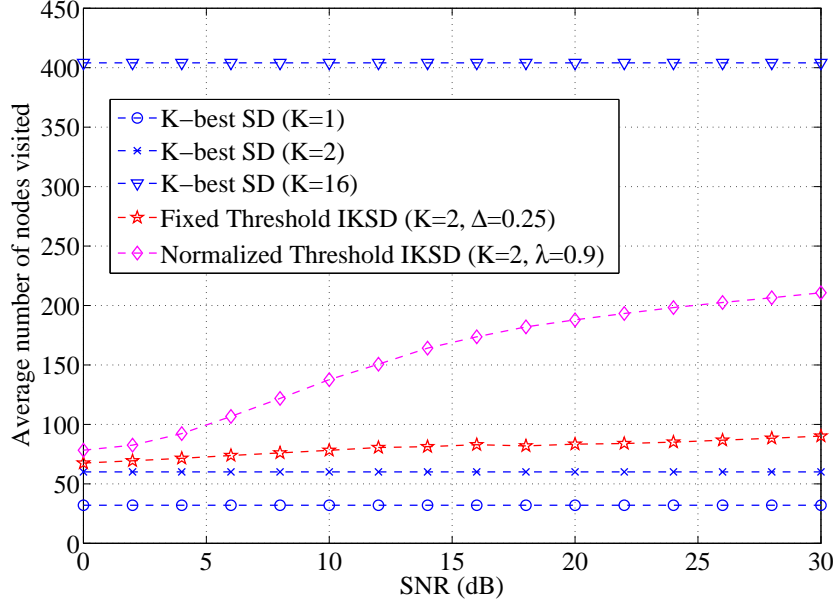
Figure 5.2: Running time for an uncoded 4×4 MIMO 16-QAM system.

A running time comparison between the IKSD and the K-best SD is also provided in Fig. 5.2. The running time of the proposed fixed-threshold IKSD is lower than that of the K-best SD when achieving the near-ML performance. For example, the conventional K-best SD ($K = 16$) searches about 4×10^2 nodes, while the fixed-threshold IKSD needs to visit only 80 nodes on average – an 80% running time savings. Moreover, for $K = 2$, with a 30% increase in running time, the fixed-threshold IKSD provides a $7\,\mathrm{dB}$ gain (at an SER of 10^{-2}) over the K-best SD. Note that, as expected, the running time curves for the conventional K-best SD are flat as a function of SNR; similarly, the fixed-threshold IKSD has a virtually flat running time curve. To quantify such flatness, a running time variability index was introduced in [47]. This index is 7×10^{-3}, affirming that the fixed-threshold IKSD has a virtually constant running time.
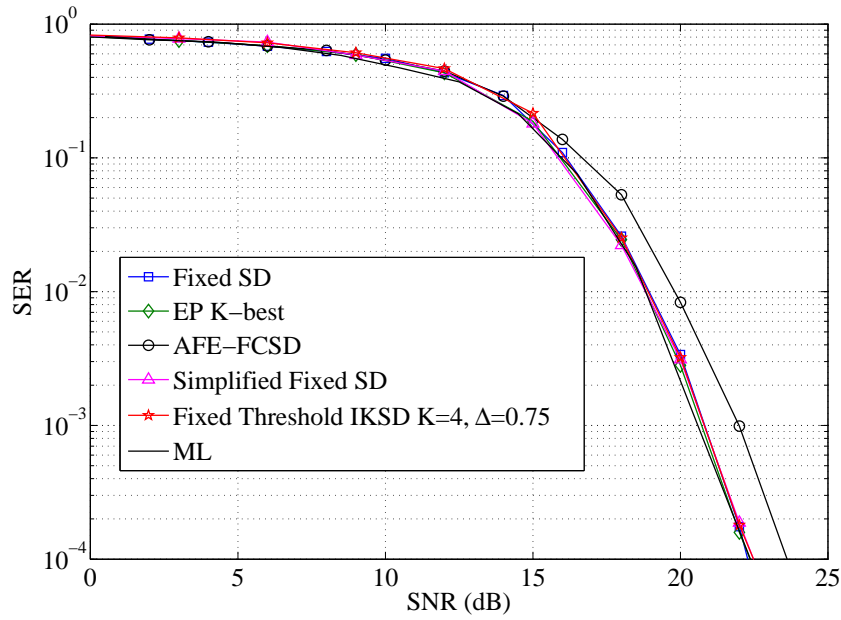
Figure 5.3: Error performance for an uncoded 8×8 MIMO 16-QAM system.
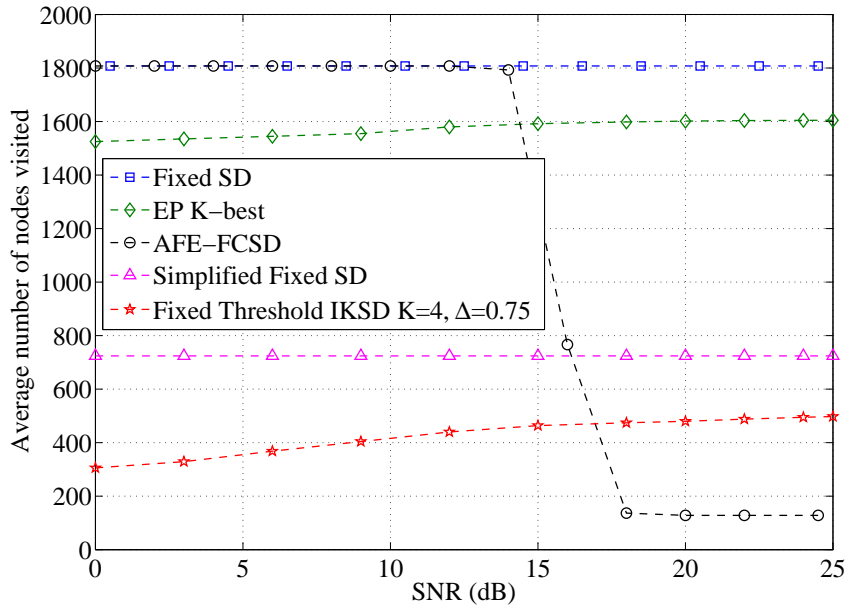
Figure 5.4: Running time for an uncoded 8×8 MIMO 16-QAM system.

In order to show the advantages of the proposed IKSD, the comparison with other algorithms (Fixed SD [30], EP K-best [66], AFE-FCSD [88], and simplified Fixed SD [87]) is shown in Figs. 5.3 and 5.4. Achieving the near-optimal SER performance, the running time of the proposed IKSD is only 23%, 27% and 59.5% of that of the Fixed SD, EP K-best and simplified Fixed SD, respectively. Although the AFE-FCSD obtains lower running time than the proposed IKSD when $\text{SNR} \geq 18 \, \text{dB}$, the latter gains $1.5 \, \text{dB}$ more than the former at an SER of 10^{-4}. Above all, the proposed IKSD achieves the best trade-off between performance and running time among all these algorithms.

Hybrid Sphere Detection: In order to verify the improvements of the proposed hybrid SD, the performance and the running time of the hybrid IKSD and the SD algorithm [85] (the hybrid K-best SD in this section) are investigated in Fig. 5.5 and Fig. 5.6. In the simulations, the number of full enumeration layers K_F is set to be 1 in order to compare the proposed hybrid IKSD with the hybrid K-best SD proposed by [85]. Moreover, 4×4 16-QAM and 64-QAM MIMO systems are considered here.
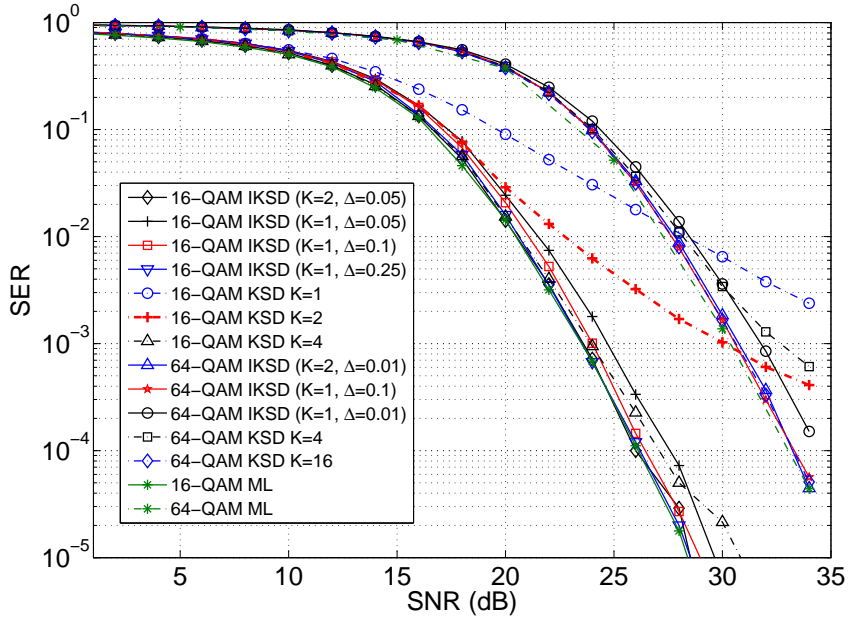
Figure 5.5: Error performance for 4×4 MIMO systems.

Let us first evaluate the SER performance. Fig. 5.5 shows the hybrid IKSD and

the hybrid K-best SD with different values of K. Clearly, for the 16-QAM system, the proposed hybrid IKSD achieves a near-ML performance when K equals 1, and Δ equals 0.25, while the hybrid K-best SD needs to choose $K = 4$ in order to obtain a near-ML performance. Interestingly, when choosing the same value for K, the proposed hybrid IKSD acquires more performance gains than the hybrid K-best SD. For example, at an SER of 10^{-3}, the hybrid IKSD gains 6.5 dB over the hybrid K-best SD with $K = 2$ and obtains a gain of more than 10 dB than the latter with $K = 1$. Although the hybrid IKSD ($K = 1$) cannot achieve a near-ML performance for all the SNRs, it still performs very close to the optimal one. Fig.5.5 also shows the performance for a 64-QAM MIMO system. Similarly, the proposed hybrid IKSD achieves a near-ML performance with a smaller K than that of the hybrid K-best SD. For example, the hybrid IKSD with $K = 1, \Delta = 0.1$ performs almost identically to the hybrid K-best SD with $K = 16$. In this figure, the performances with different values of Δ are also shown. When Δ gets larger, the performance gains more.
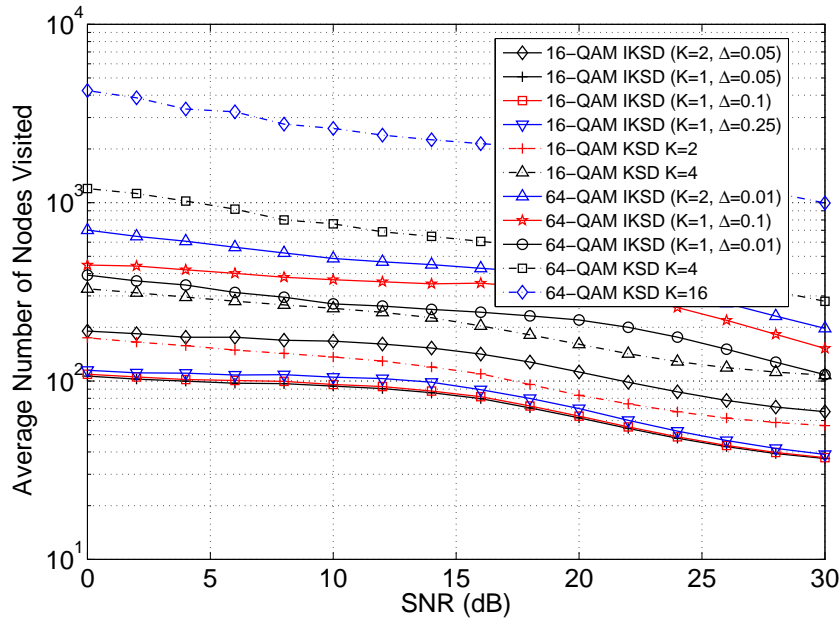
Figure 5.6: Running time for 4×4 MIMO systems.

A running time comparison for the same set-up is shown in Fig. 5.6. For the 16-QAM system, with a similar performance shown in Fig. 5.5, the hybrid IKSD with

$K = 1, \Delta = 0.25$ searches 83 nodes on average for the whole SNR region, while the hybrid K-best SD with $K = 4$ searches about 2×10^2 nodes (the former saves about 60% more than the latter). Running time savings are also achieved in a 64-QAM system. For example, the running time of the hybrid IKSD ($K = 1, \Delta = 0.1$) is 3.6×10^2, but is 2.2×10^3 for the hybrid K-best SD ($K = 16$); i.e., the proposed hybrid IKSD obtains approximately 84% running time savings over the hybrid K-best SD.

Detection for Coded MIMO systems: The advantages of the IKSD are now accessed in a 4×4 coded MIMO system. The performance measured by BER, and the running time of generating the candidate list are investigated. The systematic recursive convolutional code with rate $R = 1/2$ is used to encode the transmitted bits sequence **b** with the frame length $M_b = 8192$, where the feed-forward and feedback-generating polynomials are $G_1(D) = 1 + D^2$ and $G_2(D) = 1 + D + D^2$ with memory length 2 [10], respectively. A random interleaver is used here.
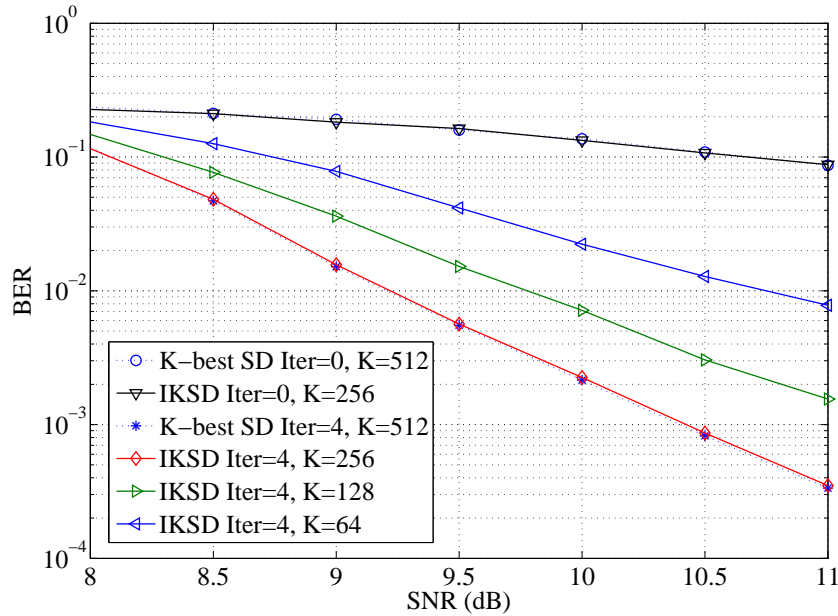
Figure 5.7: Error performance for a coded 4×4 MIMO 16-QAM system.

In order to show the effects of K, the performance and running time for different K are shown in Figs. 5.7 and 5.8. By increasing K, more nodes are visited in the search process, resulting in the increasing running time of the iterative detection and

decoding. However, the BER performance improves when K is larger. As shown in the left axis, by using 4 maximum iterations, the proposed list IKSD with $K = 256$ achieves the performance of the conventional K-best SD with $K = 512$.
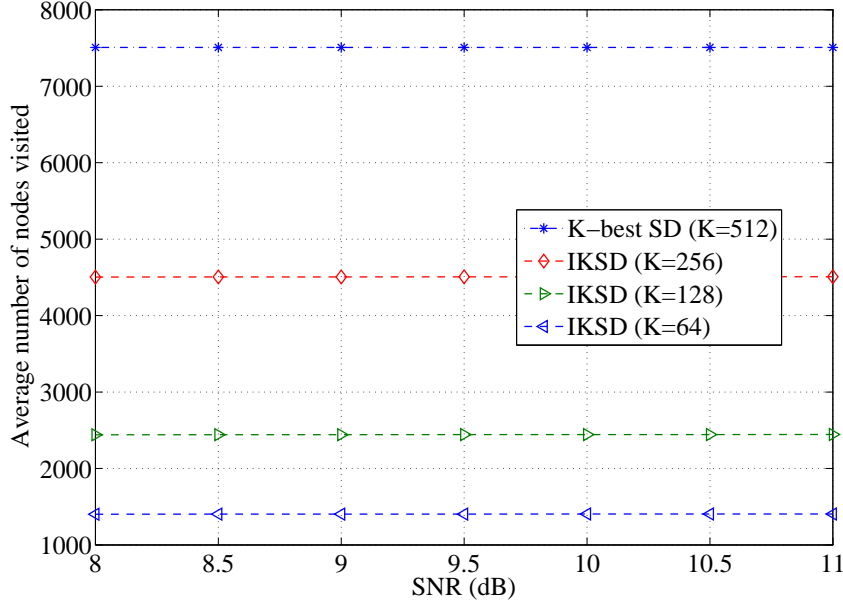
Figure 5.8: Running time for a coded 4×4 MIMO 16-QAM system.

As shown in Fig. 5.8, when K decreases, the degradation of the running time increases. For example, the average number of nodes visited is around 4.5×10^3 with $K = 256$, approximately 2.4×10^3 with $K = 128$, and about 1.4×10^3 with $K = 64$, respectively. However, the conventional list K-best SD visits about 7.5×10^3 nodes with $K = 512$. The proposed list IKSD gains 40% running time savings with the same performance.

5.6 Conclusions

This chapter proposed an improved K-best SD (IKSD), which achieved a near-ML performance at a reduced and roughly fixed running time. Unlike the conventional K-best SD, which retains a fixed number of K nodes per layer, the proposed IKSD expanded this number to all the nodes whose cost was less than $f_K + \Delta$. The conventional K-best SD is thus a special case when $\Delta = 0$. The motivation for keeping

additional nodes is to further reduce the likelihood that the conventional K-best SD will discard the ML solution early. The proposed IKSD was further extended to propose a general hybrid SD in order to further improve the performance, verifying that the main idea of the IKSD could be adopted with different variants of the conventional K-best SD. For coded MIMO systems, a soft extension of the IKSD was developed as the list IKSD. It used the IKSD to generate the candidate list for joint iterative detection and decoding, resulting in running time savings over the conventional list K-best SD.

$$\sim$$

Chapter 6

Estimate-and-Forward Relay Strategy

Sphere detection algorithms are also needed for MIMO relay networks to reduce the detection running time. This chapter proposes and analyses an EF scheme for MIMO relay networks. The EF relay forwards the MMSE estimate of the source data to the destination and performs like AF and DF for the low and high SNR regions, respectively. Further, two approximate EF schemes for large MIMO relay networks are proposed to reduce the number of computational operations. The first one, called list EF, computes a list-SD-based MMSE estimate and retains the advantages of the exact EF relay at a negligible performance loss, while the second one computes a Gaussian estimate. [1]

6.1 Introduction

The conventional AF and DF relays were introduced in Section 2.4. At the relay nodes, AF simply amplifies the received signal, while DF detects the transmit signal depending on the received signal. Another relay strategy called EF [49] is a powerful approach for uncoded single antenna relay networks. Unlike the AF and DF relays, the EF relay computes and transmits an unconstrained MMSE estimate, resulting in an optimized relay function for all SNRs. Due to its advantages, the single-antenna EF relay has been investigated [92–98]. A ML receiver for EF relaying was derived in [92]; moreover, [93] extended EF relaying into coded single

---

[1]*A version of this chapter has been submitted to IEEE Trans. Wireless Commun. (2013).*

antenna relay networks. However, EF relaying has not been extended to MIMO relays, and the high number of computational operations of EF for large MIMO networks with high-order constellations and/or a large number of antennas has also not been investigated.

The joint source-to-relay signal transmission design was investigated in [99, 100], and [101–103] worked on proposing relay/antenna selection techniques for performance improvements. In this chapter, we focus on the relay-signal-processing algorithm design and propose the MIMO EF relay strategy [104].

The main contributions of this chapter are summarized as follows.

1. The concept of the MIMO EF relay is developed. It forwards a scaled version of an unconstrained MMSE estimate of the source-transmitted signal. The scaling factor is chosen to satisfy the relay average power constraint. Unlike AF and DF, the proposed EF works equally well for both low and high SNRs, and thus no algorithm switching is required.

2. To illustrate the proposed EF relay function, two examples are provided. They involve a single antenna relay and a 2×2 MIMO relay. Both examples show the convergence of EF to AF and DF for low and high SNRs. Inspired by these two examples, we analyse and prove the convergence of EF to AF and DF for general MIMO relay networks with an arbitrary number of antennas. Thus, in the low and high SNR regions, the EF converges to AF and DF, respectively.

3. To provide a quality measure, the mean square error (MSE) expressions of AF, DF and EF are derived. Moreover, as expected, the MSE comparison reveals that EF achieves the lowest MSE for all SNRs. Thus, it performs best across all SNRs and eliminates the need for switching between algorithms for different SNRs.

4. To reduce the number of computational operations when there are high-order constellations and/or a large number of antennas (large MIMO), we propose a list EF relay, which computes MMSE estimate by using a sphere decoder

(such as [22, 25, 47, 48]) to generate a list of candidate vectors. A 2×2 16-QAM MIMO relay system is examined.

5. To reduce the number of computational operations of the MMSE estimate, the discrete sum of the terms in the exact MMSE estimate is approximately a Gaussian integral, which can be evaluated in a closed-form. This resulting relay strategy is called Gaussian EF.

6. To compute the error rates of AF, DF and EF, extensive numerical and simulation results are generated. Both high-order constellation 64-QAM and 2×2 16-QAM systems are evaluated for a single relay network. Moreover, to verify the advantages of the proposed list EF, a parallel (two relay) and a hybrid relay network are also simulated. The simulation results confirm our EF analysis, which found that the proposed EF outperforms AF and DF for all SNRs.

This chapter is organized as follows: Section 6.2 describes MIMO relay strategies including AF, DF and EF. Section 6.3 presents the proposed list EF and Gaussian EF. The proposed EF relays are extended to MIMO two-way relay networks in Section 6.4. Simulation results and discussions are given in Section 6.5. Finally, conclusions are drawn in Section 6.6.

6.2 Relay Strategies

Throughout this chapter, we assume that the channel state information is available at the relay and the destination, and can be, for example, estimated by using the transmitted pilot symbols [56]. Single-relay networks are investigated first, and for multiple relays networks, we assume identical relays that do not cooperate. Our simulation results will be discussed in Section 6.5. Due to the valuable spatial diversity arising from a direct link [105, 106], collaborative relaying with a direct link outperforms that of the case without a direct link. One simulation example is given in Section 6.5.

The performance of MIMO memoryless relay networks depends critically on the relay function. In this section, only single-relay networks are considered for

analysis, and thus $\mathbf{H}$ and $\mathbf{G}$ denote the source-relay and relay-destination channels and have the same definition as $\mathbf{H}_k$ and $\mathbf{G}_k$ in (2.16) and (2.17), respectively. Several memoryless relay functions for MIMO are discussed next. The system model is as given in Fig. 2.4.

From the discussion of AF and DF relay schemes in Section 2.4, it follows that AF outperforms DF for low SNRs while the reverse is true for high SNRs. Therefore, adaptive forwarding strategies [107, 108] have been developed, which switch between AF and DF for different SNRs. We develop the EF relay as an alternative. It achieves the advantages of AF and DF for all SNRs without switching between the algorithms.

6.2.1 Estimate-and-Forward

This section presents the main idea of this chapter. Unlike DF relay, which transmits the hard decisions, the EF relay transmits soft information. The soft information which helps data detection at the destination is a scaled unconstrained MMSE estimate of the transmitted signal $\mathbf{x}$ at the relay. The MMSE estimate is the conditional mean of $\mathbf{x}$, given the received signal $\mathbf{r}$ and channel $\mathbf{H}$, and may be stated as

$$\hat{\mathbf{x}} = \mathcal{E}(\mathbf{x}|\mathbf{r}, \mathbf{H}) = \frac{\sum_{\mathbf{x} \in \mathcal{Q}^{M_s}} \mathbf{x} f(\mathbf{r}|\mathbf{x}, \mathbf{H}) P(\mathbf{x})}{\sum_{\mathbf{x} \in \mathcal{Q}^{M_s}} f(\mathbf{r}|\mathbf{x}, \mathbf{H}) P(\mathbf{x})}, \tag{6.1}$$

where $P(\mathbf{x})$ is the priori probability of the transmitted signal $\mathbf{x}$, and $f(\mathbf{r}|\mathbf{x}, \mathbf{H})$ is the PDF of $\mathbf{r}$ conditional on $\mathbf{x}$ and $\mathbf{H}$. Because the addition noise vector is i.i.d Gaussian, the PDF $f(\mathbf{r}|\mathbf{x}, \mathbf{H})$ may be written as

$$f(\mathbf{r}|\mathbf{x}, \mathbf{H}) = \frac{1}{(\pi \sigma_1^2)^{M_s}} \exp\left(-\frac{\|\mathbf{r} - \mathbf{H}\mathbf{x}\|^2}{\sigma_1^2} \right). \tag{6.2}$$

Assuming equal priori probabilities for all transmitted symbols, the EF relay computes the MMSE estimate

$$\hat{\mathbf{x}} = \frac{\sum_{\mathbf{x} \in \mathcal{Q}^{M_s}} \mathbf{x} \exp\left(-\frac{\|\mathbf{r} - \mathbf{H}\mathbf{x}\|^2}{\sigma_1^2} \right)}{\sum_{\mathbf{x} \in \mathcal{Q}^{M_s}} \exp\left(-\frac{\|\mathbf{r} - \mathbf{H}\mathbf{x}\|^2}{\sigma_1^2} \right)}. \tag{6.3}$$

89

To satisfy the relay power constraint, the scaling factor for EF relaying, like that for AF and DF relaying, is given by

$$\beta = \sqrt{\frac{P_r}{\mathcal{E}(\|\hat{\mathbf{x}}\|^2)}} = \sqrt{\frac{P_r}{\int_{-\infty}^{\infty} \|\hat{\mathbf{x}}(\mathbf{r})\|^2 f(\mathbf{r}) d\mathbf{r}}}. \tag{6.4}$$

By using the total probability law [23], the PDF of received signal $\mathbf{r}$ can be obtained as

$$f(\mathbf{r}) = \sum_{\mathbf{x} \in \mathcal{Q}^{M_s}} f(\mathbf{r}|\mathbf{x}, \mathbf{H}) P(\mathbf{x}) = \sum_{\mathbf{x} \in \mathcal{Q}^{M_s}} \frac{1}{(\pi \sigma_1^2)^{M_s}} \exp\left(-\frac{\|\mathbf{r} - \mathbf{H}\mathbf{x}\|^2}{\sigma_1^2}\right) \frac{1}{|\mathcal{Q}|^{M_s}}. \tag{6.5}$$

Thus, the relay retransmits the scaled version of the MMSE estimate $\beta\hat{\mathbf{x}}$ to the destination. The EF relay function is therefore

$$\mathcal{G}_{EF}(\mathbf{r}) = \sqrt{\frac{P_r}{\int_{-\infty}^{\infty} \|\hat{\mathbf{x}}\|^2 f(\mathbf{r}) d\mathbf{r}}} \times \frac{\sum_{\mathbf{x} \in \mathcal{Q}^{M_s}} \mathbf{x} \exp\left(-\frac{\|\mathbf{r} - \mathbf{H}\mathbf{x}\|^2}{\sigma_1^2}\right)}{\sum_{\mathbf{x} \in \mathcal{Q}^{M_s}} \exp\left(-\frac{\|\mathbf{r} - \mathbf{H}\mathbf{x}\|^2}{\sigma_1^2}\right)}. \tag{6.6}$$

To demonstrate the EF relay scheme, two examples are discussed next.

Example 1 (BPSK and $M_s = N_r = M_r = N_d = 1$): Begin from the simplest case of a signal antenna system using BPSK modulation. In this case, the MMSE estimate in (6.3) can be written as

$$\hat{x} = \mathcal{E}(x|r, h) = \tanh\left(\frac{hr}{\sigma_1^2}\right), \tag{6.7}$$

where $\tanh(x) = \frac{e^x - e^{-x}}{e^x + e^{-x}}$.

To investigate the behaviour of this relay, the $\hat{x}$ is discussed for low and high SNRs, respectively. In the low-SNR region (the region with high noise power), by expanding $\tanh(x)$, the estimate at the relay becomes

$$\begin{aligned}
\hat{x} &= \lim_{\sigma_1^2 \to \infty} \tanh\left(\frac{hr}{\sigma_1^2}\right) = \lim_{\sigma_1^2 \to \infty} \frac{\exp(\frac{hr}{\sigma_1^2}) - \exp(-\frac{hr}{\sigma_1^2})}{\exp(\frac{hr}{\sigma_1^2}) + \exp(-\frac{hr}{\sigma_1^2})} \\
&= \lim_{\sigma_1^2 \to \infty} \frac{(1 + \frac{hr}{\sigma_1^2}) - (1 - \frac{hr}{\sigma_1^2})}{(1 + \frac{hr}{\sigma_1^2}) + (1 - \frac{hr}{\sigma_1^2})} = \lim_{\sigma_1^2 \to \infty} \frac{hr}{\sigma_1^2},
\end{aligned} \tag{6.8}$$

where the fact that $e^x \approx 1 + x$ when $x \to 0$ is used. This MMSE estimate resembles AF relaying with an amplify factor $\frac{h}{\sigma_1^2}$.

In the high-SNR region, the MMSE estimation of the received signal can be written as

$$\hat{x} = \lim_{\sigma_1^2 \to 0} \tanh\left(\frac{hr}{\sigma_1^2}\right) = \lim_{\sigma_1^2 \to 0} \frac{\exp(\frac{hr}{\sigma_1^2}) - \exp(-\frac{hr}{\sigma_1^2})}{\exp(\frac{hr}{\sigma_1^2}) + \exp(-\frac{hr}{\sigma_1^2})}$$

$$= \begin{cases} -1 & : \frac{hr}{\sigma_1^2} < 0 \\ 1 & : \frac{hr}{\sigma_1^2} > 0 \end{cases} = \text{sgn}\left(\frac{hr}{\sigma_1^2}\right), \tag{6.9}$$

where the fact that $\lim_{x \to -\infty} e^x = 0$, and $\text{sgn}(x)$ is an odd mathematical function that extracts the sign of a real number is used. (6.9) reveals that MMSE relaying approaches DF when SNR is high enough.

To further confirm the advantages of the EF relay, the power of the MMSE estimate $\mathcal{E}(\|\hat{x}\|^2)$ is also discussed here. This power is given by

$$\mathcal{E}(\|\hat{\mathbf{x}}\|^2) = \frac{\exp\left(-\frac{h^2}{2\sigma_1^2}\right)}{2\sqrt{2\pi}\sigma_1^2} \int_{-\infty}^{\infty} \frac{\left(\exp\left(\frac{hr}{\sigma_1^2}\right) - \exp\left(-\frac{hr}{\sigma_1^2}\right)\right)^2}{\exp\left(\frac{hr}{\sigma_1^2}\right) + \exp\left(-\frac{hr}{\sigma_1^2}\right)} \exp\left(-\frac{r^2}{2\sigma_1^2}\right) dr$$

$$\approx \begin{cases} \dfrac{\exp\left(-\frac{h^2}{2\sigma_1^2}\right)}{2\sqrt{2\pi}\sigma_1^2} \int_{-\infty}^{\infty} \dfrac{\exp\left(\frac{2hr}{\sigma_1^2}\right) - \exp\left(-\frac{2hr}{\sigma_1^2}\right) - 2}{2} \exp\left(-\frac{r^2}{2\sigma_1^2}\right) dr \\ \qquad\qquad\qquad \text{when } \sigma_1^2 \to \infty \\ \int_{-\infty}^{\infty} 1^2 \times \frac{1}{2\sqrt{2\pi}\sigma_1^2} \left(\exp\left(-\frac{(r-h)^2}{2\sigma_1^2}\right) + \exp\left(-\frac{(r+h)^2}{2\sigma_1^2}\right)\right) dr \\ \qquad\qquad\qquad \text{when } \sigma_1^2 \to 0 \end{cases} .$$

$$= \begin{cases} \frac{h^2}{\sigma_1^2} & \text{when } \sigma_1^2 \to \infty \\ 1 & \text{when } \sigma_1^2 \to 0 \end{cases} \tag{6.10}$$

This equation shows that the power of the MMSE estimate is close to being a scaled transmit power at low SNR and approaches the power of hard decision at the relay at high SNR. Therefore, (6.8) and (6.9) are affirmed. This example theoretically verifies and agrees with the numerical results of the relay function (shown as Fig. 1 in [49])

Example 2 (BPSK and $M_s = N_r = M_r = N_d = 2$): Next, a 2×2 MIMO relay system with BPSK inputs is considered. A real-valued MIMO relay system and constellation vector $\mathcal{Q}^2 = \left\{ \begin{pmatrix} -1 \\ -1 \end{pmatrix}, \begin{pmatrix} -1 \\ 1 \end{pmatrix}, \begin{pmatrix} 1 \\ -1 \end{pmatrix}, \begin{pmatrix} 1 \\ 1 \end{pmatrix} \right\}$ are assumed. The received signal at the relay is

$$\mathbf{r} = \begin{bmatrix} r_1 \\ r_2 \end{bmatrix} = \begin{bmatrix} h_{11} & h_{12} \\ h_{21} & h_{22} \end{bmatrix} \begin{bmatrix} x_1 \\ x_2 \end{bmatrix} + \begin{bmatrix} n_1 \\ n_2 \end{bmatrix}. \tag{6.11}$$

Thus, the relay function of the MMSE estimate can be derived by (6.6).
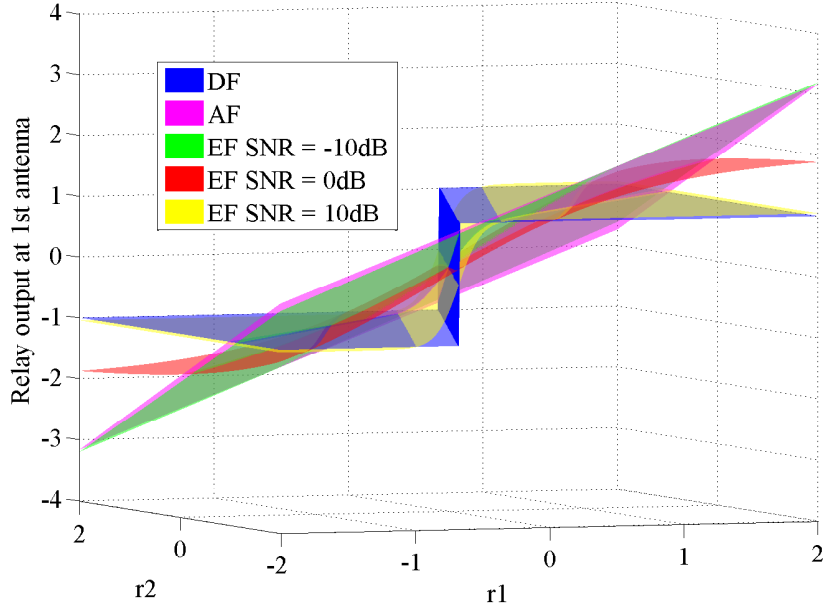
Figure 6.1: Relay function at different SNRs for the $N_r = 2$, BPSK system.

The relay functions can be shown by Fig. 6.1, where only the transmitted signal at one antenna is shown, and the MIMO channel $\mathbf{H} \sim \mathcal{CN}(0, 1)$ is a randomly generated Gaussian variable $\mathbf{H} = [-1.1756 + 0.7771i, -0.7670 + 1.6233i; 1.3744 + 0.1041i, 0.1604 + 1.9464i]$. Note that the EF relay function is almost linear for small values of $|\mathbf{r}|$ like AF. Its slope gradually decreases and finally becomes flat like the slope of DF. Another observation is that EF performs similarly to AF for low SNR $(-10\,\mathrm{dB})$ and closer to DF for high SNR $(10\,\mathrm{dB})$.

6.2.2 Relationships among AF, DF and EF

Examples 1 and 2 indicate that EF approximates AF and DF in the low SNR and high SNR regions. In this subsection, it is theoretically shown that this relationship indeed holds in general MIMO relay networks with an arbitrary number of antennas. The constellation is assumed to be symmetric; i.e., $x \in \mathcal{Q} \Leftrightarrow -x \in \mathcal{Q}$.

Low SNR Case: When the receive SNR at the relay is low, by using (6.3), the

MMSE estimate can be derived as

$$\lim_{\sigma_1^2 \to \infty} \hat{\mathbf{x}} = \lim_{\sigma_1^2 \to \infty} \frac{\sum_{\mathbf{x} \in \mathcal{Q}^{M_s}} \mathbf{x} \exp\left(-\frac{\|\mathbf{r} - \mathbf{H}\mathbf{x}\|^2}{\sigma_1^2}\right)}{\sum_{\mathbf{x} \in \mathcal{Q}^{M_s}} \exp\left(-\frac{\|\mathbf{r} - \mathbf{H}\mathbf{x}\|^2}{\sigma_1^2}\right)}$$

$$= \lim_{\sigma_1^2 \to \infty} \frac{\sum_{\mathbf{x} \in \mathcal{Q}^{M_s}} \mathbf{x} \exp\left(-\frac{-\mathbf{x}^H \mathbf{H}^H \mathbf{r} - \mathbf{r}^H \mathbf{H} \mathbf{x} + \mathbf{x}^H \mathbf{H}^H \mathbf{H} \mathbf{x}}{\sigma_1^2}\right)}{\sum_{\mathbf{x} \in \mathcal{Q}^{M_s}} \exp\left(-\frac{-\mathbf{x}^H \mathbf{H}^H \mathbf{r} - \mathbf{r}^H \mathbf{H} \mathbf{x} + \mathbf{x}^H \mathbf{H}^H \mathbf{H} \mathbf{x}}{\sigma_1^2}\right)}. \quad (6.12)$$

Because the constellation is symmetric, and thus $\sum x f(x) = 0$ if $f(x)$ is an even function in x, the above equality can be derived as

$$\lim_{\sigma_1^2 \to \infty} \hat{\mathbf{x}} = \lim_{\sigma_1^2 \to \infty} \frac{\sum_{\mathbf{x} \in \mathcal{Q}^{M_s}} \mathbf{x} \left(1 - \frac{-\mathbf{x}^H \mathbf{H}^H \mathbf{r} - \mathbf{r}^H \mathbf{H} \mathbf{x} + \mathbf{x}^H \mathbf{H}^H \mathbf{H} \mathbf{x}}{\sigma_1^2}\right)}{\sum_{\mathbf{x} \in \mathcal{Q}^{M_s}} \left(1 - \frac{-\mathbf{x}^H \mathbf{H}^H \mathbf{r} - \mathbf{r}^H \mathbf{H} \mathbf{x} + \mathbf{x}^H \mathbf{H}^H \mathbf{H} \mathbf{x}}{\sigma_1^2}\right)}.$$

Furthermore, it is known that $\lim_{\sigma_1^2 \to \infty} \frac{n_1}{\sigma^2} = 0$ with probability one and $\lim_{x \to 0} e^x = \lim_{x \to 0} 1 + x$; thus,

$$\lim_{\sigma_1^2 \to \infty} \hat{\mathbf{x}} = \lim_{\sigma_1^2 \to \infty} \frac{\sum_{\mathbf{x} \in \mathcal{Q}^{M_s}} \mathbf{x} \frac{\mathbf{x}^H \mathbf{H}^H \mathbf{r} + \mathbf{r}^H \mathbf{H} \mathbf{x}}{\sigma_1^2}}{|\mathcal{Q}|^{M_s} - \sum_{\mathbf{x} \in \mathcal{Q}^{M_s}} \frac{\mathbf{x}^H \mathbf{H}^H \mathbf{H} \mathbf{x}}{\sigma_1^2}}$$

$$= \frac{1}{\sigma_1^2 |\mathcal{Q}|^{M_s}} \left(\left(\sum_{\mathbf{x} \in \mathcal{Q}^{M_s}} \mathbf{x} \mathbf{x}^H\right) \mathbf{H}^H \mathbf{r} + \left(\sum_{\mathbf{x} \in \mathcal{Q}^{M_s}} \mathbf{x} \mathbf{x}^T\right) \mathbf{H}^T \mathbf{r}^*\right).$$

Finally, based on the property of the constellation, there are $\sum_{x_1, x_2 \in \mathcal{Q}} x_1 x_2^* = 0$, and $\sum_{x_1, x_2 \in \mathcal{Q}} x_1 x_2 = 0$. Therefore, the limitation of the MMSE estimation in the low-SNR region can be derived by

$$\lim_{\sigma_1^2 \to \infty} \hat{\mathbf{x}} = \frac{1}{\sigma_1^2 |\mathcal{Q}|} \left(\sum_{x \in \mathcal{Q}} |x|^2 \mathbf{H}^H \mathbf{r} + \sum_{x \in \mathcal{Q}} x^2 \mathbf{H}^T \mathbf{r}^*\right), \quad (6.13)$$

(6.13) shows that EF converges to AF in the low-SNR region, but in a slightly different form than that of the pure AF in (2.18). (6.13) can be further simplified for different constellations. For the real-valued MIMO relay system, such as BPSK, (6.13) can be rewritten as

$$\lim_{\sigma_1^2 \to \infty} \hat{\mathbf{x}} = \frac{2 \sum_{x \in \mathcal{Q}} x^2}{2\sigma_1^2 |\mathcal{Q}|} \mathbf{H}^T \mathbf{r} = \frac{\sum_{x \in \mathcal{Q}} x^2}{\sigma_1^2 |\mathcal{Q}|} \Re\left(\mathbf{H}^H \mathbf{r}\right). \quad (6.14)$$

When $M_s = N_r = 1$, (6.14) becomes (6.8).

For complex-valued modulations, such as M-QAM, $\sum_{x \in \mathcal{Q}} x^2 = 0$ according to the symmetric characteristic. (6.13) becomes

$$\lim_{\sigma_1^2 \to \infty} \hat{\mathbf{x}} = \frac{\sum_{x \in \mathcal{Q}} |x|^2}{\sigma_1^2 |\mathcal{Q}|} \mathbf{H}^H \mathbf{r}. \tag{6.15}$$

Let us define $\hat{\mathbf{x}}_{MF} = \mathbf{H}^H \mathbf{r}$. Then, EF becomes a matched filter AF when the transmitted power is very low. Thus, this AF is called the matched filter AF, and the relay function can defined as

$$\mathcal{G}_{MF}(\mathbf{r}) = \frac{P_r}{\mathcal{E}(\|\hat{\mathbf{x}}_{MF}\|^2)} \mathbf{H}^H \mathbf{r}. \tag{6.16}$$

High SNR Case: It is assumed that the ML detection is $\mathbf{x}_{ML}$, which can be obtained by (2.21). For high SNR, by splitting out the ML solution, the MMSE estimate can be derived as

$$
\begin{aligned}
\lim_{\sigma_1^2 \to 0} \hat{\mathbf{x}} &= \lim_{\sigma_1^2 \to 0} \frac{\sum_{\mathbf{x} \in \mathcal{Q}^{M_s}} \mathbf{x} \exp\left(-\frac{\|\mathbf{r} - \mathbf{H}\mathbf{x}\|^2}{\sigma_1^2}\right)}{\sum_{\mathbf{x} \in \mathcal{Q}^{M_s}} \exp\left(-\frac{\|\mathbf{r} - \mathbf{H}\mathbf{x}\|^2}{\sigma_1^2}\right)} \\
&= \lim_{\sigma_1^2 \to 0} \frac{\mathbf{x}_{ML} \exp\left(-\frac{\|\mathbf{r} - \mathbf{H}\mathbf{x}_{ML}\|^2}{\sigma_1^2}\right) + \sum_{\mathbf{x} \in \mathcal{A}} \mathbf{x} \exp\left(-\frac{\|\mathbf{r} - \mathbf{H}\mathbf{x}\|^2}{\sigma_1^2}\right)}{\exp\left(-\frac{\|\mathbf{r} - \mathbf{H}\mathbf{x}_{ML}\|^2}{\sigma_1^2}\right) + \sum_{\mathbf{x} \in \mathcal{A}} \exp\left(-\frac{\|\mathbf{r} - \mathbf{H}\mathbf{x}\|^2}{\sigma_1^2}\right)} \\
&= \lim_{\sigma_1^2 \to 0} \frac{\mathbf{x}_{ML} + \sum_{\mathbf{x} \in \mathcal{A}} \mathbf{x} \exp\left(-\frac{\|\mathbf{r} - \mathbf{H}\mathbf{x}\|^2 - \|\mathbf{r} - \mathbf{H}\mathbf{x}_{ML}\|^2}{\sigma_1^2}\right)}{1 + \sum_{\mathbf{x} \in \mathcal{A}} \exp\left(-\frac{\|\mathbf{r} - \mathbf{H}\mathbf{x}\|^2 - \|\mathbf{r} - \mathbf{H}\mathbf{x}_{ML}\|^2}{\sigma_1^2}\right)},
\end{aligned} \tag{6.17}
$$

where $\mathcal{A} = \{\mathbf{x} \in \mathcal{Q}^{M_s} \text{ except } \mathbf{x}_{ML}\}$. For all $\mathbf{x} \in \mathcal{A}$, it can be found that $\mathbf{x} \neq \mathbf{x}_{ML}$, and the $\|\mathbf{r} - \mathbf{H}\mathbf{x}\|^2 - \|\mathbf{r} - \mathbf{H}\mathbf{x}_{ML}\|^2$ must be greater than 0. In other words, it is lower bounded by $\epsilon > 0$ with probability one as SNR goes to infinity. Therefore, $\lim_{\sigma_1^2 \to 0} \exp\left(-\frac{\|\mathbf{r} - \mathbf{H}\mathbf{x}\|^2 - \|\mathbf{r} - \mathbf{H}\mathbf{x}_{ML}\|^2}{\sigma_1^2}\right) = 0$ is derived. The MMSE estimate thus approximates to

$$\lim_{\sigma_1^2 \to 0} \hat{\mathbf{x}} = \mathbf{x}_{ML}, \tag{6.18}$$

which is in fact DF relaying. Consequently, in the high-SNR region, EF and DF converge.

6.2.3 MSE Analysis

The error rate at the destination is greatly affected by the processed signal of the relay, and the MSE can efficiently indicate the quality of the forwarded signal. There-

fore, the MSE of different relay strategies is analyzed here. In order to facilitate the MSE analysis, the system model is assumed to be

$$\mathbf{r} = \sqrt{\frac{\rho}{M_s}} \mathbf{Hx} + \mathbf{n}, \tag{6.19}$$

where the noise variance $\sigma^2 = 1$, and ρ denotes the SNR of the MIMO system.

AF relaying: As the AF relay transmits a scaled version of the received signal as shown in (2.18), the MSE of AF relay is given as

$$\mathrm{MSE}_{AF} = \mathcal{E}\left[\left\|\mathbf{r} - \sqrt{\frac{\rho}{M_s}} \mathbf{Hx}\right\|^2\right] = \mathcal{E}\left[\|\mathbf{n}\|^2\right] = N_r. \tag{6.20}$$

LMMSE AF relaying: The MSE for this relay can be derived as

$$\begin{aligned} \mathrm{MSE}_{LMMSE} &= \mathcal{E}\left[\|\mathbf{Gr} - \mathbf{x}\|^2\right] \\ &= \mathcal{E}\left[\left\|\sqrt{\frac{\rho}{M_s}} \mathbf{GH} - \mathbf{I}\right\|^2\right] P_s + \mathcal{E}\left[\|\mathbf{G}\|^2\right] N_r, \end{aligned} \tag{6.21}$$

where $\mathbf{G} = \left(\frac{\rho}{M_s} \mathbf{H}^H \mathbf{H} + \mathbf{I}\right)^{-1} \cdot \sqrt{\frac{\rho}{M_s}} \mathbf{H}^H$.

DF relaying: According to (2.21), the MSE may be expressed as the Euclidean distance between the detected symbol and the transmitted symbol:

$$\mathrm{MSE}_{DF} = \mathcal{E}\left[\|\hat{\mathbf{x}}_{ML} - \mathbf{x}\|^2\right], \tag{6.22}$$

where $\hat{\mathbf{x}}_{ML}$ is the symbol detected by the ML algorithm according to (2.21). For MIMO systems, the transmitted symbol $\mathbf{x}$ belongs to $\mathcal{Q}^{M_s}$. Assume $\mathbf{s}_{i,j} \in \mathcal{Q}^{M_s}$, where $i = 1, 2, \ldots, M_s$ and $j = 1, 2, \ldots, |\mathcal{Q}|$. From the union bounding technique [23], the MSE for DF relaying can be derived as

$$\begin{aligned} \mathrm{MSE}_{DF} &= \mathcal{E}\left[\|\hat{\mathbf{x}}_{ML} - \mathbf{x}\|^2\right] \\ &= \sum_{i=1}^{M_s} \sum_{j=1}^{|\mathcal{Q}|} \sum_{\hat{i}=1}^{M_s} \sum_{\hat{j}=1}^{|\mathcal{Q}|} \|\hat{\mathbf{s}}_{\hat{i},\hat{j}} - \mathbf{s}_{i,j}\|^2 P(\mathbf{s}_{i,j} \to \hat{\mathbf{s}}_{\hat{i},\hat{j}}) \\ &= \sum_{i=1}^{M_s} \sum_{j=1}^{|\mathcal{Q}|} \sum_{\hat{i}=1}^{M_s} \sum_{\hat{j}=1}^{|\mathcal{Q}|} \frac{\|\hat{s}_{\hat{j}} - s_j\|^2 P(\mathbf{s}_{i,j} \to \hat{\mathbf{s}}_{\hat{i},\hat{j}})}{M_s |\mathcal{Q}|}, \end{aligned} \tag{6.23}$$

where $s_j, s_{\hat{j}} \in \mathcal{Q}$. In order to obtain the pairwise error probability (PEP), the symbol x is assumed to be drawn from a real constellation $\mathcal{Q}$. The closed form of

this PEP is

$$P(\mathbf{s}_{i,j} \to \hat{\mathbf{s}}_{\hat{i},\hat{j}}) = \mu^{M_s} \sum_{k=1}^{M_s-1} \binom{M_s - 1 - k}{k} (1 - \mu)^k, \qquad (6.24)$$

where $\mu = \frac{1}{2} \left(1 - \sqrt{\frac{\rho(|s_j|^2 + |s_{\hat{j}}|^2)}{4 + \rho(|s_j|^2 + |s_{\hat{j}}|^2)}} \right)$. By plugging (6.24) into (6.23), the MSE closed-form for DF relaying can be rewritten as

$$\begin{aligned}
\mathrm{MSE}_{DF} &= \frac{1}{M_s|\mathcal{Q}|} \sum_{i=1}^{M_s} \sum_{j=1}^{|\mathcal{Q}|} \sum_{\hat{i}=1}^{M_s} \sum_{\hat{j}=1}^{|\mathcal{Q}|} \|\hat{s}_{\hat{j}} - s_j\|^2 \mu^{M_s} \sum_{k=1}^{M_s-1} \binom{M_s - 1 - k}{k} (1 - \mu)^k \\
&= \frac{1}{|\mathcal{Q}|} \sum_{i=1}^{|\mathcal{Q}|} \sum_{j=1}^{|\mathcal{Q}|} M_s \|\hat{s}_{\hat{j}} - s_j\|^2 \mu^{M_s} \sum_{k=1}^{M_s-1} \binom{M_s - 1 - k}{k} (1 - \mu)^k.
\end{aligned}$$
$$(6.25)$$

EF relaying: Based on (6.3) the MSE at the relay can be derived as

$$\begin{aligned}
\mathrm{MSE}_{EF} &= \mathcal{E} \left[\|\hat{\mathbf{x}} - \mathbf{x}\|^2 \right] \\
&= \mathcal{E} \left[\left\| \frac{\sum_{\mathbf{x} \in \mathcal{Q}^{M_s}} \mathbf{x} \exp \left(-\frac{\|\mathbf{r} - \mathbf{H}\mathbf{x}\|^2}{\sigma_1^2} \right)}{\sum_{\mathbf{x} \in \mathcal{Q}^{M_s}} \exp \left(-\frac{\|\mathbf{r} - \mathbf{H}\mathbf{x}\|^2}{\sigma_1^2} \right)} - \mathbf{x} \right\|^2 \right] \\
&\approx \begin{cases} \mathcal{E} \left[\left\| \frac{\sum_{x \in \mathcal{Q}} |x|^2}{\sigma_1^2 |\mathcal{Q}|} \mathbf{H}^H \mathbf{r} - \mathbf{x} \right\|^2 \right] &, \quad \rho \to 0 \\ \mathcal{E} \left[\|\mathbf{x}_{ML} - \mathbf{x}\|^2 \right] &, \quad \rho \to \infty \end{cases}.
\end{aligned}$$

Based on the cyclic permutations property of the trace

$$\mathcal{E} \left[\Re(\mathbf{x}^H \mathbf{H}^H \mathbf{x}) \right] = \mathcal{E} \left[\Re(\mathbf{x}^H \mathbf{H}^H \mathbf{x}) \right] = \mathcal{E} \left[\Re(\mathrm{Tr}(\mathbf{H}^H \mathbf{x}\mathbf{x}^H)) \right] = 0. \qquad (6.26)$$

MSE_{EF} is then derived as

$$\begin{aligned}
\mathrm{MSE}_{EF} &\approx \begin{cases} \lim_{\sigma_1^2 \to \infty} \mathcal{E} \left[\left\| \frac{\sum_{x \in \mathcal{Q}} |x|^2}{\sigma_1^2 |\mathcal{Q}|} \mathbf{H}^H \mathbf{r} \right\|^2 \right] + P_s, \ \rho \to 0 \\ \mathcal{E} \left[\|\mathbf{x}_{ML} - \mathbf{x}\|^2 \right], \ \rho \to \infty \end{cases} \\
&= \begin{cases} \mathrm{MSE}_{AF}, \ \rho \to 0 \\ \mathrm{MSE}_{DF}, \ \rho \to \infty \end{cases}.
\end{aligned}$$
$$(6.27)$$

Therefore, the MSEs of EF and AF relays converge in the low-SNR region, while those of EF and DF relays converge in the high-SNR region. This behaviour is anticipated in Section 6.2.2.

Example 3 (BPSK and $M_s = N_r = 2$): In this case, for a 2×2 MIMO channel, the MSEs of all the relays are compared in Fig. 6.2. As expected, EF is the best
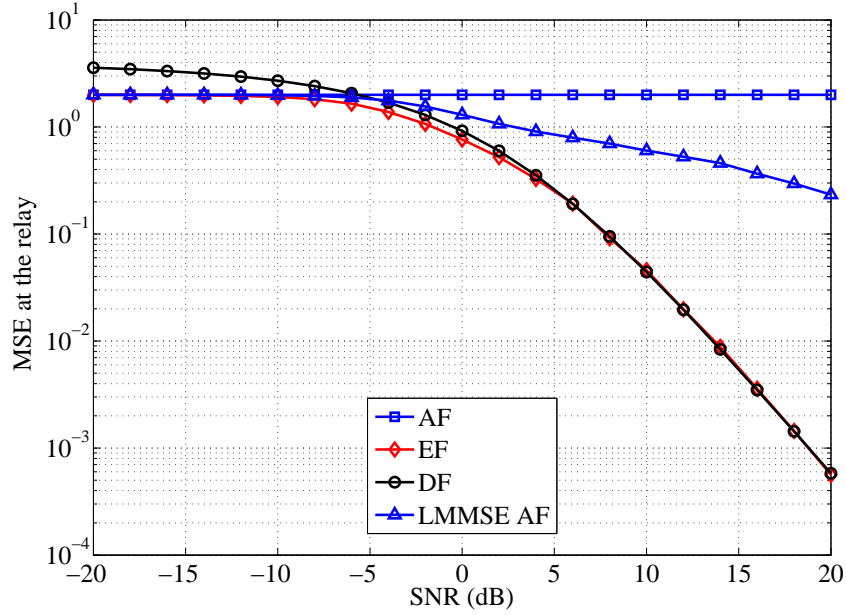
Figure 6.2: MSE at different SNRs for the $M_s = N_r = 2$ BPSK system.

performing scheme. DF performs the worst in the low-SNR region (at less than $-5\,\mathrm{dB}$) but close to the EF scheme in the high-SNR region; the reverse is found for the AF relay scheme. As well, the LMMSE AF relay scheme outperforms AF. Above all, due to its small MSE, the EF relay is expected to yield an optimal performance at the destination.

6.3 Approximate Estimate-and-Forward

According to (6.3), if $|\mathcal{Q}|^{M_s}$ is small, it is easy to compute $\hat{\mathbf{x}}$. However, when $|\mathcal{Q}|^{M_s}$ is large, the direct computation of $\hat{\mathbf{x}}$ in (6.3) is expensive. In this section, two approximate EF relays are proposed for large MIMO systems.

6.3.1 List Estimate-and-Forward

Before introducing list EF, the motivation for this idea will be explained. First the term $\psi = \exp\left(-\frac{\|\mathbf{r}-\mathbf{Hx}\|^2}{\sigma_1^2}\right)$ in (6.3) is analysed. As $\mathbf{n_1}$ is an AWGN, $\frac{\|\mathbf{r}-\mathbf{Hx}\|^2}{\sigma_1^2} \sim \chi^2(M_s)$, which is a chi-square distribution with M_s degrees of freedom. Therefore,

the PDF of ψ can be derived as

$$f_{\Psi}(\psi) = \frac{1}{\psi} \times \frac{(-\log \psi)^{M_s/2-1} \exp(\frac{\log \psi}{2})}{2^{M_s/2}\Gamma(M_s/2)}, \qquad (6.28)$$

where Gamma function $\Gamma(\frac{n}{2}) = \sqrt{\pi}\frac{(n-2)!!}{2^{(n-1)/2}}$. Thus, the probability of $\psi \geq a$ can be obtained as

$$F_{\Psi}(\psi \geq a) = \int_a^1 f_{\Psi}(\psi)d\psi. \qquad (6.29)$$

For example, when $M_s = 2$, $F_{\Psi}(\psi \geq a) = \frac{1-\sqrt{a}}{\Gamma(1)}$. If a is a number close to 1, then the tail probability $F_{\Psi}(\psi \geq a)$ would be small value, suggesting that the probability of a large ψ is very small. The above is the main motivation for developing list EF.

Consequently, most of the terms in the sum of (6.3) are small and contribute very little to the sum, especially in the high-SNR region. Intuitively, one can find a subset of $\mathcal{Q}^{M_s}$ to compute the sum in (6.3). Assume that this subset can be denoted by $\mathcal{L}$, and then (6.3) can be approximated to be

$$\hat{\mathbf{x}} \approx \frac{\sum_{\mathbf{x}\in\mathcal{L}} \mathbf{x}\exp\left(-\frac{\|\mathbf{r}-\mathbf{Hx}\|^2}{\sigma_1^2}\right)}{\sum_{\mathbf{x}\in\mathcal{L}} \exp\left(-\frac{\|\mathbf{r}-\mathbf{Hx}\|^2}{\sigma_1^2}\right)}. \qquad (6.30)$$

In this chapter, the size of the list $N_{\mathcal{L}}$ is used to obtain the trade-offs between the computational accuracy and operations. When $N_{\mathcal{L}}$ is small, $\hat{\mathbf{x}}$ is computed with low running time. In the high-SNR region, because of the limit of the exponential function ($\lim_{x\to-\infty} e^x = 0$),

$$\lim_{P_s\to+\infty} \exp\left(-\frac{\|\mathbf{r}-\mathbf{H\tilde{x}}\|^2}{\sigma_1^2}\right) = \lim_{\sigma^2\to 0} \exp\left(-\frac{\|\mathbf{r}-\mathbf{H\tilde{x}}\|^2}{\sigma_1^2}\right) = 0, \qquad (6.31)$$

where $\tilde{\mathbf{x}} \neq \hat{\mathbf{x}}$. This result means the real $\mathbf{x}$ plays a uniquely important rule in the computation of the MMSE estimate. Specifically, when $N_{\mathcal{L}} = 1$, list EF becomes DF. Therefore, list EF can achieve the exact computation of the MMSE estimate even with a very small set for the high-SNR region.

Computing list $\mathcal{L}$ is the main challenge. The SD [25] reduces the number of computational operations of MIMO detection by performing a search limited to a hypersphere. This approach can also be used to significantly reduce the running

time of detection for coded MIMO systems by adapting the list SD to generate a small list for the iterative detection and decoding process [10].

In this chapter, list SD is utilized for the EF MIMO relay. The SD generates a list of $\mathbf{x}$ satisfying $\|\mathbf{r} - \mathbf{H}\mathbf{x}\|^2 \leq d^2$. Intuitively, the constraint radius d^2 can be defined to be $d^2 = -\sigma_1^2 \ln a, (0 < a < 1)$ based on (6.29). Therefore, the list size can be controlled via a, which gives a trade-off between the estimation accuracy and running time. Another more effective method of controlling the list size is to predefine the list size $N_{\mathcal{L}}$. This method is used in this chapter.

The process of generating the list is similar to that for the list SD in [10, 32]. This process is shown below for completeness:

1. Set the initial radius to be ∞, keep the first $N_{\mathcal{L}}$ nodes in the list $\mathcal{L}$, and update the radius to be the smallest cost of the existing leaf nodes.

2. When the list is full, compare the cumulative cost of the next node in the hypersphere with the largest cost in the list; then keep the node with a smaller cost; otherwise, remove the node from the list.

3. At the end of the search process, a list with $N_{\mathcal{L}}$ nodes having the smallest costs is obtained.

After obtaining the $\hat{\mathbf{x}}$ by using (6.30), the relay function can be given as

$$\mathcal{G}_{EF}(\mathbf{r}) = \beta \frac{\sum_{\mathbf{x} \in \mathcal{L}} \mathbf{x} \exp\left(-\frac{\|\mathbf{r} - \mathbf{H}\mathbf{x}\|^2}{\sigma_1^2}\right)}{\sum_{\mathbf{x} \in \mathcal{L}} \exp\left(-\frac{\|\mathbf{r} - \mathbf{H}\mathbf{x}\|^2}{\sigma_1^2}\right)}, \tag{6.32}$$

where β can be derived by using (6.4). Thus, the scaled MMSE estimation at the relay will be retransmitted to the destination.

Example 4 (16-QAM and $M_s = N_r = M_r = N_d = 2$): In this case, the list size is assumed to be 16 for the proposed list EF. However, for the exact MMSE at the relay, there are $\mathcal{Q}^{M_s} = 16^2 = 256$ elements, where the 16-QAM constellation

$$\mathcal{Q} = \left\{ \frac{1}{\sqrt{10}}(a + bi), \quad a, b \in \{-3, -1, 1, 3\} \right\}.$$

By using the sphere decoder, list EF chooses only the size-16 subset of $\mathcal{Q}^{M_s}$ having the smaller costs of $\|\mathbf{r} - \mathbf{H}\mathbf{x}\|^2$. For a random generated channel matrix $\mathbf{H} = \frac{1}{\sqrt{2}}[h_{11}, h_{12}; h_{21}, h_{22}]$, where $h_{ij} \sim \mathcal{CN}(0, 1)$ with $i, j \in \{1, 2\}$ ($\mathbf{H} =$
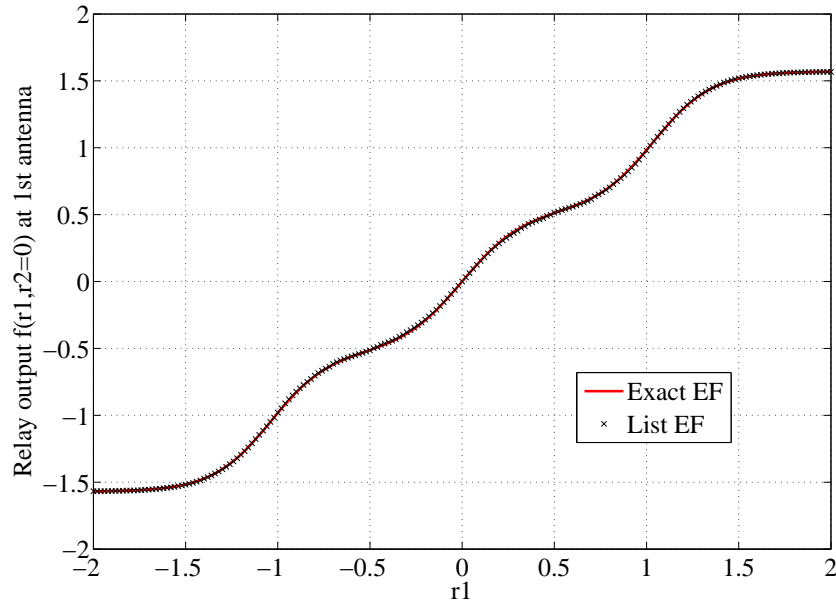
Figure 6.3: The real part of relay functions at one of the relay antennas when $\text{SNR} = 10\,\text{dB}$ for the $N_r = 2$, 16-QAM system.

$[1.0036 - 0.5688i, 0.1398 + 0.5904i; 0.2061 + 0.4925i, 1.1226 - 0.1723i])$, the relay functions of list EF and exact EF for an SNR of $10\,\text{dB}$ are shown in Fig. 6.3, where the y-axis is the real part of the transmitted signal at the first antenna of the relay. Fig. 6.3 shows that list EF and exact EF have virtually identical relay functions. This observation confirms that our proposed list EF efficiently computes the MMSE estimation while achieving the performance of the exact EF relay.

6.3.2   Gaussian EF

To reduce the number of computational operations of the MMSE estimation at the relay, another approximate method is proposed here. The high number of computational operations is due to the discrete sum in (6.3) needing $|\mathcal{Q}|^{M_s}$ terms to be computed. Instead of computing $\mathbf{x}$ in (6.3) vector-by-vector, it is proposed to compute $\hat{\mathbf{x}} = [\hat{x}_1, \hat{x}_2, \ldots \hat{x}_{M_s}]$ entry-by-entry for large systems. Thus, the MMSE

estimation at the relay can be rewritten as

$$\hat{x}_i = E(x_i|\mathbf{r}, \mathbf{H}) = \frac{\sum_{x_i \in \mathcal{Q}} x_i \sum_{\mathbf{x}_{-\mathbf{i}} \in \mathcal{Q}^{M_s-1}} \exp\left(-\frac{\|\mathbf{r}-\mathbf{Hx}\|^2}{\sigma_1^2}\right)}{\sum_{x_i \in \mathcal{Q}} \sum_{\mathbf{x}_{-\mathbf{i}} \in \mathcal{Q}^{M_s-1}} \exp\left(-\frac{\|\mathbf{r}-\mathbf{Hx}\|^2}{\sigma_1^2}\right)}$$

$$= \frac{\sum_{x_i \in \mathcal{Q}} x_i \sum_{\mathbf{x}_{-\mathbf{i}} \in \mathcal{Q}^{M_s-1}} \exp\left(-\frac{\|\mathbf{r}-\mathbf{H}_{-\mathbf{i}}\mathbf{x}_{-\mathbf{i}}-\mathbf{h}_{\mathbf{i}}x_i\|^2}{\sigma_1^2}\right)}{\sum_{x_i \in \mathcal{Q}} \sum_{\mathbf{x}_{-\mathbf{i}} \in \mathcal{Q}^{M_s-1}} \exp\left(-\frac{\|\mathbf{r}-\mathbf{H}_{-\mathbf{i}}\mathbf{x}_{-\mathbf{i}}-\mathbf{h}_{\mathbf{i}}x_i\|^2}{\sigma_1^2}\right)}, \quad (6.33)$$

where $\mathbf{x}_{-i}$ denotes the vector containing all the other entries except x_i.

The sums in the numerator and denominator are hard to compute if $|\mathcal{Q}|^{M_s}$ is large. In this chapter, the second sum in the denominator and numerator of (6.33) can be approximated by an integral. This approximation can be accurate, especially for high-order constellations and large antenna systems. (6.33) is thus approximated as

$$\hat{x}_i \approx \frac{\sum_{x_i \in \mathcal{Q}} x_i \int \exp\left(-\frac{\|\mathbf{x}_{-\mathbf{i}}\|^2}{\sigma_x^2}\right) \exp\left(-\frac{\|\mathbf{r}-\mathbf{H}_{-\mathbf{i}}\mathbf{x}_{-\mathbf{i}}-\mathbf{h}_{\mathbf{i}}x_i\|^2}{\sigma_1^2}\right) d\mathbf{x}_{-\mathbf{i}}}{\sum_{x_i \in \mathcal{Q}} \int \exp\left(-\frac{\|\mathbf{x}_{-\mathbf{i}}\|^2}{\sigma_x^2}\right) \exp\left(-\frac{\|\mathbf{r}-\mathbf{H}_{-\mathbf{i}}\mathbf{x}_{-\mathbf{i}}-\mathbf{h}_{\mathbf{i}}x_i\|^2}{\sigma_1^2}\right) d\mathbf{x}_{-\mathbf{i}}}. \quad (6.34)$$

The conventional MMSE estimation requires the sum over all the $|\mathcal{Q}|^{M_s}$ terms, while only $|\mathcal{Q}|$ elements in the constellation are summed by using the proposed integral approximation as shown in (6.34). In a MIMO system with a large constellation, Gaussian approximations are common [109], allowing for the closed-form evaluation of the integrals. Assuming $\mathbf{x}_{-\mathbf{i}}$ to be a Gaussian vector with mean zero and matched variance σ_x^2 derived from the constellation, the finite sum in (6.33) can be replaced by an integration as shown in (6.34), where the integral can be derived by using the vector integration.

For Gaussian vector $\mathbf{x}$, it is known that

$$\int \exp\left[-\frac{1}{2}(\mathbf{x}-\mathbf{m})^H \mathbf{\Sigma}^{-1}(\mathbf{x}-\mathbf{m})\right] d\mathbf{x} = \sqrt{\det(2\pi\mathbf{\Sigma})}. \quad (6.35)$$

By using the integration of the Gaussian vector in (6.35) and decomposition and combination of the vectors, the integration in (6.34) can be derived in a closed-form, which leads to

$$\hat{x}_i = \frac{\sum_{x_i \in \mathcal{Q}} x_i \left[\sqrt{\det\left(\pi\sigma_1^2\sigma_x^2\mathbf{A}^{-1}\right)} \exp\left(-\frac{\|\mathbf{h}_{\mathbf{i}}x_i\|^2}{\sigma_1^2} - \frac{\mathbf{C}-(\mathbf{A}^{-1}\mathbf{B}^{\mathbf{H}})^H \mathbf{A}(\mathbf{A}^{-1}\mathbf{B}^{\mathbf{H}})}{\sigma_x^2\sigma_1^2}\right)\right]}{\sum_{x_i \in \mathcal{Q}} \left[\sqrt{\det\left(\pi\sigma_1^2\sigma_x^2\mathbf{A}^{-1}\right)} \exp\left(-\frac{\|\mathbf{h}_{\mathbf{i}}x_i\|^2}{\sigma_1^2} - \frac{\mathbf{C}-(\mathbf{A}^{-1}\mathbf{B}^{\mathbf{H}})^H \mathbf{A}(\mathbf{A}^{-1}\mathbf{B}^{\mathbf{H}})}{\sigma_x^2\sigma_1^2}\right)\right]},$$

$$(6.36)$$

where

$$
\begin{aligned}
\mathbf{A} &= \sigma_1^2 \mathbf{I} + \sigma_x^2 \mathbf{H_{-i}}^H \mathbf{H_{-i}} \\
\mathbf{B} &= \sigma_x^2 \left(\mathbf{r} - \mathbf{h_i} x_i \right)^H \mathbf{H_{-i}} \\
\mathbf{C} &= \sigma_x^2 \left(\mathbf{r}^H \mathbf{r} - \mathbf{r}^H \mathbf{h_i} x_i - \left(\mathbf{h_i} x_i \right)^H \mathbf{r} \right).
\end{aligned}
\tag{6.37}
$$

Similarly, all the estimations of the symbol $\hat{x}_i$ in the $\hat{\mathbf{x}} = [\hat{x}_1, \hat{x}_2, \dots \hat{x}_{M_s}]^T$ can be derived by using (6.36). After deriving $\hat{\mathbf{x}}$, the relay function can be given as

$$
\mathcal{G}_{EF}(\mathbf{r}) = \beta \hat{\mathbf{x}},
\tag{6.38}
$$

where β is a scaling factor satisfying the transmit power constraint at the relay and can also be derived according to (6.4).

Example 5 (BPSK and $M_s = N_r = M_r = N_d = 2$): In this example, the relay function of Gaussian approximation EF is discussed. It is assumed that $\sigma_x^2 = 1$, $\mathbf{H} = [\mathbf{h_1}, \mathbf{h_2}] = \mathbf{I}_2$, $\mathcal{Q} = \{-1, 1\}$ and a real-valued system. As shown in (6.11), the received signal at the relay is

$$
\mathbf{r} = \begin{bmatrix} \mathbf{h_1} & \mathbf{h_2} \end{bmatrix} \begin{bmatrix} x_1 \\ x_2 \end{bmatrix} + \begin{bmatrix} n_1 \\ n_2 \end{bmatrix},
\tag{6.39}
$$

where $\mathbf{h_1} = \begin{bmatrix} 1 \\ 0 \end{bmatrix}$, $\mathbf{h_2} = \begin{bmatrix} 0 \\ 1 \end{bmatrix}$ and $\mathbf{r} = \begin{bmatrix} r_1 \\ r_2 \end{bmatrix}$. According to (6.36), the closed-from of EF function is given by

$$
\begin{aligned}
\hat{x}_i &= \frac{\sum_{x_i \in \mathcal{Q}} x_i \left[\sqrt{\det \left(2\pi \sigma_1^2 \sigma_x^2 \mathbf{A}^{-1} \right)} \exp \left(-\frac{\|x_i\|^2}{2\sigma_1^2} - \frac{\mathbf{C} - (\mathbf{A}^{-1}\mathbf{B^H})^H \mathbf{A}(\mathbf{A}^{-1}\mathbf{B^H})}{2\sigma_1^2} \right) \right]}{\sum_{x_i \in \mathcal{Q}} \left[\sqrt{\det \left(2\pi \sigma_1^2 \sigma_x^2 \mathbf{A}^{-1} \right)} \exp \left(-\frac{\|x_i\|^2}{2\sigma_1^2} - \frac{\mathbf{C} - (\mathbf{A}^{-1}\mathbf{B^H})^H \mathbf{A}(\mathbf{A}^{-1}\mathbf{B^H})}{2\sigma_1^2} \right) \right]} \\
&= \frac{\exp \left(-\frac{1 + r_1^2 + r_2^2 - 2r_1 - \frac{r_2^2}{\sigma_1^2 + 1}}{2\sigma_1^2} \right) - \exp \left(-\frac{1 + r_1^2 + r_2^2 + 2r_2 - \frac{r_1^2}{\sigma_1^2 + 1}}{2\sigma_1^2} \right)}{\exp \left(-\frac{1 + r_1^2 + r_2^2 - 2r_1 - \frac{r_2^2}{\sigma_1^2 + 1}}{2\sigma_1^2} \right) + \exp \left(-\frac{1 + r_1^2 + r_2^2 + 2r_2 - \frac{r_1^2}{\sigma_1^2 + 1}}{2\sigma_1^2} \right)},
\end{aligned}
\tag{6.40}
$$

where

$$
A = \sigma_1^2 + 1, \quad B = r_{-i}^H, \quad C = r_1^2 + r_2^2 - r_i(x_i + x_i^H).
$$

Example 6 (16-QAM and $M_s = N_r = M_r = N_d = 2$): Fig. 6.4 compares the relay functions of the proposed Gaussian EF and the exact EF for a $10\,\mathrm{dB}$
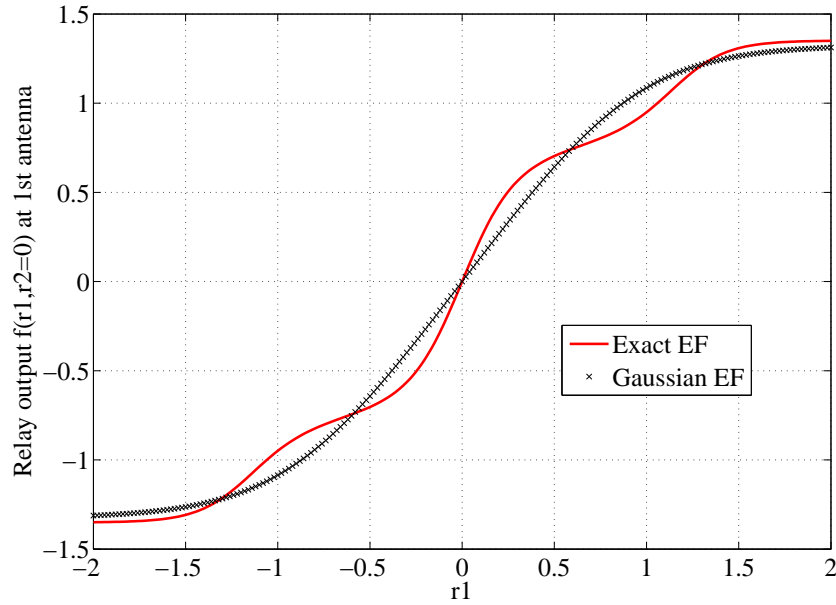
Figure 6.4: The relay functions at one of the relay antennas when $\mathrm{SNR} = 10\,\mathrm{dB}$ for the $N_r = 2$, BPSK system.

SNR and a random generated channel matrix $\mathbf{H} = [0.0852 - 0.3322i, 0.8470 - 0.9795i; -0.7000 + 0.6268i, -0.4191 - 1.3836i]$. Note that the Gaussian EF approximately coincides with the exact EF relay, while computing only 16 summations instead of $16^2 = 256$ for the exact EF.

6.4 EF in Two-Way Relay Networks
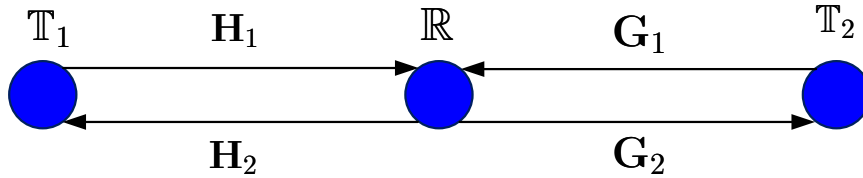
Figure 6.5: A two-way relay system model.

A two-way relay network [110–113] is illustrated in Fig 6.5, where the first terminal node $\mathbb{T}_1$ has $N_{T1} \geq 1$ antennas, the relay $\mathbb{R}$ has $N_r \geq 1$ receive antennas, and $M_r \geq 1$ transmit antennas, and the second terminal node $\mathbb{T}_2$ has $N_{T2} \geq 1$

103

antennas. For simplicity, we assume only one relay in this two-way relay network, where the two terminals exchange information via the relay.

In the first time slot, the two terminals send the transmitted signal to the relay at the same time. The relay receives the transmitted signal from both $\mathbb{T}_1$ and $\mathbb{T}_2$. This signal can be given as

$$\mathbf{r} = \mathbf{H}_1\mathbf{x}_1 + \mathbf{G}_1\mathbf{x}_2 + \mathbf{n}, \tag{6.41}$$

where $\mathbf{H}_1 = [h_{ij}] \in \mathcal{C}^{N_r \times N_{T1}}$ and $\mathbf{G}_1 = [h_{ij}] \in \mathcal{C}^{N_r \times N_{T2}}$ denotes the MIMO channel between $\mathbb{T}_1$ and $\mathbb{R}$ and between $\mathbb{T}_2$ and $\mathbb{R}$, respectively. The elements of $\mathbf{H}_1$ and $\mathbf{G}_1$ are i.i.d. complex Gaussian ($h_{ij}, g_{ij} \sim \mathcal{CN}(0,1)$); $\mathbf{n} = [n_1, n_2, \ldots n_{N_r}]^T$, and $n_i \sim \mathcal{CN}(0, \sigma^2)$ ($i = 1, 2, \ldots, N_r$) is an AWGN with mean zero and variance σ^2; The transmitted signals at $\mathbb{R}_1$ and $\mathbb{R}_2$ are denoted by $\mathbf{x}_1 = [x_{11}, x_{12}, \ldots, x_{1N_{T1}}]^T$ and $\mathbf{x}_2 = [x_{21}, x_{22}, \ldots, x_{2N_{T2}}]^T$, respectively. We also assume each transmitted symbol is chosen from the same constellation; i.e., $x_{ij} \in \mathcal{Q}$ ($i = 1, 2$), and the average transmitted power is $\mathcal{E}[\|\mathbf{x_i}\|^2] = P_t$, where P_t is the transmitted power, and $\mathcal{E}(x)$ is the expectation of x.

In the second time slot, a memoryless relay receives the signals from $\mathbb{T}_1$ and $\mathbb{T}_2$ and generates and transmits the processed signal to the opposite terminal. Its relay function $\mathcal{G}(\mathbf{r})$ uses the current received signal $\mathbf{r}$ only. With the assumption of the relay average power P_r, the transmitted signal $\mathcal{G}(\mathbf{r})$ should satisfy the power constraint $\mathcal{E}[\|\mathcal{G}(\mathbf{r})\|^2] = P_r$. Therefore, after the relay retransmits the processed signals, the received signal at $\mathbb{T}_1$ and $\mathbb{T}_2$ may be written as

$$\mathbf{y}_1 = \mathbf{H}_2\mathcal{G}(\mathbf{r}) + \mathbf{n_1}, \tag{6.42}$$

$$\mathbf{y}_2 = \mathbf{G}_2\mathcal{G}(\mathbf{r}) + \mathbf{n_2}, \tag{6.43}$$

respectively, where $\mathbf{H}_2 = [h_{ij}] \in \mathcal{C}^{N_{T1} \times M_r}$ and $\mathbf{G}_2 = [g_{ij}] \in \mathcal{C}^{N_{T2} \times M_r}$ denote the MIMO channel between $\mathbb{R}$ and $\mathbb{T}_1$ and between $\mathbb{R}$ and $\mathbb{T}_2$, respectively. The elements of $\mathbf{H}_2$ and $\mathbf{G}_2$ are i.i.d. complex Gaussian, and $\mathbf{n_1} = [n_{11}, n_{12}, \ldots n_{1N_{T1}}]^T$ and $\mathbf{n_2} = [n_{21}, n_{22}, \ldots n_{2N_{T2}}]^T$ ($n_{ij} \sim \mathcal{CN}(0, \sigma_1^2)$).

EF Relay Function: Based on Section 6.2.1, the MMSE estimate of the re-

ceived signal $\mathbf{r}$ at the relay may be given as

$$
\begin{aligned}
\hat{\mathbf{r}} &= \mathcal{E}(\mathbf{H}_1\mathbf{x}_1 + \mathbf{G}_1\mathbf{x}_2|\mathbf{r}) \\
&= \sum_{\mathcal{A}} (\mathbf{H}_1\mathbf{x}_1 + \mathbf{G}_1\mathbf{x}_2) \, P(\mathbf{H}_1\mathbf{x}_1 + \mathbf{G}_1\mathbf{x}_2|\mathbf{r}) \\
&= \frac{\sum_{\mathcal{A}} (\mathbf{H}_1\mathbf{x}_1 + \mathbf{G}_1\mathbf{x}_2) \, f(\mathbf{r}|\mathbf{x}_1, \mathbf{x}_2, \mathbf{H}_1, \mathbf{G}_1)}{\sum_{\mathcal{A}} f(\mathbf{r}|\mathbf{x}_1, \mathbf{x}_2, \mathbf{H}_1, \mathbf{G}_1)},
\end{aligned}
\tag{6.44}
$$

where $\mathcal{A}$ is the set of satisfying $\mathbf{x}_1 \in \mathcal{Q}^{N_{T1}}$ and $\mathbf{x}_2 \in \mathcal{Q}^{N_{T2}}$. $f(\mathbf{r}|\mathbf{x}_1, \mathbf{x}_2, \mathbf{H}_1, \mathbf{G}_1)$ is the PDF of $\mathbf{r}$ conditional on $\mathbf{x}_1$, $\mathbf{x}_2$, $\mathbf{H}_1$ and $\mathbf{G}_1$. Because the addition noise vector is i.i.d Gaussian, the PDF $f(\mathbf{r}|\mathbf{x}_1, \mathbf{x}_2, \mathbf{H}_1, \mathbf{G}_1)$ may be written as

$$
\begin{aligned}
&f(\mathbf{r}|\mathbf{x}_1, \mathbf{x}_2, \mathbf{H}_1, \mathbf{G}_1) \\
&= \frac{1}{(\pi\sigma^2)^{N_{T1}+N_{T2}}} \exp\left(-\frac{\|\mathbf{r} - \mathbf{H}_1\mathbf{x}_1 - \mathbf{G}_1\mathbf{x}_2\|^2}{\sigma^2}\right).
\end{aligned}
\tag{6.45}
$$

The EF relay computes the MMSE estimate

$$
\hat{\mathbf{r}} = \frac{\sum_{\mathcal{A}} (\mathbf{H}_1\mathbf{x}_1 + \mathbf{G}_1\mathbf{x}_2) \exp\left(-\frac{\|\mathbf{r} - \mathbf{H}_1\mathbf{x}_1 - \mathbf{G}_1\mathbf{x}_2\|^2}{\sigma^2}\right)}{\sum_{\mathcal{A}} \exp\left(-\frac{\|\mathbf{r} - \mathbf{H}_1\mathbf{x}_1 - \mathbf{G}_1\mathbf{x}_2\|^2}{\sigma^2}\right)}.
\tag{6.46}
$$

As with AF and DF relaying, to satisfy the relay power constraint, the scaling factor is given by

$$
\beta = \sqrt{\frac{P_r}{\mathcal{E}(\|\hat{\mathbf{r}}\|^2)}} = \sqrt{\frac{P_r}{\int_{-\infty}^{\infty} \|\hat{\mathbf{r}}\|^2 f(\mathbf{r}) d\mathbf{r}}}.
\tag{6.47}
$$

By using the total probability law, the PDF of the received signal $\mathbf{r}$ can be derived as

$$
\begin{aligned}
f(\mathbf{r}) &= \sum_{\mathcal{A}} f(\mathbf{r}|\mathbf{x}) P(\mathbf{x}) \\
&= \sum_{\mathcal{A}} \frac{1}{(\pi\sigma^2|\mathcal{Q}|)^{N_{T1}+N_{T2}}} \exp\left(-\frac{\|\mathbf{r} - \mathbf{H}\mathbf{x}\|^2}{\sigma^2}\right),
\end{aligned}
\tag{6.48}
$$

where $\mathbf{x} = [\mathbf{x}_1; \mathbf{x}_2]$ and $\mathbf{H} = [\mathbf{H}_1\mathbf{G}_1]$. Thus, the relay retransmits the scaled version of MMSE estimate $\beta\hat{\mathbf{x}}$ to the destination. The EF relay function is therefore

$$
\mathcal{G}_{EF}(\mathbf{r}) = \sqrt{\frac{P_r}{\int_{-\infty}^{\infty} \|\hat{\mathbf{r}}\|^2 f(\mathbf{r}) d\mathbf{r}}} \times \hat{\mathbf{r}}.
\tag{6.49}
$$

Similarly, the list EF can also be extended and applied to reduce the running time in large MIMO two-way relay networks. In this thesis, we have omitted the details.

105

6.5 Simulation Results

In this section, the performance measured by SER is compared for different strategies (the proposed list EF, DF, AF, LMMSE AF, and matched filter AF), where the power at the source and the relay are equal ($P_s = P_r$) and noise variance $\sigma_1^2 = \sigma_2^2$. At the destination, the received signal (2.17) is decoded by using the SD [21]. The list size of the proposed list EF is chosen to be 4 for comparison where necessary.

One-way Relay Networks:
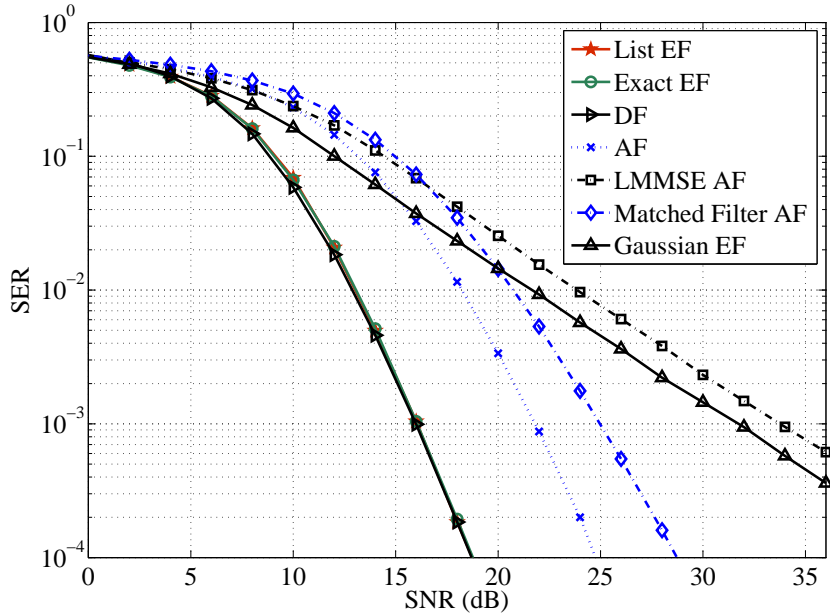
Figure 6.6: Error performance in a 4×4 MIMO relay system with 4-QAM.

Firstly, The SER performance of different relay strategies is given for a 4×4 4-QAM MIMO relay network in Fig. 6.6. The three proposed EF relay schemes are compared with the classical DF and AF schemes. According to Section 6.2.1, exact EF needs to compute all the $4^4 = 256$ terms in $\mathcal{Q}^{M_s}$. In contrast, list EF (4 terms) and Gaussian EF (4 terms) significantly reduce the number of computational operations. Interestingly, list EF outperforms Gaussian EF. Further, in the low-SNR region, list EF achieves a similar performance to that of AF, LMMSE AF and the matched filter AF, and this finding agrees with the result in (6.15). Both AF and matched filter AF achieve the full diversity order 4 in the high-SNR region.

Moreover, the full diversity order is also achieved by list EF, exact EF and the DF relay. However, the full diversity order cannot be obtained by LMMSE and Gaussian AF, both of which obtain diversity order 1. This loss may be caused by the low quality of the forwarded signal at the relay. Interestingly, Gaussian EF outperforms LMMSE AF by $2\,\text{dB}$. However, the proposed List EF outperforms all the AFs. For example, at an SER of 10^{-3}, list EF gains $6.5\,\text{dB}$, $9\,\text{dB}$ and $18\,\text{dB}$ over the pure AF, matched filter AF and LMMSE AF, respectively. These observations confirm the benefits of the list EF relay.
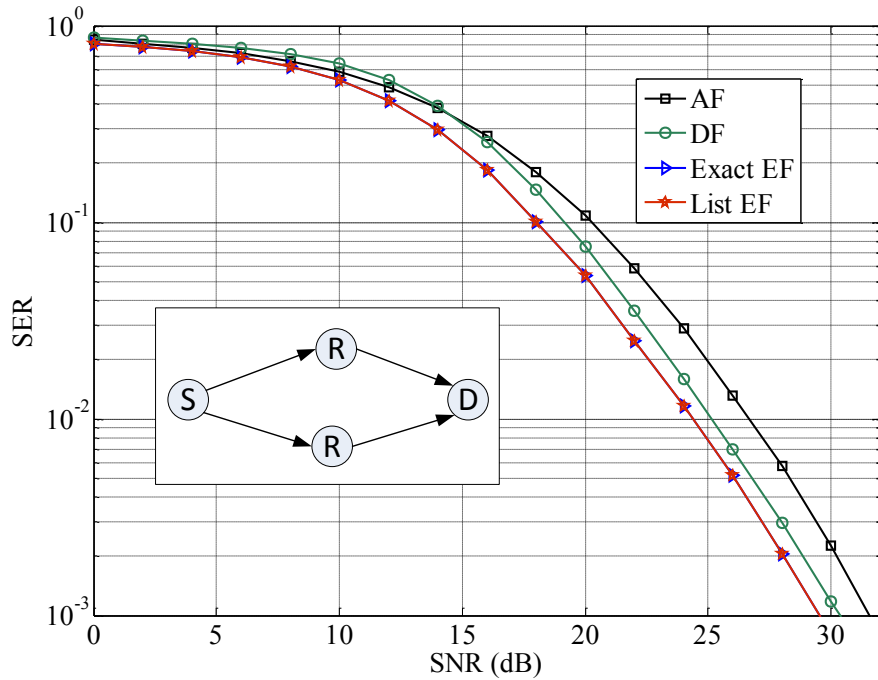
Figure 6.7: Error performance in a parallel 2×2 MIMO relay network with 16-QAM.

In this chapter, the advantages of single EF relay networks have been shown, but their extension to parallel multiple EF relay networks is straightforward. Furthermore, while DF suffers severe performance degradation, the soft EF provides a better performance. In order to verify this performance gain, the simulation results for a two-relay network are provided in Fig. 6.7, which compares the SER of list EF, Exact EF, AF and DF. Note that list EF performs very close to exact EF. Fur-

thermore, at an SER of 10^{-3}, both the exact and list EF gain $1\,\mathrm{dB}$ and $2\,\mathrm{dB}$ over the DF and AF relay strategies, respectively. Reliable soft information thus helps to achieve performance gains even over AF and DF in parallel relay networks, and this advantage will increase with the number of relays.
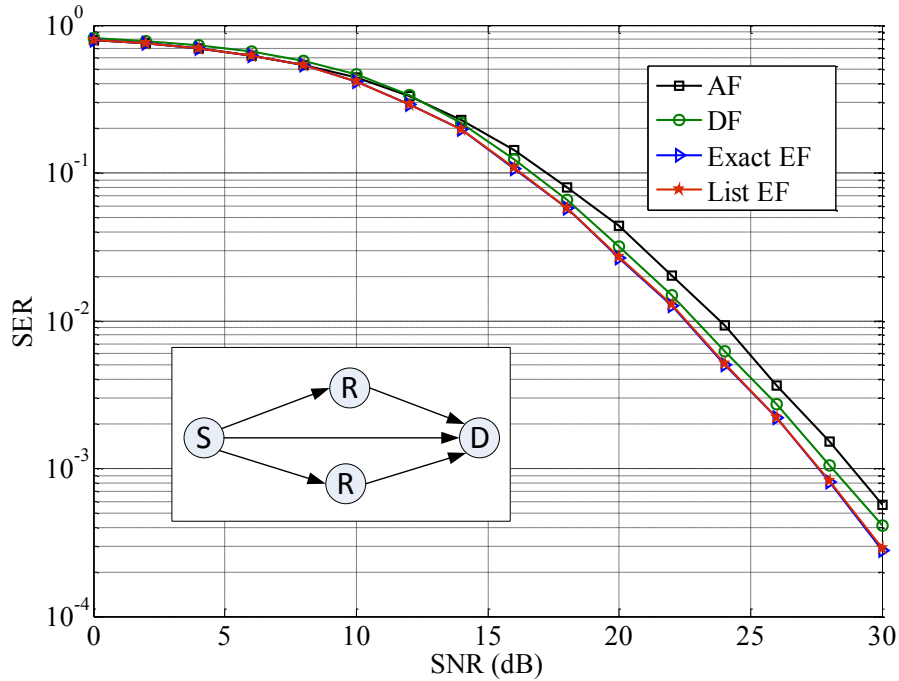
Figure 6.8: Error performance in a parallel 2×2 MIMO relay network with direct link and 16-QAM.

As an example of a collaborative relay network, a two-relay parallel network with direct link is represented in Fig. 6.8. The two relays are assumed to be at the middle point between the source and destination ($d_{sr} = d_{rd} = 0.5 \times d_{sd}$), and the path loss exponent $\alpha = 3$. As discussed in Section 6.2, the case with a direct link outperforms the case without a direct link (Fig. 6.7). However, the achieved performance gain by the proposed EF scheme is smaller than that for the case without a direct link. That is, for an SER of 10^{-3}, both the exact EF and list EF obtain $0.5\,\mathrm{dB}$ and $1.3\,\mathrm{dB}$ performance gains over the DF and AF relay case, respectively, because the direct link brings more reliable information for the destination here.
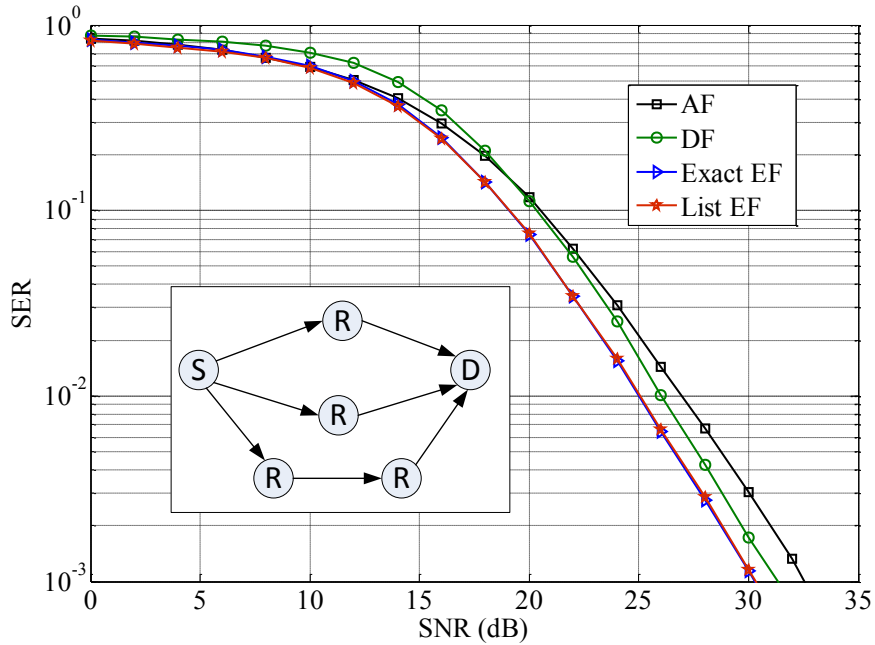
Figure 6.9: Error performance in a hybrid 2×2 MIMO relay network with 16-QAM.

For a collaborative relaying case (a hybrid relay network), the SER of the proposed EF is demonstrated in Fig. 6.9. The system now has three parallel paths, and the last path consists of 2 serial relay nodes. Clearly, from this figure, the proposed list EF and exact EF perform identically, and outperform AF and DF with $2.5\,\mathrm{dB}$ and $1\,\mathrm{dB}$ at an SER of 10^{-3}, respectively. Furthermore, AF performs better than DF in the low-SNR region ($\mathrm{SNR} \leq 19\,\mathrm{dB}$), while the reverse is true for high SNRs. However, the proposed EF and list EF strategies always achieve a better performance than AF and DF for all SNRs.

The above simulation results show that the exact EF relay outperforms DF and AF in all SNRs for the large MIMO relay networks. Moreover, even the proposed list EF performs almost identically to exact EF. Although the proposed Gaussian EF performs below list EF, it offers another option for reducing the number of computational operations of the relay. Finally, the advantage of EF is that switching between AF and DF as SNR changes is unnecessary. A unified algorithm works for all cases.

EF in two-way relays: In this section, the performances measured by SER for

different strategies (the proposed list EF, EF, DF, and AF) are compared in SISO and MIMO two-way relay networks, where the power at the source and the relay are equal ($P_t = P_r$), and the noise variance $\sigma^2 = \sigma_1^2 = \sigma_2^2$. At the second terminal, the received signal (6.42) is decoded by using the sphere detection method [24]. We choose the list size of the proposed list EF to be 4.
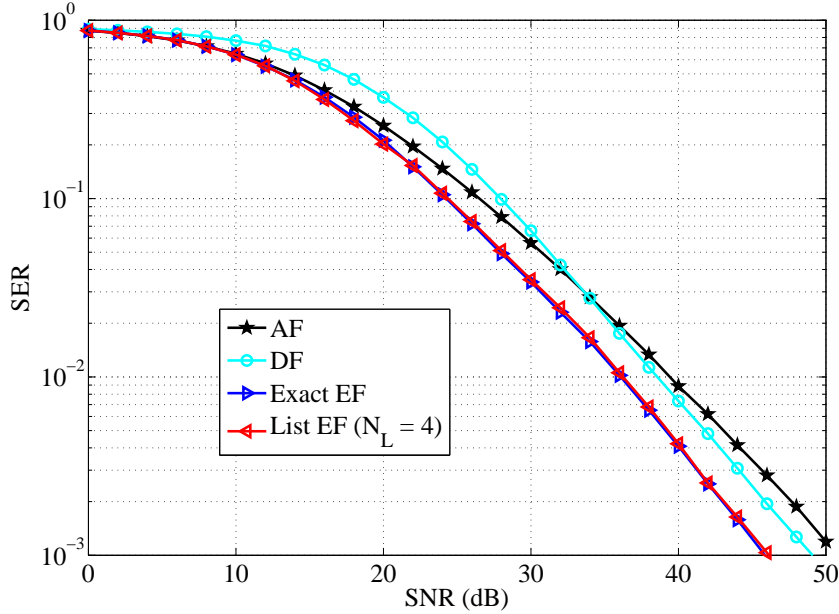
Figure 6.10: Error performance in a single antenna two-way relay network with 16-QAM.

First, the SER performance for a SISO two-way relay system with a 16 QAM is given in Fig. 6.10, which compares the proposed EF relay with the classical relays (AF and DF) for different SNRs. As expected, both list EF and exact EF all achieve performance gains over DF and AF. For example, at an $\mathrm{SER} = 10^{-2}$, the proposed exact EF gains $2\,\mathrm{dB}$ and $3\,\mathrm{dB}$ over the DF and AF relay, respectively. Furthermore, the proposed exact EF needs to compute all the $16^2 = 256$ terms in $\mathcal{Q}^{N_{T1}+N_{T2}}$, while list EF computes only 4 terms. Nevertheless, list EF performs approximately the same as exact EF over all SNRs. Therefore, although list EF generates only an approximate MMSE estimate, its performance is excellent, and its number of computational operations is low. Another interesting observation is that AF outperforms DF in the low-SNR region, while it performs worse than DF

in the high-SNR region. However, the proposed two EF strategies obtain the best SER performance for all SNRs without switching algorithms.
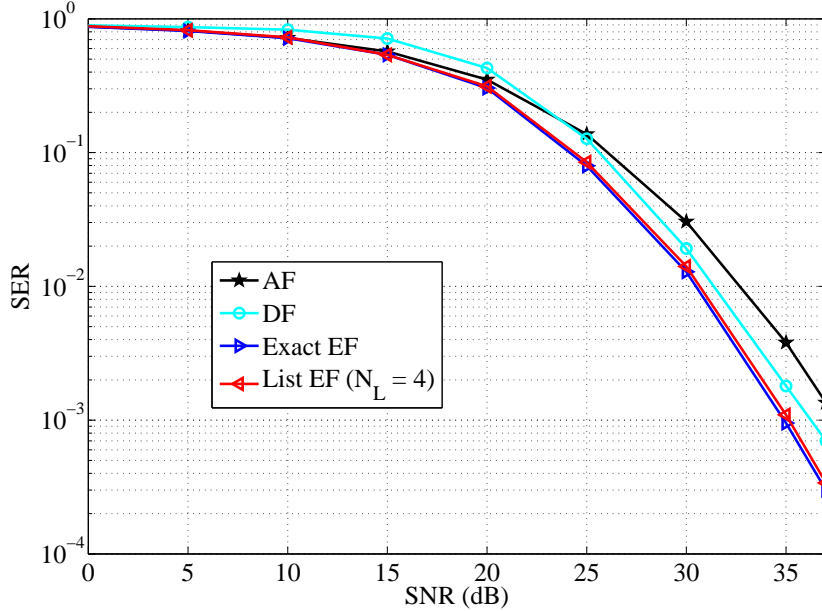
Figure 6.11: Error performance in a 2×2 two-way relay network, with 16-QAM.

In order to evaluate the benefits of the proposed EF relay for MIMO two-way relay networks. The SER performance of different relay strategies for a 2×2 16-QAM relay network is given in Fig. 6.11. The two proposed EF relay schemes are compared with the classical DF and AF schemes. Exact EF needs to compute all $16^{2+2} = 65536$ terms. In contrast, list EF (4 terms) significantly reduces the number of computational operations. Note that EF outperforms the DF and AF strategies. For example, at an $\mathrm{SER} = 10^{-3}$, EF gains $1.5\,\mathrm{dB}$ and $3\,\mathrm{dB}$ over DF and AF, respectively. Furthermore, with a small list size $N_{\mathcal{L}} = 4$, list EF approaches the performance of exact EF with $N_{\mathcal{L}} = 65536$ with negligible performance loss.

6.6   Conclusions

For MIMO one-way and two-way relay networks, this chapter proposed an estimate-and-forward (EF) relay strategy. The transfer characteristics of the EF relay and its MSE were analysed, showing its minimum MSE compared to that of AF and DF

for all SNRs. It was shown that this relay performed similarly to AF and DF in the low and high SNR regions. With a large number of antennas and/or high-order constellations, two approximate EF relays were also proposed to reduce the number of computational operations:

1. **List EF**: This relay uses the sphere decoder for generating the reduced list. Thus, its number of the computational operations is reduced, especially for large MIMO relay networks, while it attains nearly the performance of the exact EF relay. Consequently, it offers a flexible trade-off between accuracy and computational operations.

2. **Gaussian EF**: In exact EF, the estimate (6.3) is based on all the vectors $\mathbf{x} \in \mathcal{Q}^{M_s}$, and the computing of this estimate involves high number of computational operations. To overcome this issue, the Gaussian EF reduces the M_s-dimensional estimation to an one-dimensional MMSE solution. This reduction is achieved by replacing the discrete sum with a Gaussian integral.

Both the proposed list EF and Gaussian EF significantly reduced the number of computational operations, especially for the MIMO relay networks with a high-order constellation and/or a large number of antennas. The simulation results confirmed that the proposed EF outperformed AF and DF for all the SNRs. Moreover, for multiple parallel networks, the performance gains of EF over AF and DF are expected to increase with an increasing number of relay nodes.

$\sim$

Chapter 7

Conclusions and Future Work

Next-generation wireless communication systems must provide high data rates and improved reliability. These goals are achieved by: (1) MIMO technology based on multiple-antenna transmitter and receiver terminals and (2) cooperation between wireless nodes enabling intermediate nodes (relays) to forward messages from source to destination. Both MIMO and cooperative communication [4] have the potential for tremendous improvements in coverage area, data rates, reliability and transmit power reduction.

   This thesis developed MIMO and cooperative detection algorithms that achieved near-optimal performance with low running time. These algorithms may thus lead to the development of networks with large signal constellations and large numbers of antennas, which are prohibitively complex with conventional strategies despite their great potential to improve spectral efficiency. The research outcomes may permit the implementation of a simpler and cheaper hardware, making the communication systems easy to develop and saving unnecessary capital expenses (energy costs, as discussed in Section 2.1.2).

- Chapter 3 introduced an SRC-SD, which achieved a reduced running time and a reduced variability for near-ML performance. This SD tightened the radius of the conventional SD by a heuristic SNR-dependent factor. Its application in coded MIMO and relay networks was also investigated to confirm that the proposed SRC-SD indeed had a near-optimal performance and a roughly constant running time.

- A probability-distribution-based SPSD was developed in Chapter 4. Uniform pruning, geometric pruning, threshold pruning, hybrid pruning and depth-dependent pruning were proposed and analysed. All of these rules achieved lower running time than the conventional SD in the low-SNR region. In particular, the threshold pruning rule obtained the most significant running time savings while achieving the full diversity order, and the running time savings increased with the number of transmit antennas.

- In Chapter 5, an IKSD was proposed, which had lower running time than the conventional K-best SD. The proposed IKSD, which achieved a near-ML performance at a reduced and roughly fixed running time, expanded the fixed K nodes and all the additional nodes whose cost was within a small threshold value Δ of the cost of the k-th node. This algorithm was extended to create a hybrid SD by combining the full enumeration with the proposed IKSD. Finally, a soft version of the IKSD was also developed as the list IKSD.

- Chapter 6 proposed an EF relay and investigated forwarding strategies in MIMO one-way and two-way relay networks. Analysis and simulation results verified that EF outperformed the conventional AF and DF strategies for all SNRs without switching algorithms. Furthermore, the performance gains increased with the number of relays.

Further research could focus on developing and examining novel relay functions and sphere detection technologies for multiple-antenna relay networks:

- ***Coded MIMO Relay Networks:*** Soft information relaying [114, 115] combines the advantages of the classical relay protocols AF and DF. DF achieves a coding gain, but suffers from propagation of the errors of the decoder at the relay. AF lacks the benefits of channel coding, but avoids error propagation and preserves reliability information. Chapter 6 developed optimal relay functions and the resulting performance analysis, low running time and enhanced relay strategies and detection process for uncoded MIMO. These algorithms could be readily extended for coded MIMO.

- *Systems without Perfect Channel Information:* Since wireless channels are time-varying, the relay and the destination need accurate and up-to-date CSI. While relay strategies and detection algorithms take perfect CSI for granted, the available CSI in actual systems is generally imperfect [116,117], resulting in suboptimal performance. Hence, further research could develop robust relaying methods and signal detection algorithms and studying the performance of the developed strategies.

  Furthermore, when perfect CSI is not available, the relay and the destination need to update past (imperfect) CSI. This refinement could be achieved by advanced signal processing techniques, relying on any correlation of CSI at a given time instant with its past values (e.g., as in an autoregressive model). Iterating between such channel estimation and detection stages would thus enable better symbol detection.

$$\sim$$

Bibliography

[1] (2013, Feb.) Cisco visual networking index: Global mobile data traffic forecast update. [Online]. Available: http://www.cisco.com/en/US/solutions/collateral/ns341/ns525/ns537/ns705/ns827/white_paper_c11-520862.html

[2] "Mobile broadband capacity constraints and the need for optimization," Rysavy research, Tech. Rep., Feb. 2010.

[3] E. Biglieri, R. Calderbank, A. Constantinides, A. Goldsmith, A. Paulraj, and H. V. Poor, *MIMO Wireless Communications*. New York, NY, USA: Cambridge University Press, 2007.

[4] A. Nosratinia, T. Hunter, and A. Hedayat, "Cooperative communication in wireless networks," *IEEE Commun. Mag.*, vol. 42, no. 10, pp. 74 – 80, Oct. 2004.

[5] *Wireless LAN Medium Access Control (MAC)and Physical Layer (PHY) Specifications Amendment 5: Enhancements for Higher Throughput*, IEEE Std 802.11n Std., Oct. 2009.

[6] *Technical Specification Group Radio Access Network; Evolved Universal Terrestrial Radio Access (E-UTRA); LTE physical layer; General description (Release 9)*, 3GPP 3GPP TS 36.201 V9.1 Std., Mar. 2010.

[7] "IEEE standard for local and metropolitan area networks part 16: Air interface for fixed and mobile broadband wireless access systems amendment 2: Physical and medium access control layers for combined fixed and mobile operation in licensed bands and corrigendum 1," *IEEE Std 802.16e-2005 and*

IEEE Std 802.16-2004/Cor 1-2005 (Amendment and Corrigendum to IEEE Std 802.16-2004), pp. 1 –822, 2006.

[8] F. J. MacWilliams and N. J. A. Sloane, *The Theory of Error-Correcting Codes*. North Holland, Jun. 1988.

[9] T.-D. Chiueh and P.-Y. Tsai, *OFDM Baseband Receiver Design for Wireless Communications*. Wiley Publishing, 2007.

[10] B. Hochwald and S. ten Brink, "Achieving near-capacity on a multiple-antenna channel," *IEEE Trans. Commun.*, vol. 51, no. 3, pp. 389 – 399, Mar. 2003.

[11] A. Ghosh, R. Ratasuk, B. Mondal, N. Mangalvedhe, and T. Thomas, "LTE-advanced: next-generation wireless broadband technology [invited paper]," *IEEE Wireless Commun.*, vol. 17, no. 3, pp. 10 –22, Jun. 2010.

[12] Q. Li, R. Hu, Y. Qian, and G. Wu, "Cooperative communications for wireless networks: techniques and applications in LTE-advanced systems," *IEEE Wireless Commun.*, vol. 19, no. 2, pp. 22 –29, Apr. 2012.

[13] "IEEE Standard for Information technology–Telecommunications and information exchange between systems–Local and metropolitan area networks–Specific requirements-Part 11: Wireless LAN Medium Access Control (MAC) and Physical Layer (PHY) Specifications Amendment 3: Enhancements for Very High Throughput in the 60 GHz Band," *IEEE Std 802.11ad-2012 (Amendment to IEEE Std 802.11-2012, as amended by IEEE Std 802.11ae-2012 and IEEE Std 802.11aa-2012)*, pp. 1–628, 2012.

[14] Z. Guo and P. Nilsson, "Algorithm and implementation of the K-best sphere decoding for MIMO detection," *IEEE J. Sel. Areas Commun.*, vol. 24, no. 3, pp. 491 – 503, Mar. 2006.

[15] B. C. Levy, *Principles of Signal Detection and Parameter Estimation*. Springer Publishing Company, Incorporated, 2008.

[16] W. Guo and T. OFarrell, "Reducing energy consumption of wireless communications," 2011.

[17] W. Zhang, *State Space Search: Algorithms, Complexity and Applications*. New York: Springer-Verlag, 1999.

[18] J. M. Rabaey, A. Chandrakasan, and B. Nikolic, *Digital integrated circuits-A design perspective*, 2nd ed.   Prentice Hall, 2004.

[19] T. H. Cormen, C. E. Leiserson, R. L. Rivest, and C. Stein, *Introduction to Algorithms*, 3rd ed.   The MIT Press, 2009.

[20] J. Jalden and B. Ottersten, "On the complexity of sphere decoding in digital communications," *IEEE Trans. Signal Process.*, vol. 53, no. 4, pp. 1474 – 1484, Apr. 2005.

[21] B. Hassibi and H. Vikalo, "On the sphere-decoding algorithm I. expected complexity," *IEEE Trans. Signal Process.*, vol. 53, no. 8, pp. 2806 – 2818, Aug. 2005.

[22] T. Cui and C. Tellambura, "An efficient generalized sphere decoder for rank-deficient MIMO systems," *IEEE Commun. Lett.*, vol. 9, no. 5, pp. 423 – 425, May 2005.

[23] A. Papoulis and S. Pillai, *Probability, Random Variables and Stochastic Processes*.   McGraw-Hill Education, Dec. 2001.

[24] O. Damen, A. Chkeif, and J.-C. Belfiore, "Lattice code decoder for space-time codes," *IEEE Commun. Lett.*, vol. 4, no. 5, pp. 161–163, May 2000.

[25] E. Viterbo and J. Boutros, "A universal lattice code decoder for fading channels," *IEEE Trans. Inf. Theory*, vol. 45, no. 5, pp. 1639–1642, Jul. 1999.

[26] E. Agrell, T. Eriksson, A. Vardy, and K. Zeger, "Closest point search in lattices," *IEEE Trans. Inf. Theory*, vol. 48, no. 8, pp. 2201 – 2214, Aug. 2002.

[27] M. Damen, H. El Gamal, and G. Caire, "On maximum-likelihood detection and the search for the closest lattice point," *IEEE Trans. Inf. Theory*, vol. 49, no. 10, pp. 2389 – 2402, Oct. 2003.

[28] U. Fincke and M. Pohst, "Improved methods for calculating vectors of short length in a lattice, including a complexity analysis," *Math. Comput.*, vol. 44, pp. 463–471, Apr. 1985.

[29] C. P. Schnorr and M. Euchner, "Lattice basis reduction: Improved practical algorithms and solving subset sum problems," *Math. Programming*, vol. 66, pp. 181–191, 1994.

[30] L. Barbero and J. Thompson, "Fixing the complexity of the sphere decoder for MIMO detection," *IEEE Trans. Wireless Commun.*, vol. 7, no. 6, pp. 2131–2142, Jun. 2008.

[31] M. Tuchler and A. C. Singer, "Turbo equalization: An overview," *IEEE Trans. Inf. Theory*, vol. 57, no. 2, pp. 920 –952, Feb. 2011.

[32] S. Han, T. Cui, and C. Tellambura, "Improved K-Best sphere detection for uncoded and coded MIMO systems," *IEEE Wireless Commun. Lett.*, vol. 1, no. 5, pp. 472 –475, Oct. 2012.

[33] S. Han and C. Tellambura, "Soft-output extension of an SNR-adaptive sphere decoder for coded MIMO systems," in *Proc. 2012 IEEE Canadian Conf. on Elect. and Comput. Eng.*, Montreal, Quebec, Apr. 29-May 2 2012.

[34] C. Berrou, A. Glavieux, and P. Thitimajshima, "Near Shannon limit error-correcting coding and decoding: Turbo-codes. 1," in *Proc. IEEE Int. Conf. on Commun.(ICC), Geneva*, vol. 2, May 1993, pp. 1064–1070.

[35] L. Barbero and J. Thompson, "Extending a fixed-complexity sphere decoder to obtain likelihood information for turbo-MIMO systems," *IEEE Trans. Veh. Technol.*, vol. 57, no. 5, pp. 2804 –2814, Sep. 2008.

[36] J. Laneman, D. Tse, and G. Wornell, "Cooperative diversity in wireless networks: Efficient protocols and outage behavior," *IEEE Trans. Inf. Theory*, vol. 50, no. 12, pp. 3062 – 3080, Dec. 2004.

[37] G. Amarasuriya, C. Tellambura, and M. Ardakani, "Performance analysis framework for transmit antenna selection strategies of cooperative MIMO AF relay networks," *IEEE Trans. Veh. Technol.*, vol. 60, no. 7, pp. 3030 – 3044, Sep. 2011.

[38] ——, "Asymptotically-exact performance bounds of AF multi-hop relaying over Nakagami fading," *IEEE Trans. Commun.*, vol. 59, no. 4, pp. 962 –967, Apr. 2011.

[39] Y. Jing and B. Hassibi, "Distributed space-time coding in wireless relay networks," *IEEE Trans. Wireless Commun.*, vol. 5, no. 12, pp. 3524 –3536, Dec. 2006.

[40] G. Amarasuriya, C. Tellambura, and M. Ardakani, "Joint relay and antenna selection for dual-hop Amplify-and-Forward MIMO relay networks," *IEEE Trans. Wireless Commun.*, vol. 11, no. 2, pp. 493 –499, Feb. 2012.

[41] G. Sharma, V. Ganwani, U. Desai, and S. Merchant, "Performance analysis of maximum likelihood detection for decode and forward MIMO relay channels in Rayleigh fading," *IEEE Trans. Wireless Commun.*, vol. 9, no. 9, pp. 2880 –2889, Sep. 2010.

[42] G. Amarasuriya, C. Tellambura, and M. Ardakani, "Performance analysis of hop-by-hop beamforming for dual-hop MIMO AF relay networks," *IEEE Trans. Commun.*, vol. 60, no. 7, pp. 1823 –1837, Jul. 2012.

[43] K. Amiri, M. Wu, J. Cavallaro, and J. Lilleberg, "Cooperative partial detection using MIMO relays," *IEEE Trans. Signal Process.*, vol. 59, no. 10, pp. 5039 –5049, Oct. 2011.

[44] A. Sabharwal and U. Mitra, "Bounds and protocols for a rate-constrained relay channel," *IEEE Trans. Inf. Theory*, vol. 53, no. 7, pp. 2616 –2624, Jul. 2007.

[45] A. Scaglione, D. Goeckel, and J. Laneman, "Cooperative communications in mobile ad hoc networks," *IEEE Signal Process. Mag.*, vol. 23, no. 5, pp. 18 – 29, Sep. 2006.

[46] D. Gesbert, "Robust linear MIMO receivers: a minimum error-rate approach," *IEEE Trans. Signal Process.*, vol. 51, no. 11, pp. 2863 – 2871, Nov. 2003.

[47] S. Han and C. Tellambura, "A complexity-efficient sphere decoder for MIMO systems," in *Proc. IEEE Int. Conf. on Commun.*, Kyoto, Japan, Jun. 2011, pp. 1–5.

[48] T. Cui, T. Ho, and C. Tellambura, "Statistical pruning for near maximum likelihood detection of MIMO systems," in *Proc. of IEEE Int. Conf. on Commun. (ICC)*, Jun. 2007, pp. 5462 –5467.

[49] K. S. Gomadam and S. A. Jafar, "Optimal relay functionality for SNR maximization in memoryless relay networks," *IEEE J. Sel. Areas Commun.*, vol. 25, no. 2, pp. 390 –401, Feb. 2007.

[50] A. Murugan, H. El Gamal, M. Damen, and G. Caire, "A unified framework for tree search decoding: rediscovering the sequential decoder," *IEEE Trans. Inf. Theory*, vol. 52, no. 3, pp. 933 –953, Mar. 2006.

[51] T. Cui and C. Tellambura, "Generalized feedback detection for spatial multiplexing multi-antenna systems," *IEEE Trans. Wireless Commun.*, vol. 7, no. 2, pp. 594 –603, Feb. 2008.

[52] J.-S. Kim, S.-H. Moon, and I. Lee, "A new reduced complexity ML detection scheme for MIMO systems," *IEEE Trans. Commun.*, vol. 58, no. 4, pp. 1302–1310, Apr. 2010.

[53] B. Shim and I. Kang, "Sphere decoding with a probabilistic tree pruning," *IEEE Trans. Signal Process.*, vol. 56, no. 10, pp. 4867–4878, Oct. 2008.

[54] ——, "On further reduction of complexity in tree pruning based sphere search," *IEEE Trans. Commun.*, vol. 58, no. 2, pp. 417–422, Feb. 2010.

[55] K. Su and I. Wassell, "A new ordering for efficient sphere decoding," in *Proc. IEEE Int. Conf. on Commun.(ICC)*, vol. 3, May 2005, pp. 1906 – 1910.

[56] T. Cui and C. Tellambura, "Joint data detection and channel estimation for OFDM systems," *IEEE Trans. Commun.*, vol. 54, no. 4, pp. 670 – 679, Apr. 2006.

[57] ——, "Generalized feedback detection for MIMO systems," in *Proc. of IEEE GLOBECOM*, 2005, pp. 3077–3081.

[58] A. Wiesel, X. Mestre, A. Pages, and J. Fonollosa, "Efficient implementation of sphere demodulation," in *Proc. IEEE Workshop on Signal Process. Advances in Wireless Commun.*, Jun. 2003, pp. 36 – 40.

[59] J. Anderson and S. Mohan, "Sequential coding algorithms: A survey and cost analysis," *IEEE Trans. Commun.*, vol. 32, no. 2, pp. 169 – 176, Feb. 1984.

[60] L. Barbero and J. Thompson, "A fixed-complexity MIMO detector based on the complex sphere decoder," in *Proc. of IEEE 7th Workshop on Signal Process. Advances in Wireless Commun.*, Jul. 2006, pp. 1 –5.

[61] R. Gowaikar and B. Hassibi, "Efficient statistical pruning for maximum likelihood decoding," in *Proc. IEEE Int. Conf. on Acoustics Speech and Signal Process. (ICASSP)*, vol. 5, Apr. 2003, pp. 49–52.

[62] W. Zhao and G. Giannakis, "Sphere decoding algorithms with improved radius search," *IEEE Trans. Commun.*, vol. 53, no. 7, pp. 1104 – 1109, Jul. 2005.

[63] Z. Guo and P. Nilsson, "Reduced complexity Schnorr-Euchner decoding algorithms for MIMO systems," *IEEE Commun. Lett.*, vol. 8, no. 5, pp. 286 – 288, May 2004.

[64] A. Younis, R. Mesleh, H. Haas, and P. Grant, "Reduced complexity sphere decoder for spatial modulation detection receivers," in *Proc. IEEE Global Commun. Conf.*, Dec. 2010, pp. 1 –5.

[65] I.-W. Lai, G. Ascheid, H. Meyr, and T.-D. Chiueh, "Efficient channel-adaptive MIMO detection using just-acceptable error rate," *IEEE Trans. Wireless Commun.*, vol. 10, no. 1, pp. 73 –83, Jan. 2011.

[66] Y. H. Wu, Y. T. Liu, H.-C. Chang, Y.-C. Liao, and H.-C. Chang, "Early-pruned K-best sphere decoding algorithm based on radius constraints," in *Proc. IEEE Int. Conf. on Commun.(ICC)*, 19-23 2008, pp. 4496 –4500.

[67] Y. Fan and J. Thompson, "MIMO configurations for relay channels: Theory and practice," *IEEE Trans. Wireless Commun.*, vol. 6, no. 5, pp. 1774–1786, May 2007.

[68] J. Chen, X. Yu, and C.-C. Kuo, "V-BLAST receiver and performance in MIMO relay networks with imperfect CSI," in *Proc. IEEE Int. Conf. on Commun.(ICC)*, May 2008, pp. 4436 –4440.

[69] S. Han, C. Tellambura, and T. Cui, "SNR-dependent radius control sphere detection for MIMO systems and relay networks," *Trans. Emerging Tel. Tech.*, Feb. 2013.

[70] T. Cui, J. Tang, F. Gao, and C. Tellambura, "Moment-based parameter estimation and blind spectrum sensing for quadrature amplitude modulation," *IEEE Trans. Commun.*, vol. 59, no. 2, pp. 613–623, 2011.

[71] P. Wolniansky, G. Foschini, G. Golden, and R. Valenzuela, "V-BLAST: an architecture for realizing very high data rates over the rich-scattering wireless channel," in *Proc. URSI Int. Symposium on Signals, Systems and Electonics (ISSSE)*, Sep. 1998, pp. 295 –300.

[72] Z. Ma, B. Honary, P. Fan, and E. Larsson, "Stopping criterion for complexity reduction of sphere decoding," *IEEE Commun. Lett.*, vol. 13, no. 6, pp. 402 –404, Jun. 2009.

[73] P. Robertson, E. Villebrun, and P. Hoeher, "A comparison of optimal and sub-optimal MAP decoding algorithms operating in the log domain," in *Proc. IEEE Int. Conf. on Commun.(ICC), Seattle*, vol. 2, Jun. 1995, pp. 1009 –1013 vol.2.

[74] R. Gowaikar and B. Hassibi, "Statistical pruning for near-maximum likelihood decoding," *IEEE Trans. Signal Process.*, vol. 55, no. 6, pp. 2661 –2675, Jun. 2007.

[75] A. Ghaderipoor and C. Tellambura, "A statistical pruning strategy for Schnorr-Euchner sphere decoding," *IEEE Commun. Lett.*, vol. 12, no. 2, pp. 121 –123, Feb. 2008.

[76] J. Ahn, H.-N. Lee, and K. Kim, "Schnorr-Euchner sphere decoder with statistical pruning for MIMO systems," in *Proc. the 6th Int. Symposium on Wireless Commun. Systems (ISWCS)*, Sep. 2009, pp. 619 –623.

[77] S. Lei, Q. Tu, D. Yang, and J. Chen, "Probabilistic tree pruning for fixed-complexity sphere decoder in MIMO systems," in *Proc. Int. Conf. on Wireless Commun. and Signal Process. (WCSP)*, Oct. 2010, pp. 1 –6.

[78] S. Han and C. Tellambura, "Complexity-efficient detection for MIMO relay networks," in *Proc. 12th IEEE Canadian Workshop on Inform. Theory*, Kelowna, Canada, May 2011, pp. 126 –129.

[79] S. Lei, X. Zhang, C. Xiong, and D. Yang, "An efficient statistical pruning algorithm for fixed-complexity sphere decoder," *IEICE Trans. Commun.*, vol. E94.B, no. 3, pp. 834–837, 2011.

[80] R. Y. Chang and W.-H. Chung, "Efficient tree-search MIMO detection with probabilistic node ordering," in *Proc. of IEEE ICC*, Jun. 2011, pp. 1 –5.

[81] J. Maurer, G. Matz, and D. Seethaler, "On the diversity-complexity tradeoff in MIMO spatial multiplexing systems," in *Proc. Fortieth Asilomar Conf. on Signals, Systems and Computers*, Nov. 2006, pp. 2077 –2081.

[82] J. Maurer, J. Jalden, D. Seethaler, and G. Matz, "Achieving a continuous diversity-complexity tradeoff in wireless MIMO systems via pre-equalized sphere-decoding," *IEEE J. Sel. Topics Signal Process.*, vol. 3, no. 6, pp. 986 –999, Dec. 2009.

[83] T. Cui, S. Han, and C. Tellambura, "Probability-distribution-based node pruning for sphere decoding," *IEEE Trans. Veh. Technol.*, vol. 62, no. 4, pp. 1586–1596, May 2013.

[84] X. Zhu and R. D. Murch, "Performance analysis of maximum likelihood detection in a MIMO antenna system," *IEEE Trans. Commun.*, vol. 50, pp. 187–191, Feb. 2002.

[85] C.-A. Shen and A. Eltawil, "A radius adaptive K-best decoder with early termination: Algorithm and VLSI architecture," *IEEE Trans. Circuits Syst. I, Reg. Papers*, vol. 57, no. 9, pp. 2476 –2486, Sep. 2010.

[86] T.-H. Kim and I.-C. Park, "Small-area and low-energy K-best MIMO detector using relaxed tree expansion and early forwarding," *IEEE Trans. Circuits Syst. I, Reg. Papers*, vol. 57, no. 10, pp. 2753 –2761, Oct. 2010.

[87] C. Xiong, X. Zhang, K. Wu, and D. Yang, "A simplified fixed-complexity sphere decoder for V-BLAST systems," *IEEE Commun. Lett.*, vol. 13, no. 8, pp. 582 –584, Aug. 2009.

[88] K.-C. Lai, C.-C. Huang, and J.-J. Jia, "Variation of the fixed-complexity sphere decoder," *IEEE Commun. Lett.*, vol. 15, no. 9, pp. 1001 –1003, Sep. 2011.

[89] P. Bengough and S. Simmons, "Sorting-based VLSI architectures for the M-algorithm and T-algorithm trellis decoders," *IEEE Trans. Commun.*, vol. 43, no. 3, pp. 514 –522, Mar. 1995.

[90] S. Simmons, "Breadth-first trellis decoding with adaptive effort," *IEEE Trans. Commun.*, vol. 38, no. 1, pp. 3 –12, Jan. 1990.

[91] N. Heidmann, T. Wiegand, and S. Paul, "Architecture and FPGA-implementation of a high throughput K+-best detector," in *Proc. Europe Conf. Exhibition in Design, Automation Test*, Mar. 2011, pp. 1 –6.

[92] P. Weitkemper and G. Dietl, "Maximum likelihood receiver for MMSE relaying," in *Proc. of IEEE ICC, (ICC)*, Jun. 2011, pp. 1 –5.

[93] P. Weitkemper, D. Wubben, and K.-D. Kammeyer, "Minimum MSE relaying for arbitrary signal constellations in coded relay networks," in *Proc. IEEE 69th Veh. Technol. Conf. (VTC Spring)*, Apr. 2009, pp. 1 –5.

[94] C. Serediuc, J. Lilleberg, and B. Aazhang, "MAP detection with soft information in an estimate and forward relay network," in *Proc. the Forty Fourth Asilomar Conference on Signals, Systems and Computers*, Nov. 2010, pp. 121 –125.

[95] A. Chakrabarti, A. Sabharwal, and B. Aazhang, "Practical quantizer design for half-duplex estimate-and-forward relaying," *IEEE Trans. Commun.*, vol. 59, no. 1, pp. 74 –83, Jan. 2011.

[96] R. Dabora and S. Servetto, "On the role of estimate-and-forward with time sharing in cooperative communication," *IEEE Trans. Inf. Theory*, vol. 54, no. 10, pp. 4409 –4431, Oct. 2008.

[97] W. Li and J. Lilleberg, "Optimized discrete-estimate-and-forward relaying strategy," in *Proc. IEEE Wireless Commun. and Networking Conf. (WCNC)*, Apr. 2012, pp. 963 –967.

[98] R. Thobaben and E. Larsson, "Sensor-network-aided cognitive radio: On the optimal receiver for estimate-and-forward protocols applied to the relay channel," in *Proc. Forty-First Asilomar Conference on Signals, Systems and Computers*, Nov. 2007, pp. 777 –781.

[99] O. Munoz-Medina, J. Vidal, and A. Agustin, "Linear transceiver design in nonregenerative relays with channel state information," *IEEE Trans. Signal Process.*, vol. 55, no. 6, pp. 2593 –2604, Jun. 2007.

[100] F.-S. Tseng, W.-R. Wu, and J.-Y. Wu, "Joint source/relay precoder design in nonregenerative cooperative systems using an MMSE criterion," *IEEE Trans. Wireless Commun.*, vol. 8, no. 10, pp. 4928 –4933, Oct. 2009.

[101] G. Amarasuriya, C. Tellambura, and M. Ardakani, "Joint relay and antenna selection for dual-hop amplify-and-forward MIMO relay networks," *IEEE Trans. Wireless Commun.*, vol. 11, no. 2, pp. 493–499, 2012.

[102] ——, "Two-way amplify-and-forward MIMO relay networks with antenna selection," in *proc. IEEE Global Telecommunications Conference (GLOBE-COM)*, 2011, pp. 1–5.

[103] ——, "Transmit antenna selection strategies for cooperative MIMO AF relay networks," in *proc. IEEE Global Telecommunications Conference (GLOBE-COM)*, 2010, pp. 1–5.

[104] S. Han, T. Cui, and C. Tellambura, "Estimate-and-Forward relay strategy for MIMO relay networks," *IEEE Trans. Wireless Commun.*, 2013, revised.

[105] Y. Rong, "Optimal joint source and relay beamforming for MIMO relays with direct link," *IEEE Commun. Lett.*, vol. 14, no. 5, pp. 390–392, 2010.

[106] H. Wan, W. Chen, and J. Ji, "Efficient linear transmission strategy for MIMO relaying broadcast channels with direct links," *IEEE Wireless Commun. Lett.*, vol. 1, no. 1, pp. 14–17, 2012.

[107] J. Fricke, M. Butt, and P. Hoeher, "Quality-oriented adaptive forwarding for wireless relaying," *IEEE Commun. Lett.*, vol. 12, no. 3, pp. 200 –202, Mar. 2008.

[108] Q. Li, S. Ting, A. Pandharipande, and Y. Han, "Adaptive two-way relaying and outage analysis," *IEEE Trans. Wireless Commun.*, vol. 8, no. 6, pp. 3288 –3299, Jun. 2009.

[109] H. El Gamal and J. Hammons, A.R., "Analyzing the turbo decoder using the Gaussian approximation," *IEEE Trans. Inf. Theory*, vol. 47, no. 2, pp. 671 –686, Feb. 2001.

[110] Q. You, Z. Chen, and Y. Li, "A multihop transmission scheme with detect-and-forward protocol and network coding in two-way relay fading channels," *IEEE Trans. Veh. Technol.*, vol. 61, no. 1, pp. 433 –438, Jan. 2012.

[111] T. Cui, F. Gao, T. Ho, and A. Nallanathan, "Distributed space time coding for two-way wireless relay networks," *IEEE Trans. Signal Process.*, vol. 57, no. 2, pp. 658 –671, Feb. 2009.

[112] S. Bagheri, F. Verde, D. Darsena, and A. Scaglione, "Randomized decode-and-forward strategies for two-way relay networks," *IEEE Trans. Wireless Commun.*, vol. 10, no. 12, pp. 4214 –4225, Dec. 2011.

[113] R. Vaze and R. Heath, "On the capacity and diversity-multiplexing tradeoff of the two-way relay channel," *IEEE Trans. Inf. Theory*, vol. 57, no. 7, pp. 4219 –4234, Jul. 2011.

[114] J. Du, M. Xiao, and M. Skoglund, "Cooperative network coding strategies for wireless relay networks with Backhaul," *IEEE Trans. Commun.*, vol. 59, no. 9, pp. 2502 –2514, Sep. 2011.

[115] D. Kim, H.-M. Kim, and G.-H. Im, "Improved network-coded cooperative transmission with low-complexity adaptation to wireless channels," *IEEE Trans. Commun.*, vol. 59, no. 10, pp. 2916 –2927, Oct. 2011.

[116] P. Ubaidulla and A. Chockalingam, "Relay precoder optimization in MIMO-relay networks with imperfect CSI," *IEEE Trans. Signal Process.*, vol. 59, no. 11, pp. 5473 –5484, Nov. 2011.

[117] B. Chalise and L. Vandendorpe, "MIMO relay design for multipoint-to-multipoint communications with imperfect channel state information," *IEEE Trans. Signal Process.*, vol. 57, no. 7, pp. 2785 –2796, Jul. 2009.

$\sim$

Appendix A

Proof of the ML Rule in MIMO Relay Networks

Proof: According to the norm expansion $||\mathbf{H}||^2 = \mathbf{H}^H\mathbf{H}$, (3.16) is expanded as

$$
\begin{aligned}
\hat{\mathbf{x}}_d &= \arg\min_{\mathbf{x}\in\mathcal{Q}^{N_s}} \left(\sum_{i=1}^{N_{re}} ||\mathbf{y}_i - \mathbf{G}_i\mathbf{x}||^2 + ||\mathbf{y}_d - \mathbf{H}_{sd}\mathbf{s}_s||^2 \right). \\
&= \arg\min_{\mathbf{x}\in\mathcal{Q}^{N_s}} \left[\sum_{i=1}^{N_{re}} \mathbf{y}_i^H\mathbf{y}_i + \mathbf{y}_d^H\mathbf{y}_d - \mathbf{x}^H \left(\sum_{i=1}^{N_{re}} \mathbf{G}_i^H\mathbf{y}_i + \mathbf{H}_{sd}^H\mathbf{y}_d \right) \right. \\
&\quad \left. - \left(\sum_{i=1}^{N_{re}} \mathbf{y}_i^H\mathbf{G}_i + \mathbf{y}_d^H\mathbf{H}_{sd} \right) \mathbf{x}^H + \mathbf{x}^H \left(\sum_{i=1}^{N_{re}} \mathbf{G}_i^H\mathbf{G}_i + \mathbf{H}_{sd}^H\mathbf{H}_{sd} \right) \mathbf{x} \right].
\end{aligned}
\tag{A.1}
$$

Assuming $\mathbf{y}'$ and $\mathbf{H}'$ are derived, the ML expression can be expanded similarly as

$$
\begin{aligned}
\hat{\mathbf{x}}_d &= \arg\min_{\mathbf{x}\in\mathcal{Q}^{N_s}} ||\mathbf{y}' - \mathbf{H}'\mathbf{x}||^2 \\
&= \arg\min_{\mathbf{x}\in\mathcal{Q}^{N_s}} \left(\mathbf{y}'^H\mathbf{y}' - \mathbf{x}^H\mathbf{H}'^H\mathbf{y}' - \mathbf{y}'^H\mathbf{H}'\mathbf{x} + \mathbf{x}^H\mathbf{H}'^H\mathbf{H}'\mathbf{x} \right). \quad \text{(A.2)}
\end{aligned}
$$

By comparing (A.1) and (A.2), it is clear that

$$
\mathbf{H}'^H\mathbf{H}' = \sum_{i=1}^{N_{re}} \mathbf{G}_i^H\mathbf{G}_i + \mathbf{H}_{sd}^H\mathbf{H}_{sd},
\tag{A.3a}
$$

$$
\mathbf{H}'^H\mathbf{y}' = \sum_{i=1}^{N_{re}} \mathbf{G}_i^H\mathbf{y}_i + \mathbf{H}_{sd}^H\mathbf{y}_d.
\tag{A.3b}
$$

Further, because of $\left(\sum\limits_{i=1}^{N_{re}} \mathbf{G}_i^H \mathbf{G}_i + \mathbf{H}_{sd}^H \mathbf{H}_{sd} \right)^H = \sum\limits_{i=1}^{N_{re}} \mathbf{G}_i^H \mathbf{G}_i + \mathbf{H}_{sd}^H \mathbf{H}_{sd}$, (A.3a) can be shown to yield

$$
\begin{aligned}
\mathbf{H}'^H \mathbf{H}' &= \left[\left(\sum_{i=1}^{N_{re}} \mathbf{G}_i^H \mathbf{G}_i + \mathbf{H}_{sd}^H \mathbf{H}_{sd} \right)^H \left(\sum_{i=1}^{N_{re}} \mathbf{G}_i^H \mathbf{G}_i + \mathbf{H}_{sd}^H \mathbf{H}_{sd} \right) \right]^{\frac{1}{2}} \\
&= \left[\left(\sum_{i=1}^{N_{re}} \mathbf{G}_i^H \mathbf{G}_i + \mathbf{H}_{sd}^H \mathbf{H}_{sd} \right)^{\frac{1}{2}} \right]^H \left(\sum_{i=1}^{N_{re}} \mathbf{G}_i^H \mathbf{G}_i + \mathbf{H}_{sd}^H \mathbf{H}_{sd} \right)^{\frac{1}{2}}.
\end{aligned}
\tag{A.4}
$$

Thus, the equivalent channel matrix $\mathbf{H}'$ is

$$
\mathbf{H}' = \left(\sum_{i=1}^{N_{re}} \mathbf{G}_i^H \mathbf{G}_i + \mathbf{H}_{sd}^H \mathbf{H}_{sd} \right)^{1/2},
\tag{A.5}
$$

where $\mathbf{H}' = \mathbf{H}'^H$.

According to the equivalent channel matrix (A.1) and (A.2), the equivalent received signal $\mathbf{y}'$ are derived as

$$
\mathbf{y}' = (\mathbf{H}'^H)^{-1} \left(\sum_{i=1}^{N_{re}} \mathbf{G}_i^H \mathbf{y}_i + \mathbf{H}_{sd}^H \mathbf{y}_{sd} \right) = (\mathbf{H}')^{-1} \left(\sum_{i=1}^{N_{re}} \mathbf{G}_i^H \mathbf{y}_i + \mathbf{H}_{sd}^H \mathbf{y}_{sd} \right).
\tag{A.6}
$$

∎

∼

Appendix B

Proof of the FER of Statistical Pruning SD

B.1 Proof for Uniform Pruning

Proof: In order to derive the FER upper bound for the uniform rule, we can let $\mathbf{s}^{(1)} = \left[s_1^{(1)}, \ldots, s_n^{(1)} \right]^T$ denote the transmitted vector and $\hat{\mathbf{s}} = [\hat{s}_1, \ldots, \hat{s}_n]^T$ denote the vector returned by the SPSD. It can be derived that $P_f = \Pr(\hat{\mathbf{s}} \neq \mathbf{s}^{(1)})$. Denote A as the event that $\mathbf{s}^{(1)}$ is visited. By using the total probability theorem [23], the FER can be expressed as

$$
\begin{aligned}
P_f &= \Pr(\hat{\mathbf{s}} \neq \mathbf{s}^{(1)}|A^c) \Pr(A^c) + \Pr\left(\hat{\mathbf{s}} \neq \mathbf{s}^{(1)}|A\right) \Pr(A) \\
&= \Pr(A^c) + \Pr\left(\hat{\mathbf{s}} \neq \mathbf{s}^{(1)}|A\right) \Pr(A),
\end{aligned}
\tag{B.1}
$$

where $\Pr(\hat{\mathbf{s}} \neq \mathbf{s}^{(1)}|A^c) = 1$. First $\Pr(A^c)$ (or $1 - \Pr(A)$) is derived and then the second term of (B.1) is analysed. Let $\tilde{\mathbf{s}} = [\tilde{s}_1, \ldots, \tilde{s}_n]^T$ be the temporary value for $\mathbf{s} = [s_1, \ldots, s_n]^T$ during the statistical pruning search as in Algorithm I, which corresponds to a leaf node in the search tree. A_i denotes the event that $s_i^{(1)}$ is visited. Note that $\Pr(A) = \Pr(\tilde{\mathbf{s}} = \mathbf{s}^{(1)})$, the probability that the leaf node corresponding to $\mathbf{s}^{(1)}$ is visited and is given by

$$
\begin{aligned}
\Pr(A) &= \Pr(\tilde{\mathbf{s}} = \mathbf{s}^{(1)}|\tilde{s}_n = s_n^{(1)}) \Pr(\tilde{s}_n = s_n^{(1)}) \\
&\quad + \Pr(\tilde{\mathbf{s}} = \mathbf{s}^{(1)}|\tilde{s}_n \neq s_n^{(1)}) \Pr(\tilde{s}_n \neq s_n^{(1)}) \\
&= \Pr(\tilde{\mathbf{s}} = \mathbf{s}^{(1)}|\tilde{s}_n = s_n^{(1)}) \Pr(A_n),
\end{aligned}
\tag{B.2}
$$

132

where $\Pr(\tilde{s}_n = s_n^{(1)}) = \Pr(A_n)$, and $\Pr(\tilde{\mathbf{s}} = \mathbf{s}^{(1)}|\tilde{s}_n \neq s_n^{(1)}) = 0$. By a similar argument, (B.2) can be expanded as

$$\Pr(A) = \Pr(A_n) \prod_{i=1}^{n-1} \Pr(A_i|\tilde{s}_{i+1} = s_{i+1}^{(1)}, \ldots, \tilde{s}_n = s_n^{(1)}). \qquad \text{(B.3)}$$

Let B_i denote the event that $s_i^{(1)}$ is not the first element of $\mathcal{A}$ in Algorithm I. It can be derived as

$$\begin{aligned}
\Pr(A_n^c) &= \Pr(A_n^c|B_n)\Pr(B_n) + \Pr(A_n^c|B_n^c)\Pr(B_n^c) \\
&= (1-p)\Pr(B_n),
\end{aligned} \qquad \text{(B.4)}$$

where $\Pr(A_n^c|B_n) = 1 - p$, and $\Pr(A_n^c|B_n^c) = 0$. The union bound for $\Pr(B_n)$ is given by

$$\begin{aligned}
\Pr(B_n) \leq & E_{r_{n,n}} E_{s_n^{(1)}} \Bigg[\sum_{s_n^{(2)} \neq s_n^{(1)}} \Pr\left(\left|z_n - r_{n,n}s_n^{(2)}\right|^2 \right. \\
& \left. < \left|z_n - r_{n,n}s_n^{(1)}\right|^2 \Big| s_n^{(1)}, r_{n,n} \right) \Bigg],
\end{aligned} \qquad \text{(B.5)}$$

where $s_n^{(2)}$ is the nearest neighbor of $s_n^{(1)}$. From [23], the squared norm of the entries of upper-triangular matrix $\mathbf{R}$ have χ^2 distribution with different degrees of freedom without column reordering, specifically, $|r_{i,i}|^2 \sim \chi^2(2(n-i+1))$, for $i = 1, \ldots, n$ and $|r_{i,j}|^2 \sim \chi^2(2)$, for $j > i$, where $\chi^2(k)$ denotes the chi-squared distribution with k degrees of freedom. It can be obtained as

$$\begin{aligned}
& \Pr\left(\left|z_n - r_{n,n}s_n^{(2)}\right|^2 < \left|z_n - r_{n,n}s_n^{(1)}\right|^2 \Big| s_n^{(1)}, r_{n,n} \right) \\
& = Q\left(\sqrt{\left|r_{n,n}\left(s_n^{(2)} - s_n^{(1)}\right)\right|^2 / 2\sigma^2} \right).
\end{aligned} \qquad \text{(B.6)}$$

where $Q(\cdot)$ is the Q-function. Using the Chernoff bound for the Q-function, $\Pr(B_n)$ can be bounded as

$$\begin{aligned}
\Pr(B_n) \leq & E_{r_{n,n}} E_{s_n^{(1)}} \left[\sum_{s_n^{(2)} \neq s_1^{(1)}} \exp\left(\frac{-r_{n,n}^2 \left|s_n^{(2)} - s_n^{(1)}\right|^2}{4\sigma^2} \right) \right] \\
& = E_{s_n^{(1)}} \sum_{s_n^{(2)} \neq s_1^{(1)}} \frac{1}{1 + \frac{\left|s_n^{(2)} - s_n^{(1)}\right|^2}{4\sigma^2}} \leq \frac{|\mathcal{Q}|}{1 + d_{\min}^2/4\sigma^2},
\end{aligned} \qquad \text{(B.7)}$$

133

where $d_{\min}$ is the minimum Euclidean distance of $\mathcal{Q}$, and the equality comes from the moment generating function of $r_{n,n}$, $M_{r_{n,n}}(t) = E\{e^{tr_{n,n}}\}$. Therefore, $\Pr(A_n^c)$ can be bounded as

$$\Pr(A_n^c) \leq (1-p)\frac{|\mathcal{Q}|}{1 + d_{\min}^2/4\sigma^2}. \tag{B.8}$$

Similarly, the conditional probability is bounded as

$$\begin{aligned}
&\Pr(A_i^c|\tilde{s}_{i+1} = s_{i+1}^{(1)}, \ldots, \tilde{s}_n = s_n^{(1)}) \\
&\leq (1-p)\frac{|\mathcal{Q}|}{(1 + d_{\min}^2/4\sigma^2)^{n-i+1}}, \; i = 1, \ldots, n-1.
\end{aligned} \tag{B.9}$$

Finally, an upper bound on $\Pr(A^c)$ is obtained as

$$\begin{aligned}
\Pr(A^c) =& 1 - \Pr(A) \\
=& 1 - \Pr(A_n) \prod_{i=1}^{n-1} \Pr(A_i|\tilde{s}_{i+1} = s_{i+1}^{(1)}, \ldots, \tilde{s}_n = s_n^{(1)}) \\
=& 1 - (1 - \Pr(A_n^c)) \prod_{i=1}^{n-1} \left(1 - \Pr(A_i^c|\tilde{s}_{i+1} = s_{i+1}^{(1)}, \ldots, \tilde{s}_n = s_n^{(1)})\right).
\end{aligned} \tag{B.10}$$

In the high-SNR region, $\Pr(A_n^c)$ and $\Pr(A_i^c|\tilde{s}_{i+1} = s_{i+1}^{(1)}, \ldots, \tilde{s}_n = s_n^{(1)})$, $i = 1, \ldots, n-1$ are small. $\Pr(A^c)$ can be well approximated as

$$\begin{aligned}
\Pr(A^c) \approx& \Pr(A_n^c) + \sum_{i=1}^{n-1} \Pr(A_i^c|\tilde{s}_{i+1} = s_{i+1}^{(1)}, \ldots, \tilde{s}_n = s_n^{(1)}) \\
\leq& (1-p) \sum_{i=1}^{n} \frac{|\mathcal{Q}|}{(1 + d_{\min}^2/4\sigma^2)^i}.
\end{aligned} \tag{B.11}$$

$\Pr\left(\hat{\mathbf{s}} \neq \mathbf{s}^{(1)}|A\right)$ in (B.1) is then bounded in the following. Denote the set of all the visited leaf nodes by $\mathcal{I}$, which is the candidate set for the output of the statistical pruning detection. Since some leaf nodes may be pruned, $|\mathcal{I}| \leq |\mathcal{Q}|^n$. In case of A, $\mathbf{s}^{(1)} \in \mathcal{I}$. The union bound for $\Pr\left(\hat{\mathbf{s}} \neq \mathbf{s}^{(1)}|A\right)$ is given by

$$\begin{aligned}
\Pr\left(\hat{\mathbf{s}} \neq \mathbf{s}^{(1)}|A\right) \leq& \frac{1}{|\mathcal{Q}|^n} \sum_{\mathbf{s}^{(1)} \in \mathcal{Q}^n} \sum_{\mathbf{s}^{(2)} \in \mathcal{I}, \mathbf{s}^{(2)} \neq \mathbf{s}^{(1)}} \\
& \Pr\left(\left\|\mathbf{z} - \mathbf{R}\mathbf{s}^{(2)}\right\|^2 \leq \left\|\mathbf{z} - \mathbf{R}\mathbf{s}^{(1)}\right\|^2\right).
\end{aligned} \tag{B.12}$$

By using the Chernoff bound for the Q-function to the summand in (B.12), it can be readily obtained that

$$
\Pr\left(\hat{\mathbf{s}} \neq \mathbf{s}^{(1)}|A\right) \leq \frac{1}{|\mathcal{Q}|^n} \sum_{\mathbf{s}^{(1)} \in \mathcal{Q}^n} \sum_{\mathbf{s}^{(2)} \in \mathcal{I}, \mathbf{s}^{(2)} \neq \mathbf{s}^{(1)}} \frac{1}{\left(1 + \frac{d_{\min}^2}{4\sigma^2}\right)^n}
$$
$$
\leq |\mathcal{I}| \frac{1}{\left(1 + \frac{d_{\min}^2}{4\sigma^2}\right)^n} \leq \left(\frac{|\mathcal{Q}|}{1 + \frac{d_{\min}^2}{4\sigma^2}}\right)^n .
$$

(B.13)

Combining (B.13) and (B.11), the frame error rate can be bounded as

$$
P_f = \Pr(A^c) + \Pr\left(\hat{\mathbf{s}} \neq \mathbf{s}^{(1)}|A\right)\Pr(A)
$$
$$
\leq (1 - p) \sum_{i=1}^{n} \frac{|\mathcal{Q}|}{\left(1 + \frac{d_{\min}^2}{4\sigma^2}\right)^i} + \left(\frac{|\mathcal{Q}|}{1 + \frac{d_{\min}^2}{4\sigma^2}}\right)^n
$$

(B.14)

∎

B.2 Proof for Threshold Pruning

Proof: For threshold rule, the approach is similar to the analysis of uniform rule. All the events are defined the same as before. For the threshold pruning rule, the union bound for $P(A_n^c)$ is given by

$$
P(A_n^c) \leq E_{r_{n,n}} E_{s_n^{(1)}}\left[\Pr\left(|n_n|^2 > \delta_n\right)\right]
$$
$$
= \int_{\frac{\delta_n}{\sigma^2}}^{+\infty} f_n(x)dx = 1 - \gamma\left(1, \frac{\delta_n}{2\sigma^2}\right),
$$

(B.15)

where δ_n controls the strength of pruning as in Pruning Rule 2, $f_n(x)$ is the pdf of $\chi^2(2)$, and $\gamma(\alpha, x)$ is the incomplete gamma function. Similarly, it can be obtained as

$$
\Pr(A_i^c|\tilde{s}_{i+1} = s_{i+1}^{(1)}, \ldots, \tilde{s}_n = s_n^{(1)}) \leq \int_{\frac{\delta_i}{\sigma^2}}^{+\infty} f_i(x)dx
$$

(B.16)

where $f_i(x)$ is the pdf of $\chi^2(2(n - i + 1))$. The FER is upper bounded as

$$
P_f \leq \sum_{i=1}^{n} \int_{\frac{\delta_i}{\sigma^2}}^{+\infty} f_i(x)dx + \left(\frac{|\mathcal{Q}|}{1 + \frac{d_{\min}^2}{4\sigma^2}}\right)^n .
$$

(B.17)

∎

$\sim$